Linear and Nonlinear Acoustics With Nonuniform Entropy in Combustion Chambers

Thesis by
Joseph William Humphrey III

In Partial Fulfillment of the Requirements
for the Degree of
Doctor of Philosophy

California Institute of Technology
Pasadena, California
1987
(Submitted September 25, 1986)

Acknowledgements

I would like to take this opportunity to express my gratitude to all of the people who have helped me to make this work possible. I cannot mention everyone individually, but several deserve special mention.

The Office of Naval Research has supported this work through my Graduate Research Fellowship and ONR contract N00014-84-K-0434. China Lake Naval Weapons Center supported the experimental efforts contained in Chapter 2. My thanks to Dr. W.H. Clark and Frank Markarian for their guidance and assistance at the Naval Weapons Center.

My advisor, Professor Culick, was instrumental in providing guidance, focus, encouragement, and enlightening perspectives on problems, which, at the time, seemed almost impossible. In addition, my first advisor, Professor Marble, guided the initial phase of my research as well as providing many insightful technical conversations. Several other professors who directly influenced my work were Professors Zukoski, Cohen, and Knowles.

I would like to thank a very good friend who has been a source of food for thought and encouragement for the last three years, Michael Chobotov. Thanks also to Robert Whirley, who assisted generously in computer applications. Vigor Yang helped with many conversations and guidance in the areas of modeling and acoustics.

And last, I am very grateful to my family who have consistently encouraged my educational endeavors. Thanks especially to my wife who had to endure the trials and tribulations of being married to a graduate student.

Abstract

A one-dimensional analytical model is presented for calculating the longitudinal acoustic modes of idealized "dump-type" ramjet engines. The geometry considered is the coaxial flow type with the inlet flow opening to the combustor at a simple dump plane. Since the frequencies are very low, the dominant modes are the one-dimensional longitudinal modes and allow the predictions to be extended to more complicated geometries (such as side dump combustors) with good success. A plane flame has been studied and incorporated into the combustor model where the flame is allowed to move or oscillate in the combustor. This provides three mechanisms of interaction at the flame sheet: change in mean temperature in the combustor, energy conversion at the sheet due to upstream fluctuations, and fluctuating heat release. A supersonic inlet upstream contains a shock wave in its diffuser section while the downstream exit is terminated by a choked nozzle. The linear coupling of the acoustic and entropy waves at the inlet shock, flame sheet, and exit nozzle along with acoustic admittances at the inlet and exit are combined to determine the stability of the system as well as the acoustic modes. Since the acoustic and entropy waves travel at different velocities, the geometry is a critical factor in determining stability. Typical values of the admittances will produce damped solutions when the entropy is neglected, but, as the ratio of the entropy to acoustic fluctuations is increased, the coupling can either feed acoustic energy into or out of different modes independently. This transfer of energy has a destabilizing or stabilizing effect on the acoustic modes of the system depending on the relative phases between the acoustic and entropy waves.

In the linear case, the entropy and acoustics are decoupled in the flow field. All linear coupling occurs at the boundary conditions. For cases where the

entropy fluctuations are of the same order of magnitude as the pressure oscillations and the coupling is of comparable order, the linear stability of the acoustic field is strongly dependent upon the entropy fluctuations. The linear acoustics are predominantly governed by the boundary conditions; thus it is imperative that the entire system of inlet, combustor, and exit be considered together to determine the characteristic eigenvalues (resonant frequencies) and eigenfunctions (mode shapes). In addition, there are two modes of acoustic pressure oscillations: the classical acoustic mode and the entropy-induced mode of pressure oscillation. The nonlinear case treats the quadratic nonlinear fluid mechanic interactions in the coupling of two acoustic modes. The result is that the nonlinear acoustic-entropy interactions are much smaller than the acoustic-acoustic interactions for this case. Hence, the nonlinear acoustic field is influenced by the nonuniform entropy only by its dependence upon the linear solution which can be strongly dependent upon the entropy.

The energy in the acoustics of this model is controlled by the energy loss (gain) at the boundaries balanced with the energy gain (loss) at the flame front. Acoustic energy is typically lost at both the inlet and exit, but fluctuating entropy waves convecting with the mean flow velocity that impinge upon a choked nozzle generate acoustic waves that can, under the proper conditions, feed acoustic energy into the system. In addition, the Rayleigh condition for driving the system with a fluctuating heat release can also contribute to the stability of the system. The plane flame mechanism also contributes to the acoustic energy from the interaction of entropy and acoustic waves at a flame sheet. This allows a systematic study of the influence of entropy-acoustic wave interactions on the linear stability and modes of this combustor system.

Contents

List of Figures

List of Tables

Nomenclature

A	Entropy Constant (Complex)	M_d	Duct Mach Number
A_N	Nozzle Admittance	$\vec{n}$	$\pm\vec{\imath}$
A_{NEXIT}	Defined Admittance Eq. 4.87	$O(M^2)$	Order Mach Number Squared
A_{SH}	Linear Shock Admittance	P	Pressure
a	Speed of Sound	P_{t0}	Total Pressure
a_0	Mean Speed of Sound	P_{t4}	Combustor Pressure
B	Entropy Constant (Complex)	P_0	Upstream Pressure
b_f	Point Force	P'	Fluctuating Pressure
c_v	Specific Heat (Constant Volume)	P_{upst}	Pressure Upstream of Shock
c_p	Specific Heat (Constant Pressure)	P^+	Magnitude of Rightward Wave
e	Internal Energy	P^-	Magnitude of Leftward Wave
$\mathcal{E}$	Acoustic Energy	q	Entropy Source from 4.8 and 4.11
$F(\Omega)$	Characteristic Expression	$\dot{q}$	Heat Generation Term
$\mathcal{H}$	Nondimensional Entropy	Q	$\triangle h_f$ Enthalpy of Formation
k	Wave Number	R	Universal Gas Constant
K	Wave Number with Mean Flow	$s(x,t)$	Entropy
$\mathcal{K}$	Defined in Equation 4.88	$s_0(x,t)$	Mean Entropy
L_2	Duct 2 Length	$s'(x,t)$	Flutuating Entropy
L_1	Duct 1 Length	S	Area
L_C	Combustor Length	S_t	Flame Deflagration Speed
$\hat{m}$	Mass Source Magnitude	S_a	Relative Flame Speed
M	Mach Number	t	Time
M_0	Mean Mach Number	T	Temperature
$M_{1.5}$	Mean Mach Number in the Inlet	T_{t0}	Upstream Total Temperature
M_4	Combustor Mach Number	T_{t4}	Combustor Total Temperature

T_0	Upstream Temperature	$\phi(x)$	Phase Angle
U^+	Magnitude of Rightward Wave	ϕ_{flame}	Flame Phase Angle
U^-	Magnitude of Leftward Wave	Φ	Dissipation
$u(x,t)$	Axial Velocity	Φ	Equivalence Ratio
$u_0(x,t)$	Mean Axial Velocity	Ω	Complex Eigenfrequency
$u'(x,t)$	Fluctuating Axial Velocity	ω	Real part of Eigenfrequency
Vol	Volume	ρ	Density
w	Mass Source Term	σ	Constant
W_a	Mass Flux of Air	τ	Time for Event
x	Axial Position	τ	Period
$\hat{x}$	Axial Position from Cone Apex	$\tau_{acoustic}$	Acoustic Travel Time
x_f	Flame Position	$\tau_{convective}$	Convective Travel Time
x_{SH}	Shock Position	τ_{Inlet}	Inlet Time Delay
Z	Shock Strength Parameter	τ_{flame}	Flame Time Delay
		υ	Velocity
α	Damping Coefficient		
β_E	Acoustic Exit Reflectance	$(\,)_t$	$\frac{\partial}{\partial t}$
β_{EE}	Entropy Exit Reflectance	$(\,)_x$	$\frac{\partial}{\partial x}$
β_I	Inlet Exit Reflectance	$(\,)_1$	Perturbation Quantity
β_{EXIT}	Combined Exit Reflectance 4.85	$(\,)_1$	Cold Region of Combustor
β_{Iflame}	Flame Reflectance	$(\,)_2$	2^{nd} Order Perturbation Quantity
$\delta(x-x^*)$	Dirac Delta Function	$(\,)_2$	Hot Region of Combustor
ϵ	Knudsen Number	$(\,)_f$	Evaluated at Flame Position
γ	Ratio of Specific Heats		
λ	Total Temperature Ratio		
κ	Defined in Equation 4.59		
μ	Viscosity		
η	Time Dependance Function		

Chapter 1

Introduction

Renewed interest in ramjet engine applications has led to new efforts to study pressure oscillations in ramjet combustors. The problem of pressure oscillations in combustion chambers is not new, nor is it restricted to ramjets. Combustors of all sizes have exhibited pressure oscillations of some form from large industrial power generation burners to small rocket thrusters. The primary reason is the dependence of the chemical combustion processes on the local pressure and temperature. Propulsion systems are particularly notable for having significant pressure oscillations because these systems have very high rates of heat generation per unit volume.

Pressure oscillations in combustion chambers are frequently called combustion instabilities. This has occasionally been a misnomer, as in the case of the Pogo instability where the oscillation is due to a dynamic instability involving coupling between the fuel delivery hardware and the combustion chamber. The combustion processes are indeed complex, involving turbulent flow, shear layers, recirculating flow, turbulent mixing of fuel and oxidizer, multi-phase flow, solid and droplet burning, and finite-rate chemical kinetics, etc. In fact, understanding any one of the above processes in the presence of another is part of the imprecise

art of applied science and engineering. The problem remains, however, to control the resultant pressure oscillations in many combustion chambers.

There are several practical reasons for concern over pressure oscillations. The most obvious is the structural integrity of the chamber. Larger fluctuations require stronger chambers with the penalty of added weight. In addition, the oscillations produce vibrations in the hardware systems which can often be unacceptable for guidance systems as well as electronic hardware. Another problem related to pressure oscillations is the possibility of "flame out" or "unstart" due to a pressure induced oscillating inlet shock wave. A flame out occurs when the diffuser becomes unchoked. Usually, this is a catastrophic failure of the system which is irreversible. Finally, the combustion efficiency may be degraded or enhanced by certain pressure oscillations.

The acoustics of chambers plays a dominant role in most pressure oscillation problems. Any chamber has geometrically determined preferred oscillations or resonant modes. These modes are similar to the vibration modes of a stretched string on a violin. If it should happen that energy input occurs (from combustion or any other process) near a preferred resonant mode then oscillation or instability is likely to occur. In the case of combustion chambers, oscillations often grow to a finite amplitude steady state. There are two fundamental oscillator systems that can produce steady state oscillations: forced systems and self-excited systems.

Forced systems have an external driving mechanism. A simple example is to have a piston (or speaker) at the end of a duct. The piston is driven by some external source such as a motor (or magnetic coil) and acoustic pressure waves radiate out from the piston (for sufficiently small and slow piston excursion). The generated pressure waves are a function only of the driving. The energy input per unit area is simply the product of the local pressure on the piston and the piston velocity. Energy is lost at the walls (viscosity etc.) and at the boundary

conditions at the far end of the duct. A steady state is obtained since the driving is constantly adding energy which is acoustically radiated to the far end of the duct where it is lost through the boundary.

Self-excited systems contain driving that is a function of the oscillations in the system. An example could be heat release in a duct where the heat release is a function of the local acoustic state of the system. If the heat release is in phase with a resonant mode of the system then self-excited driving could occur. In the linear case, these systems are either damped in time, growing in time, or neutrally stable. Practically, it is difficult to obtain a linear, neutrally stable state so the response of the self-excited linear system only has the trivial steady state of no oscillation. It is through nonlinear processes that these systems can exhibit steady state oscillations.

Work in this field is by no means new. In approximately 1942, von Karman and Summerfield first stated the combustion time lag concept to explain the low frequency "chugging" phenomenon of liquid propellant rockets [1]. This work was continued and expanded by Summerfield [2] and also Crocco et al. [3] [4] in the early fifties. These were low frequency bulk modes. Bulk modes are modes where the phase distribution of the oscillation is constant; that is, the pressure fluctuates up and down uniformly throughout the chamber. These helped to explain the then current experimental results of systems that had oscillations primarily due to their fuel delivery systems. Since then many people have been involved with various aspects of the problem of pressure oscillations.

Lord Rayleigh predated all of these more current efforts in his treatment of a duct with heat addition [5]. This fundamental understanding of driving mechanisms and geometry, however, is still in order to better control the inherent pressure oscillations of combustion chambers. The goal of this work is to enhance understanding of some of these problems.

Recently, the importance and significance of entropy on the pressure oscillations in combustion chambers has attracted interest. A fluctuating heat release due to combustion instability in the chamber can produce "hot" or "cold" spots in the gas and therefore a fluctuation of entropy. It is the primary goal here to study those influences coupled with the acoustic pressure oscillations to determine the stability characteristics of combustion chambers.

An experimental study of pressure oscillations in side dump ramjet combustors was conducted in collaboration with China Lake Naval Weapons Center. The steady pressure oscillations were measured at several axial positions along the inlet and combustor for different inlet and exit boundary conditions. Chapter 2 contains the experimental part of this work and a review of other experimental work. It is placed at the beginning of this thesis to provide some of the background and motivation for the analytical work later. The data was reduced to produce pressure mode shape plots and phase distribution plots along the length of the inlet and combustor. The frequencies of interest are the low frequencies from approximately 50 to 800 Hz. Other frequencies of oscillation are discussed in Chapter 3.

A detailed description of the conceptual motivation for the analysis is given in Chapter 3. As a result, Chapter 3 is one of the most important chapters. It contains many of the physical interpretations that have shaped and guided the analysis. Chapter 3 also contains references to more recent and pertinent work.

The analysis has two phases: linear and nonlinear. The linear phase combines the superposition of acoustic waves and entropy in a chamber with boundary conditions at each end. For low frequency longitudinal modes, this can be a powerful method since some elements of the acoustic system may be treated as acoustically compact. An element is acoustically compact when its length is short compared to the wavelength of interest. As a result, many acoustic regions

can be coupled together through their common boundaries in the form of matching conditions. Specifically, a flat laminar flame is developed into an acoustically compact element which couples the upstream cool region of the combustor with the downstream hot region. Several modeling issues are discussed with respect to the boundary conditions. Among the boundary conditions used are those for inlet shock waves and choked exit nozzles. The resulting linear problem is an eigenvalue problem where the eigenvalues are the resonant modes of the system. Once the eigenvalues are determined, the linear problem is essentially solved including linear stability, pressure distributions, and velocity distributions. The linear analysis is contained in Chapters 4, 5, and 6.

The nonlinear phase utilizes the results of the linear work to find an approximate solution to the nonlinear case. The nonlinear analysis combines spatial averaging and a Galerkin expansion of the fluctuation terms to obtain a nonlinear oscillator equation. This equation is then time averaged and expanded to obtain a system of first order ordinary differential equations. The first order equations are solved numerically by a fourth order Runge-Kutta method. All nonlinear calculations were based upon two-mode interactions. The nonlinear analysis is contained in Chapter 7.

The results of the analysis show that in the linear case the entropy is very important when the fluctuating entropy is proportionately similar in magnitude to the fluctuating pressure. In addition to the classical acoustic modes of pressure oscillation there is another series of modes herein called entropy modes. Hence, the pressure modes contain both the acoustic and entropy induced modes. The linear stability is greatly altered with entropy. The critical parameters are the dimensions of the chamber, the inlet and exit reflectances, the mean flow velocity, and the forward and rearward acoustic velocities.

In the nonlinear case, entropy influences the solution with both linear and

nonlinear contributions. The nonlinear acoustic-entropy interactions are only a few percent of the acoustic-acoustic interactions. Thus, the nonlinear behavior is governed predominantly by the nonlinear acoustics *without* entropy. However, the amplitudes in the nonlinear limit cycles are functions of the linear damping and growth rate of the two modes interacting. The amplitude of the limit cycle — as well as the approach to the limit cycle — are therefore strongly dependent on the linear contribution of entropy to stability.

These results are applicable to a broad class of combustion chamber problems beyond the immediate ramjet case. It is possible from this study to make an assessment of the overall importance of entropy to an oscillating system if the relative size of either the fluctuating entropy *or* temperature is known. A formalism is also presented from which detailed calculations of a general combustor can be made once an explicit heat release model is adopted.

Chapter 2

Experimental Work

Chapter 2 summarizes some experimental pressure oscillation studies carried out in conjunction with China Lake Naval Weapons Center. These studies were initiated by NWC to study combustion instabilities in modern integral rocket ramjets. A more complete summary was published by Clark and Humphrey [6].

2.1 Experiments

This work is a continuation and an expansion of previous work [7] [8] dealing with combustion instabilities. The earlier work provided tentative identification of longitudinal acoustic modes associated with combustion-induced pressure oscillations in both a full-scale side dump engine and a laboratory-scale simulation of the same engine. A relatively simple, idealistic analytical method is outlined for predicting the longitudinal acoustic modes that may occur in a ramjet engine. The predictions are then compared with the laboratory-scale engine.

No attempt is made to predict the *actual stability* characteristics of the engine. Rather, the naturally occurring longitudinal linear acoustic modes that *may* be present are calculated, and experimental evidence is used to determine if

any of these modes are excited during unsteady combustion. Success in predicting many of the features of the excited modes which actually occur in complex, three-dimensional, chemically reacting flows gives confidence that future, more complete analyses will eventually result in useful design tools for predicting stability of a specific configuration.

2.1.1 Acoustic Model

The experimental results were compared to a linear acoustic model. The model is described here but not derived since it is actually an isentropic subset of the linear analysis of chapters 4 and 6. The analytical model is a simplified version of the technique described by Yang and Culick [9]. The current model does not include the approximate treatment of the two-dimensional features of the mean flow field in the combustor, as was done by Yang and Culick. This model is a strictly one-dimensional treatment of the configuration depicted in Figure 2.1. The idealized ramjet model consists of an inlet section with known, uniform mean flow properties connected via a sudden expansion to a combustion chamber with different, but uniform, mean flow properties. This allows for the greatly differing temperatures and sonic velocities that would typically occur between the inlet duct and the combustion chamber. At the dump plane ($x = 0$), the conditions of pressure and mass continuity result in two matching conditions.

To obtain the mass continuity relation, it is important to use the isentropic flow assumption. The exit from the combustor ($x = L_2$) is a choked nozzle with an axial length generally much shorter than the highest acoustic wavelength of interest. The acoustic admittance, A_N, is used to determine the complex reflectance, β_E, at the exit. The reflection coefficient is the ratio of reflected to incident pressure waves.

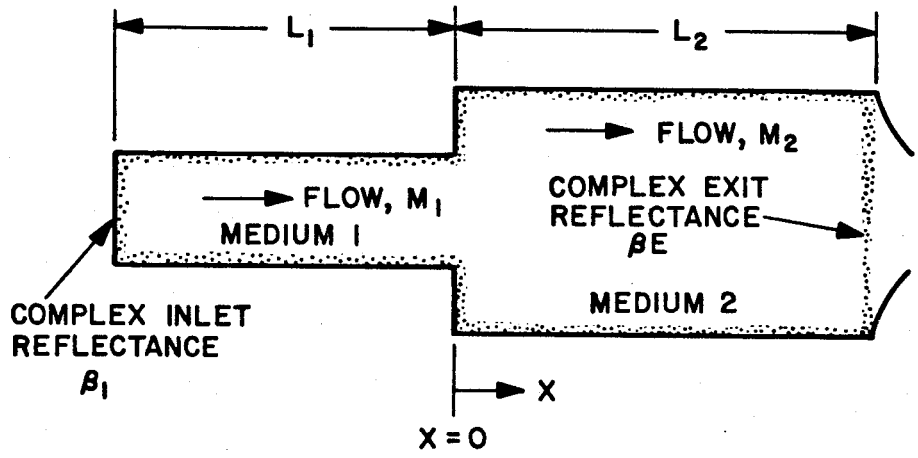

Figure 2.1: Model of Ramjet.

The inlet entrance is treated in a similar manner. The inlet admittance is more complicated than for the exit nozzle and is a function of the particular type of experimental setup. For instance, in some connected pipe tests the inlet can be approximated by an ideal open end with $\beta_I = -1$. For an actual ramjet or for a freejet test, however, a supersonic inlet operating under supercritical conditions is typical. In this case the reflection coefficient is determined by the interactions between upstream moving acoustic waves and the terminal normal shock system in the inlet diffuser. The inlet admittance function can then be estimated from the approximate theory of Culick and Rogers [10].

In the same manner as in Chapter 6, a resultant transcendental equation is solved for the eigenfrequencies from which the linear pressure mode shapes can be calculated. Humphrey [11] has published a more complete description of the calculation method as well as a listing of the numerical method for solving the equations and computing the amplitude and phase distributions. This analytical acoustic model contains no mechanisms for adding fluctuating energy to the

flows. It does however include the steady state jump in energy level at the dump plane. Furthermore, the Culick and Rogers theory of inlet shocks predicts that, in general, the normal shock at the inlet will tend to absorb most of the incident acoustic energy. Hence, all solutions obtained with the present model are stable, (the damping coefficient, α, is less than zero).

2.1.2 Side Dump Combustor Experiments

The laboratory scale, side dump engine depicted in Figure 2.2 is described by Clark [7]. This engine was tested in a direct connect mode with both inlets connected to a large plenum via the converging-diverging nozzles shown. Liquid fuel (RJ-4) was introduced into the inlet air flow through fixed-orifice injectors [7]. The pressure oscillations were measured with the high-frequency pressure transducers located as shown on Figure 2.2. Systematic variations about this "baseline" configuration were made in order to evaluate the acoustic mode predictions. In addition to the "baseline" (Configuration I), three other configurations were tested. In each case, only one geometric parameter was varied. Briefly, in Configuration II, the combustor exit nozzle area was increased in order to reduce the combustor pressure and increase the average combustor Mach number. In this case, a sharp-edged orifice plate was used at the combustor exit rather than a contoured nozzle. In Configuration III, the combustor length was decreased in order to shift the frequencies of acoustic modes. In Configuration IV, the inlet nozzles were replaced with straight pipe sections in order to simulate an acoustically open end. The pertinent test conditions for each configuration are given in Table 2.1 .

The tests with the converging-diverging inlet nozzles (Configurations I, II, and III) indicated that the nozzles were periodically unchoked during combustion. Hence, the application of Culick and Rogers theory is not strictly correct for the

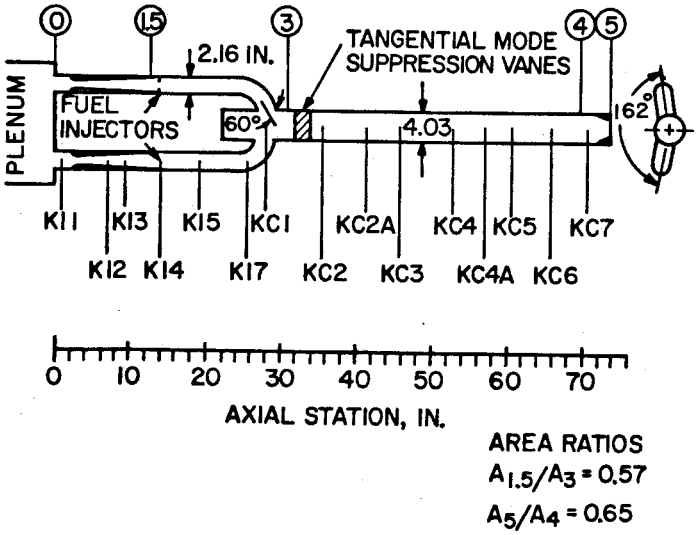

Figure 2.2: Baseline Combustor – Configuration I.

inlet boundary conditions. Nevertheless, reasonable results were obtained by estimating the average Mach number upstream of the shock to be the values shown in Table 2.1.

Results from Test 1 are plotted in Figure 2.3, which shows the pressure amplitude spectrum obtained by digital spectral analysis of the signal from one of the high-frequency transducers. The oscillations are dominated by the mode at 290 Hz, but there are also significant spectral components at 130 and 590 Hz. The agreement between experimental and theoretical frequencies is very good, as indicated. The analytical solution for the conditions of Test 1, 2, and 3 indicated that all the natural acoustic modes are highly damped. This is because the inlet reflection coefficient is approximately zero for the nearly sonic conditions listed in Table 2.1 and energy addition due to combustion has not been included. In order to obtain reasonable comparisons with experimental mode shapes and phase distributions, it was necessary to set $\alpha_j = 0$. This is physically reasonable since the simple theoretical model contains no mechanism to replace the acoustic energy lost at the anechoic inlet end, even though experimentally the oscillations

Test No.	1	2	3	4
Configuration	I	II	III	IV
T_{t_0}, $^\circ R$	1010	1061	1135	1065
T_{t_4}, $^\circ R$	4150	3680	3234	3800
$M_{1.5}$	0.23	0.27	0.28	0.26
M_{1S}	1.01	1.01	1.1	N/A
M_4	0.37	0.524	0.37	0.44
P_{t_4}, $psia$	88	63	56	75
Φ^*	0.91	0.93	**	0.91
x_{SH},in	$\approx$ .25	0.25	0.25	N/A
W_a,lb/s	5	5	3.6	5.1

* RJ-4 fuel was used with stoichiometric fuel/air ratio = 0.07.

**C_2H_4 fuel was used with unknown fuel flow rate.

Table 2.1: Test Conditions for Side Dump Combustor.

are being driven at a constant amplitude by the combustion heat addition.

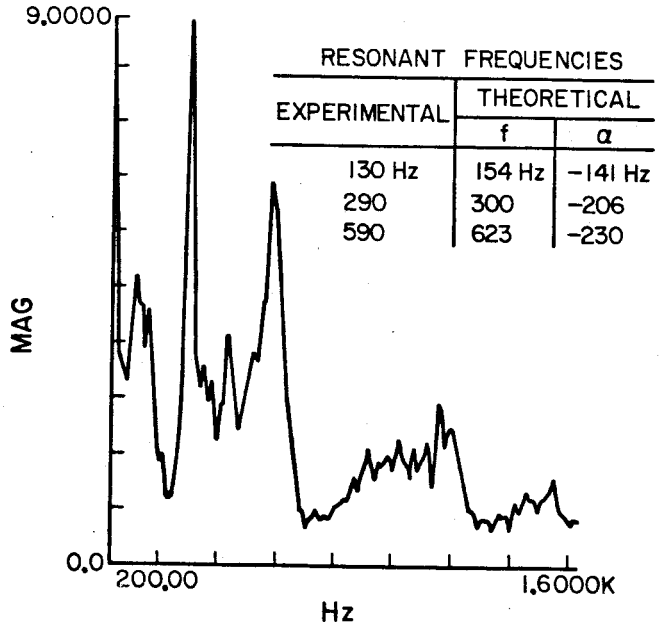

Figure 2.3: Amplitude Spectrum at KC4 for Configuration I.

The pressure amplitude mode shapes and relative phase distribution for experimental and theoretical values are compared in Figures 2.4 and 2.5 for the 290 Hz mode. The agreement between theory and experiment for pressure amplitude distributions is good in the combustor and poor in the inlet sections. The relative phase distributions agree well throughout the engine. This is also true for the 130 and 590 Hz modes (not shown). It is interesting that the mode at 130 Hz, which has been called a "bulk" mode has a corresponding predicted mode. The term "bulk" mode has been used to denote the low frequency mode with a relatively constant phase distribution so that the pressure pulsates in phase throughout the chamber. It should be noted that these "bulk" modes are not independent of the acoustics of the system.

Test 2 (Configuration II) was not significantly different from Test 1 and the agreement between theory and experiment was about the same as for Test 1 (Figures 2.6 and 2.7). The experimental frequencies were 150, 255, 500 Hz while

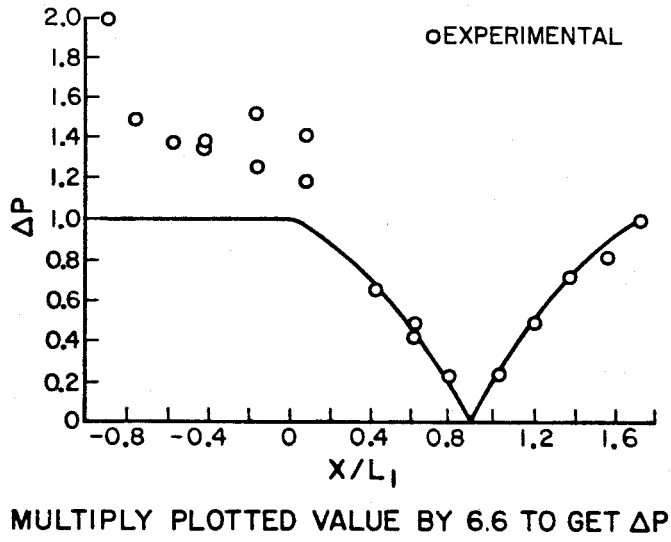

Figure 2.4: Pressure Amplitude at 290 Hz for Configuration I.

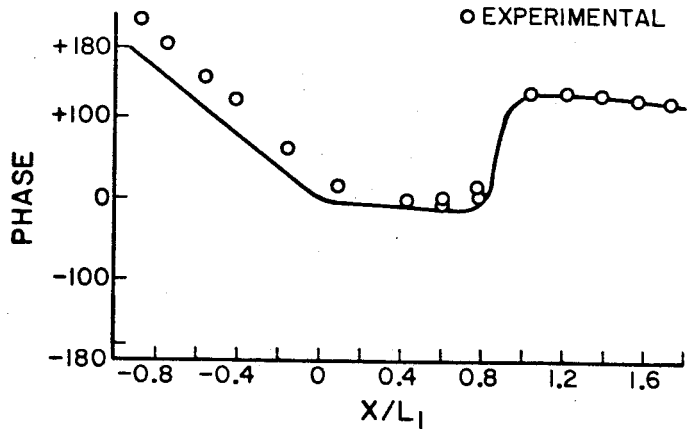

Figure 2.5: Relative Phase Distribution at 290 Hz for Configuration I.

the predicted frequencies were 129, 272, and 566 Hz.

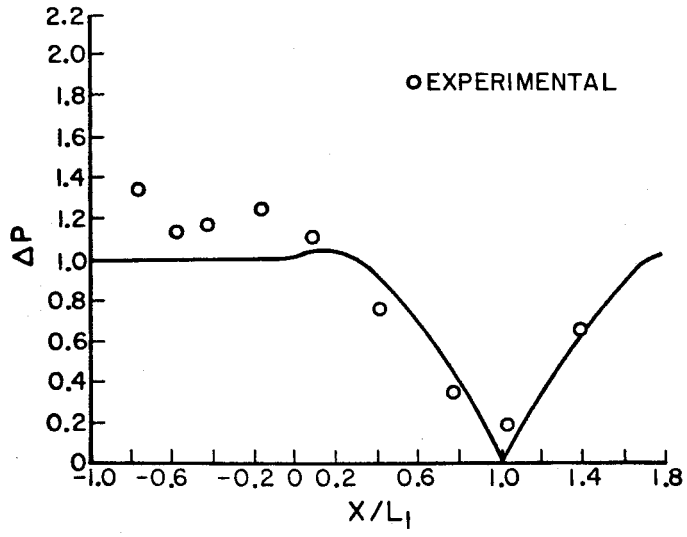

Figure 2.6: Pressure Amplitude at 255 Hz for Configuration II ($p * 14 = p$,psi).

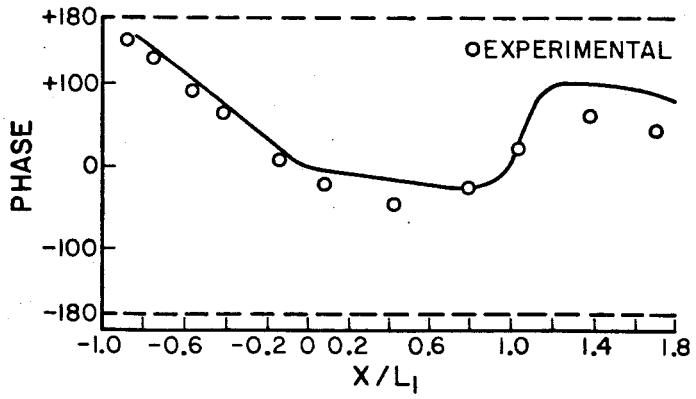

Figure 2.7: Relative Phase Distribution at 255 Hz for Configuration II.

For Test 3 (Configuration III) with the short combustor, the dominant oscillatory mode was at 223 Hz. The mode and phase plots of Figures 2.8 and 2.9 reveal that this was the same as the "bulk" mode which was present during Tests

1 and 2 for the longer combustor. In Configuration III, however, the frequency of the dominant mode was not in good agreement with the predicted value, nor was the pressure mode shape in the inlet region. The relative phase distributions (Figure 2.9) were in fair agreement. The experimental frequencies were 223, 373, and 450 Hz while the predicted frequencies were 170, 361, and 532 Hz.

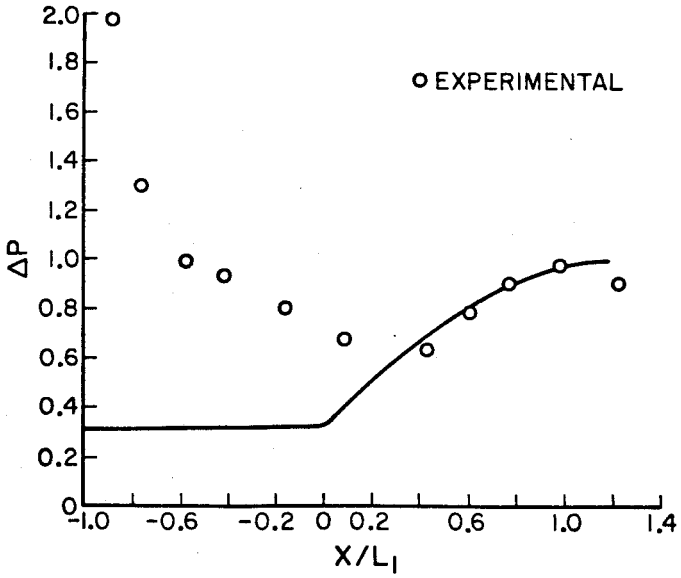

Figure 2.8: Pressure Amplitude at 223 Hz for Configuration III ($p * 4.86 = p$, psi).

For Test 4 the dominant mode was at 292 Hz. For Configuration IV with an "open" inlet as the upstream boundary condition, the ideal inlet reflection coefficient would be -1. The pressure mode shape shown in Figure 2.10 indicates that this change in end conditions did, indeed, have a profound influence on the mode shapes in the inlet section. However, the results in this case indicate a considerable discrepancy between experiment and the analysis. Further study of the boundary condition showed that the plenum chamber could no longer be ignored. When the plenum was considered in a similar acoustic analysis consisting of a plenum duct, inlet duct, and combustor duct; the predictions were similar to those of Tests 1 and 3. This analysis was similar to that used by Smith [12].

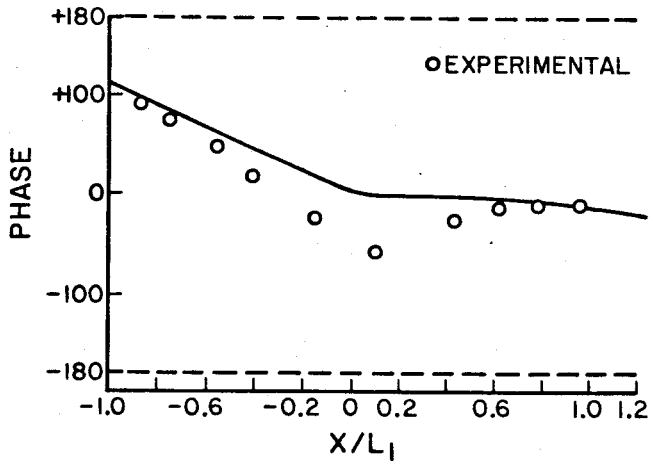

Figure 2.9: Relative Phase Distribution at 223 Hz for Configuration III.

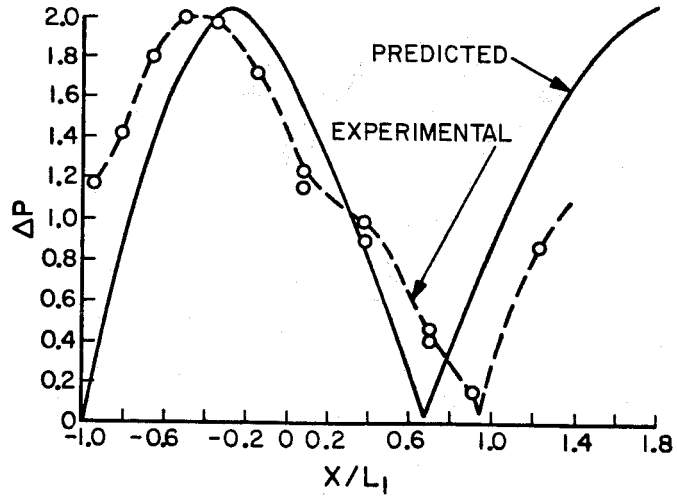

Figure 2.10: Pressure Amplitude at 290 Hz for Configuration IV.

2.1.3 Summary of Experiments

From the preceding discussions it is possible to say that a simple, one-dimensional, isentropic theory for the acoustic modes of an idealized ramjet engine is capable of correctly predicting many of the features of longitudinal pressure oscillations which are known to occur in actual practice. In general, the agreement between theoretical and measured phase distributions and between theoretical and measured pressure amplitude mode shapes in the combustor region are satisfactory. However, in the inlet sections of both the side dump and coaxial dump engines, there was considerable discrepancy between measured and theoretical pressure mode shapes. With a few exceptions, the agreement between experiment and analysis is within plus or minus 20% for the test conditions examined.

The side dump engine exhibited two types of oscillations. The first type is identified by the presence of one or more pressure node points in the combustor sections. (For examples, see Figures 2.4, 2.6, and 2.10.) Each pressure node point is associated with a rapid (approximately 180 degree) phase shift, as demonstrated in Figures 2.5, and 2.7. The other mode is identified by comparatively uniform values of the pressure oscillation amplitude and relative phase throughout the combustor section. With one exception, in the inlet section of *all* the configurations considered, the relative phase distribution varied linearly with longitudinal position and with a slope in fair agreement with the theoretical value. Theoretically, this linear variation is due to the fact that for the upstream normal shock the reflection coefficient is approximately zero. Hence, the inlet entrance does not strongly reflect the upstream moving waves. An exceptional condition arises for Configuration IV of the side dump combustor series. For this case, the upstream end should have approximated an ideal open acoustic end for which the reflection is approximately -1. The predicted and experimental pressure mode

shapes in the inlet section were in qualitative agreement while the slopes of the phase variations differed considerably. Surprisingly, the measured results show that the same linear phase variation occurred in this open-ended inlet as in the nearly choked inlet. Once the plenum chamber was included in the analysis and damping in the plenum recognized, the predicted results were in a similar degree of agreement as the other cases.

2.2 Other Experimental Work

The experiment described is only one effort of several to study longitudinal pressure oscillations. Schadow et al. ([13] [14] [15] [16] [17]) have been studying several aspects of coaxial dump combustors. This work involves quantitative studies of two-dimensional inlet shocks, hot and cold flows, velocity measurements, vortex visualization, and non-circular dump planes. Most of these efforts have been directed toward studying the multidimensional effects in a dump combustor. The shock response is important for two reasons. The upstream shock provides the upstream boundary condition for the acoustic system. If the instabilities are large enough, however, the shock position is affected sufficiently to influence the thrust of the engine. Sajben et al. [18] [19] have conducted experiments on the unsteady inlet shock response where the inlet shock has incoming Mach number greater than about 1.3. This results in a separated flow regime in the inlet diffuser which is not the case for the experiments conducted here. In addition to the experimental inlet shock studies is a numerical work by Hsieh [20] on unsteady flow fields in inlet diffusers in an attempt to calculate the results Sajben found experimentally.

Smith [12] performed some very enlightening combustion experiments with a two-dimensional dump combustor and flow visualization. The high speed films showed cases where large plugs of hot and cold gases were convecting downstream.

These were ideal entropy fluctuations but unfortunately the system was not terminated by a choked nozzle and hence no coupling between entropy and acoustics at the exit nozzle. The instabilities found were related to a two-dimensional phenomena of vortex rollup and the shear flow after the dump plane.

Another series of low frequency combustor instability experiments were conducted at the Aero Propulsion Laboratory, Air Force Wright Aeronautical Laboratories (Davis [21]). These were also filmed and measured in several configurations including with a choked exit nozzle. Abouseif et al. [22] attempted to explain some of these results with a model that included a flame sheet and entropy waves with some success. It is believed that better predictions would have been obtained if some of the simplifying assumptions had not been used. Critical to their model however is the assumption that the primary driving comes from incomplete combustion and hence a fluctuating heat release. The reason for this is that the fluctuations will result in a fluctuating residence time for a particle of fluid to remain in the combustor. If there is incomplete combustion, then more or less heat is released depending upon the residence time of each individual particle of fluid. Incomplete combustion was not the case in the China Lake experiments and oscillations were still observed. The model also neglected upstream entropy fluctuations such as those created at the inlet shock. Unfortunately, they did not publish any of the results of the pressure distributions and while it is useful to predict frequencies it is a better test of an acoustic model to be able to obtain both pressure mode shapes and phase distributions.

Craig et al. [23] conducted some experiments at the Aero Propulsion Laboratory with emphasis on the low frequency modes. One interesting result was that increasing the length to width ratio tended to promote instability which would, according to Abouseif et al.'s model, eliminate the primary driving mechanism. Reardon [24] attempted to provide an analytical interpretation of those

results. His model was based on the time lag model concept which has been developed extensively for liquid propellant rockets. Although this procedure may be successful for the bulk modes, it is not decoupled from the longitudinal acoustic modes, as purported by Reardon. Any analysis of stability depends upon steady experiments to determine parameters which are then used to predict the results of the unsteady experiment. In Reardon's study, as he mentioned, the constants for the time lag had to be multiplied by an arbitrary multiplier. It appears that the characterization of the steady flow should be the source of this discrepancy.

In summary, there seems to be sufficient experimental evidence which indicates that entropy could play an important role in the stability of a combustor system. The entropy also provides a mechanism through which energy can be fed into the acoustic system — either through boundaries or internal to the flow field — if a model for the heat release is obtained. Hence, the emphasis of this work is to study and predict the significance and influence of entropy in the problem of pressure oscillations in combustion chambers.

Chapter 3

Modes of Propagation

In addition to experimental work a considerable amount of analytical work has been accomplished. One of the earliest is obviously Rayleigh's Criterion which simply states

> "If heat be periodically communicated to, and abstracted from, a mass of air vibrating (for example) in a cylinder bounded by a piston, the effect produced will depend upon the phase of the vibration at which the transfer of heat takes place. If heat be given to the air at the moment of greatest condensation, or be taken from it at the moment of greatest rarefaction, the vibration is encouraged. On the other hand, if heat be given at the moment of greatest rarefaction, or abstracted at the moment or greatest condensation, the vibration is discouraged [25]."

For the purposes of designing ramjet combustion systems, the processes of pressure oscillations need to be understood with similar acuity to Rayleigh's Criterion for the purposes of control. It is correct to work towards control rather than elimination because some oscillations can actually enhance the performance of a system. A significant amount or work was done during the 1950's, 60's, and

70's on liquid and solid propellant rocket engines. It is upon this foundation that the ramjet studies are based.

3.1 Typical Geometry

Figure 3.1 shows a typical coaxial dump liquid-fueled ramjet inlet and combustor configuration. The flow through the inlet diffuser is choked. Immediately downstream of the throat the flow is supersonic. An upstream shock wave is contained in the diffuser beyond which the flow throughout is subsonic. The downstream subsonic end of the diffuser is connected to a constant area (or nearly constant area) inlet duct. Usually the fuel is introduced into the flow by a fuel injection mechanism in the inlet duct. Typically, a liquid droplet spray injector mixes the fuel into the oxidizing mean flow some distance upstream of the dump plane to allow for sufficient mixing and evaporation prior to burning [7].

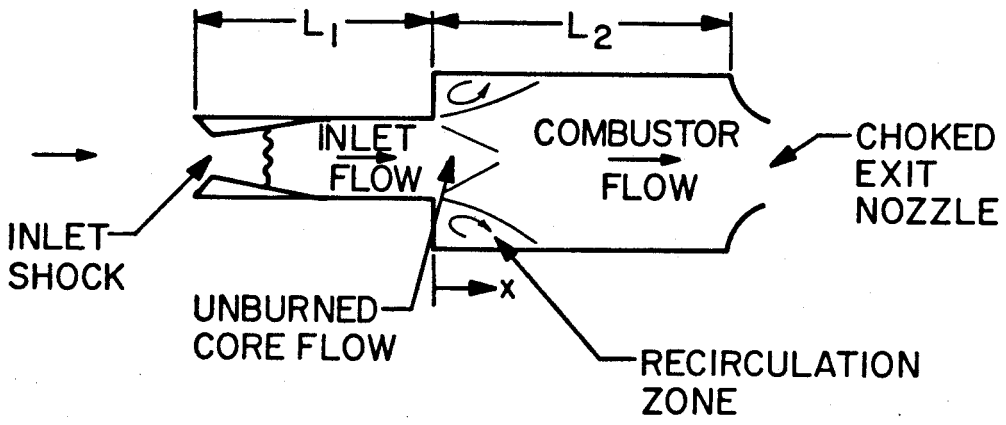

Figure 3.1: Typical Coaxial Dump Ramjet Configuration.

The inlet flow then undergoes a sudden expansion at the dump plane. The

flow is obviously complicated by shear layers, vortex generation, and recirculation, not to mention the combustion processes. The recirculation zone behind the inlet dump is primarily a region of hot burned exhaust gases. This acts as a flame holder which is one of the attractive features of the dump combustors. Typical flame holders obstruct the flow field and hence cause a total pressure loss which can be translated to a loss of thrust. The heat release takes place between the dump plane and the choked exit nozzle terminating the combustor. The actual location of the heat release is very much a function of the geometry and chemistry of each specific combustor.

The classical acoustic resonances of the system (diffuser, inlet duct, combustor, and exit nozzle) are determined by the mean flow conditions, the boundary conditions, and the matching conditions. The combustion processes provide volumetric mass sources as well as heat sources in the flow field which may or may not tend to add acoustic energy. Although it is unlikely that a general combustion model can incorporate the many flow fields along with liquid fuels, solid fuels, and varied operating conditions, it is possible to study the basic acoustic elements to determine the general conditions for stability.

3.2 Types of Oscillations

The pressure oscillations inside an axisymmetric duct are combinations of longitudinal, radial and transverse modes. In general, the longitudinal modes have frequencies in the range of 100-800 Hz while the transverse and radial modes are in the range of 2000-5000 Hz for a large range of typical combustors in tactical missiles.

The higher frequency modes, sometimes called screech, have been studied in the context of both liquid and solid propellant rockets [3], [4], [26], [27], [28],

[29], [30], [31], [32], [33].

In the case of ramjets, however, the high frequency modes tend to have smaller amplitudes [22] than the longitudinal modes or can be controlled relatively easily by flow vanes and baffles around the perimeter of the combustor [34]. The larger amplitude longitudinal modes and bulk modes have been the most troublesome and have been the focus of much of the current research in liquid fueled ramjets [35] [36]. The acoustics for the low frequency modes is predominantly one-dimensional even though the flow details are two- and three-dimensional. Hence, rather than finding multi-dimensional corrections to the one-dimensional case, most work here has been spent working on the basic physics in one dimension. Yang presented a method of averaging the axisymmetric flow details for a dump combustor which could then be used in one-dimensional acoustics [37].

The mean flow in most ramjet configurations is significant. The inlet Mach number is often in the range of .35 to .5 and in the combustor from .1 to .3 . This alters the acoustic velocities somewhat but the significant contribution is in the convection of "pockets" of gases with different thermodynamic states through the combustor. It is convenient to define some time constants. Three are particularly useful: the residence time, the thermal time and chemical time. The residence time is the length of time a particle (or small pocket of gas) resides in the chamber from dump plane to exit and is of the order of milliseconds. The thermal time is the time required for significant change in thermal energy through conduction and is of the order of seconds. Usually in propulsion system combustors, conduction is neglected since the residence time is so short compared to the thermal time. The chemical time is the time required for complete combustion of the fuel. Clearly, the residence time must be greater than the chemical time for complete combustion. The chemical time is also of the order of milliseconds. Since conduction is neglected two adjacent pockets of gas that have different thermodynamic

states can convect through the combustor without interacting (except through mixing or radiation). Thus, if the heat release from combustion is oscillatory, then oscillatory pockets of gas with differing thermodynamic states will convect downstream.

3.3 Wave Equation Form of Equations

The acoustic field can be represented by the superposition of traveling pressure waves. These waves travel, or radiate, at the acoustic velocity, which is the sonic velocity plus or minus the mean velocity. A point source, then, radiates a spherical pressure wave. In one dimension, the acoustic waves can travel leftward or rightward. It is the wave characteristic of acoustics that helps to reduce an acoustic phenomena to a physical mechanism such as a reflected traveling wave at a boundary and the superposition of traveling waves to get standing waves in organ pipes.

The general equations of motion can be written in wave equation form (as is done in Chapter 4). The classical acoustic waves are recovered but a third wave, entropy, is found. Entropy is not a wave in the acoustic sense as it does not radiate or propagate in the same manner as the acoustic pressure or velocity. The entropy is associated with the thermodynamic state of the particles of the gas and is convected with the mean flow. The entropy wave then can be thought of as pockets of fluid with different thermodynamic states convecting with the mean flow. It is the wave form of the equations of motion that makes it mathematically expedient to express temperature and heat release in terms of entropy and the acoustic terms. An excellent discussion of the wave nature of the equations of motion is given by Whitham [38].

3.4 Fluid Mechanic Interactions

Before considering modeling it is useful to discuss in some detail the fluid mechanic interactions. These are divided into linear and nonlinear interactions.

As mentioned in Chapter 1, the amplitudes of disturbances in linear self-excited systems that are unstable tend to grow exponentially. For a limit cycle to exist, a nonlinear process must occur for some finite amplitude oscillation and transfer some of the energy in the unstable mode either into another decaying mode or out of a boundary [39]. For very small values of a disturbance, the disturbance will grow exponentially. As the magnitude increases the modes will interact through nonlinear processes to produce a finite amplitude steady oscillation. These transient characteristics are often hard to measure experimentally because the time response of the measurements generally have to be faster for the transient behavior than for the steady state. Another way to get the transient behavior is to initially excite the system at a magnitude greater than the limit cycle. The oscillations should then decay to the limit cycle magnitude (presuming the initial excitation is not too large).

In the low frequency limit, it is possible to treat some processes as acoustically compact elements. When this is done, the combustor can be broken into several regions separated by elements that are simply matching conditions. Treating the source as compact elements results in the linear decoupling of the acoustic waves from the entropy in the acoustic regions between the matching or boundary conditions. This eliminates any volumetric linear interactions and leaves only linear boundary interactions between entropy and acoustics. This method can be used to treat many, varied geometry problems. For the geometry shown in Figure 3.2, the linear coupling of entropy with acoustic waves occurs at the upstream shock, the plane flame matching condition, and the choked exit nozzle.

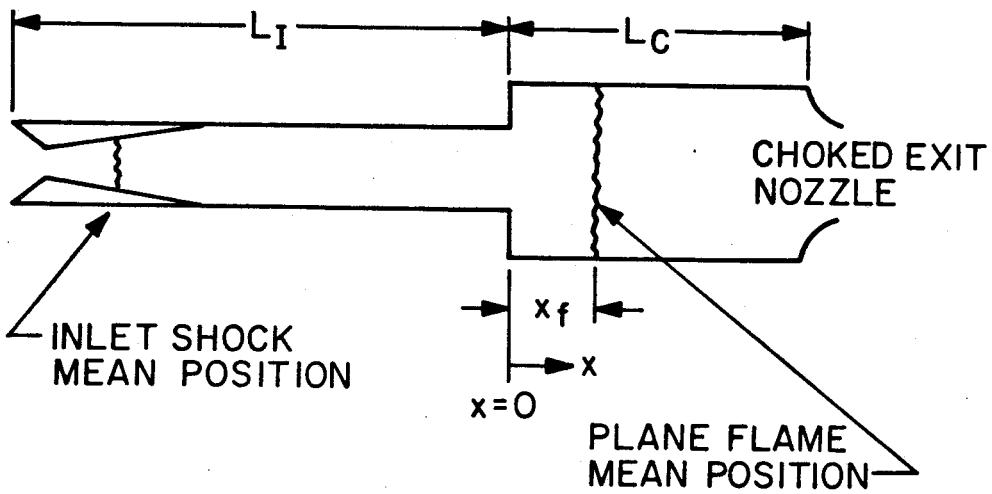

Figure 3.2: One-Dimensional Ramjet Model with Inlet Shock and Plane Flame.

The nonlinear interactions are predominantly volumetric although some nonlinear boundary conditions are discussed in Chapter 7. The following discussion of interactions is a summary of work by Kovasznay [40] and Chu and Kovasznay [41].

The equations of motion in a viscous, heat conductive, compressible medium can be expressed in terms of density, pressure, and entropy with mass sources, body forces, and heat sources. A standard perturbation expansion is performed with a non-dimensional parameter, α, characterizing the intensity of the disturbance where each of the density, pressure, entropy, and the sources are written in a power series expansion in α. Then collecting terms with like orders of α, a series of first, second, and nth order equations are derived where the kth order equations are functions of the solutions to the first through (k-1)th sets of equations.

The space-time domain considered is a small neighborhood around a point of interest and as a result is intended "to give a "local" understanding of the interaction phenomena up to a uniform degree of approximation in all fluctuation

modes [41]."

By setting the first order source terms to zero (as discussed above for linear interactions), the higher order source terms are shown to be the "apparent" rate of fluid injection, body forces, and rate of heat addition which are functions of the lower order solutions to the density, pressure, and entropy.

For α infinitesimal, the first order (linear) equations are split into three modes: sound (acoustic), entropy, and vorticity. The equations can be split arbitrarily in any number of ways. This particular choice splits the equations into physically familiar modes. The results of this choice of splitting are that the linear vorticity mode is a function of body forces; the acoustic mode is a function of mass sources, body forces, and heat sources; and the entropy mode is a function of the heat sources.

For flows with combustion, the volumetric body forces are usually negligible and the vorticity mode decouples completely from the acoustic and entropy modes. (This is not to say that there may not be linear vorticity-acoustic coupling at boundaries.) Conversely, the mass and heat sources are both pressure and entropy dependent so that the acoustics and entropy modes are coupled.

In summary, the results of the linear coupling are:[41]

> "The vorticity mode is the type of fluid motion most frequently encountered in the mechanics of viscous incompressible fluid. The sound mode is the type of fluid motion discussed in acoustics and in the theory of compressible fluids. The entropy mode has been the main subject of investigation in the theory of heat transfer in fluid."
>
> "We thus see that the solution of (3.1 [the equations of motion]) can always be thought of as consisting of the superposition of three basic modes of fluctuations that are familiar to us in one or another branch of fluid mechanics. Naturally not all the three modes of fluctuations

will enter significantly into a particular problem."

In the second order case, quadratic nonlinearity, the second order "apparent" sources, which are functions of the first order solutions, can be rewritten as the bilateral products of the three linear modes. Hence, the second order equations are functions of six modes: acoustic-acoustic, entropy-entropy, vorticity-vorticity, acoustic-entropy, acoustic-vorticity, and also entropy-vorticity. In general, fluctuations of any of the three modes will produce fluctuations in all of them. For flow in the absence of boundaries (as in a region containing small scale turbulence in a large medium) Chu and Kovasznay estimated the relative magnitude of each of the bilateral interactions which are given in Table 3.1. It is assumed that viscous and heat conduction terms are neglected in the first order terms (as is the case for combustion problems). In Table 3.1, ϵ represents the local Knudsen number and is generally less than α. The Knudsen number is the ratio of the viscous diffusion length to the wavelength. For freely propagating acoustics waves, the viscous diffusion length is of the order of the mean free path while the wavelength is of the order of feet. Thus, the Knudsen number is very small. In the low frequency, one-dimensional limit the vorticity terms are eliminated. Table 3.1 can then be reduced to Table 3.2.

In all cases the entropy-entropy mode can be neglected so that for the one-dimensional combustor the acoustic-acoustic and acoustic-entropy interactions are the dominant nonlinear terms.

The bilateral acoustic-acoustic interactions were studied extensively by Awad and Culick [39] [42]. In addition to calculating limit cycles, a sufficiency condition for the existence of two-mode limit cycles was presented. For two modes to interact and form a limit cycle it is sufficient that one mode have a linear growth rate that is less than half the decay rate of the other interacting mode.

	Sound Source	Entropy Source	Vorticity Source
Sound-Sound	"Steepening" and "Self-Scattering" $O(\alpha^2)$	$O(\alpha^2\epsilon)$	$O(\alpha^2\epsilon)$
Vorticity-Vorticity	"Generation" $O(\alpha^2)$	$O(\alpha^2\epsilon)$	"Self Convection" $O(\alpha^2)$
Entropy-Entropy	$O(\alpha^2\epsilon)$	$O(\alpha^2\epsilon)$	$O(\alpha^2\epsilon)$
Sound-Entropy	"Scattering" $O(\alpha^2)$	"Heat Convection" $O(\alpha^2)$	"Generation" $O(\alpha^2)$
Sound-Vorticity	"Scattering" $O(\alpha^2)$	$O(\alpha^2\epsilon)$	"Vorticity Convection" $O(\alpha^2)$
Vorticity-Entropy	$O(\alpha^2\epsilon)$	"Heat Convection" $O(\alpha^2)$	$O(\alpha^2\epsilon)$

Table 3.1: Order of Terms for Nonlinear Interaction between Modes [41].

	Sound Source	Entropy Source	Vorticity Source
Sound-Sound	"Steepening" and "Self-Scattering" $O(\alpha^2)$	$O(\alpha^2\epsilon)$	$O(\alpha^2\epsilon)$
Vorticity-Vorticity	"Generation" N/A	N/A	"Self Convection" N/A
Entropy-Entropy	$O(\alpha^2\epsilon)$	$O(\alpha^2\epsilon)$	$O(\alpha^2\epsilon)$
Sound-Entropy	"Scattering" $O(\alpha^2)$	"Heat Convection" $O(\alpha^2)$	"Generation" $O(\alpha^2)$
Sound-Vorticity	"Scattering" N/A	N/A	"Vorticity Convection" N/A
Vorticity-Entropy	N/A	"Heat Convection" N/A	N/A

Table 3.2: Order of Terms for Nonlinear Interaction between 1-Dimensional Modes.

3.5 Modeling Considerations

Tsien developed the transfer function for a general choked nozzle [43]. Later, Marble and Candel [44] determined that in the linear analysis, entropy waves incident upon a choked nozzle would produce acoustic waves at the nozzle. This is a linear transfer of energy into (or out of) the acoustics from the boundary. This provides one of the first mechanisms by which fluctuating entropy would interact with the acoustics in ramjet modeling. Then Culick and Rogers [10] developed a linear inlet shock theory that accounts for an oscillating shock in inlet diffuser. An oscillating shock will produce a source of entropy fluctuations in the combustor flow. In the early fifties, Chu [45] [46] [47] [48] had developed a linear plane flame matching condition. The analysis given by Chu described a planar flame in which the heat release per unit area is related to the acoustic and entropy fluctuations.

The plane flame matching condition is generalized in Chapter 5 for a diverging combustor and consideration of stability. The plane flame model also provides for the interactions of entropy and acoustics (details in Chapter 5). The present study combines each of the above mechanisms to model stability and pressure oscillations in ramjet combustors.

Previous attempts to explain the low frequency oscillations have been reasonably successful despite their lack of accuracy with respect to growth rates. This illustrates that the linear problem is dominated by the boundary conditions and geometry to determine frequencies. The growth rates, however, require an accurate accounting of the energy transfer and generation. Several previous authors have erroneously claimed that the bulk mode is not acoustic. This is usually a result of failing to recognize the acoustics of the inlet and combustor *system.* Often, the bulk mode is below the lowest classical organ pipe mode with length

equal to the combustion chamber and this has resulted in calling the mode a bulk mode. In general, however, the bulk mode should be one in which the pressure oscillates in phase throughout the combustor. In most cases, when the boundary conditions are traced thoroughly upstream and downstream, it can be shown that the bulk mode is in fact the lowest acoustic mode of the *system*.

There are four primary differences between this work and previous work. First, this work treats entropy and acoustics an a general way which allows for both bulk mode and longitudinal modes of a combustor system in a unified approach. Second, the issue of stability of a plane flame contained in a combustion chamber is studied with self-excitation. Third, the linear and nonlinear influence of entropy and acoustics is studied in detail. And fourth, all the above analysis is coupled with a formalism that permits examinations of second order nonlinear acoustics with entropy in chambers with boundary conditions far more general than previously.

Chapter 4

Linear Acoustics with Entropy

Chapter Four deals with the basic mathematical tools of linear acoustics that are used in the remainder of this investigation. It also treats several basic problems that are the foundation to understanding pressure oscillations in chambers. The examples given consist of acoustic chambers with given boundary conditions and that are subjected to mass sources, point sources, or entropy sources. Stability of each example is examined to find under what conditions the oscillation is enhanced or discouraged. The general equations are first formulated with the introduction of entropy and the physical contributions to entropy. Then methods of solution are given with conceptual examples.

The last section examines acoustic and entropy induced acoustic oscillations. The fundamental modes of pressure oscillation from acoustics and entropy are determined. Two modes are found which contain the classical acoustic modes and a newly found set of entropy modes. The important assumptions required for the given solutions are that the viscosity, thermal conduction, and dissipation are negligible.

4.1 General Formulation of the Equations

In order to set up the framework for the modeling, the governing equations of motion are formulated. These equations are formulated for more general cases and then simplified as required. This provides an easy way to determine which approximations are appropriate to each application. The formalism is often more generally applicable than the specific examples and will be noted where appropriate.

The basic equations of motion with sources can be written in differential vector form as

$$\textbf{Continuity} \qquad \frac{\partial \rho}{\partial t} + \nabla \cdot (\rho \vec{v}) = w(x,t)\,, \tag{4.1}$$

$$\textbf{Conservation of Momentum} \qquad \frac{D\vec{v}}{Dt} = -\nabla P + \mu \nabla^2 \vec{v} + \vec{b}_f + \frac{1}{3}\mu \nabla \Theta\,, \tag{4.2}$$

$$\textbf{Conservation of Energy} \qquad \rho \frac{De}{Dt} = -P\Theta + \nabla \cdot (k \nabla T) + \dot{q} + \Phi\,, \tag{4.3}$$

where

$$\Theta = \nabla \cdot \vec{v}\,, \qquad \frac{D(\ )}{Dt} = \frac{\partial(\ )}{\partial t} + \vec{u} \cdot \nabla(\ )\,. \tag{4.4}$$

In addition to the equations of motion are the equation of state and definition for polytropic gases,

$$P = \rho R T\,, \tag{4.5}$$

and

$$P\rho^{-\gamma} = e^{s/c_v}\,. \tag{4.6}$$

The choice of introducing entropy through the equation of polytropic gases is a natural one when the equations are considered in wave form. The equations will reduce to propagating acoustic and convected entropy waves and thus the use of entropy greatly simplifies the algebra as well as clarifying the physical mechanisms.

An alternate form of the energy equation for an ideal gas is

$$\frac{1}{c_v}\frac{Ds}{Dt} = \frac{1}{P}\frac{DP}{Dt} - \frac{\gamma}{\rho}\frac{D\rho}{Dt}, \tag{4.7}$$

which can be derived from 4.6. Another way to obtain 4.7 is to consider the first law of thermodynamics, the ideal gas law, and the definition of specific heats. It is convenient to define another term, $q(\vec{x},t)$,

$$q(\vec{x},t) = \frac{1}{c_v}\frac{Ds}{Dt}. \tag{4.8}$$

The internal energy, e, is the composition of the internal, potential, and stored chemical energies. For reversible processes the internal thermal energy in a gas is given by

$$\int_{T_0}^{T} c_v dT = c_v(T - T_0) \tag{4.9}$$

when c_v is a constant.

The hydrostatic position is not an important factor in most acoustics problems so the potential energy can be neglected. The chemical energy is due to the atomic bonding of the molecules and will be denoted $\mathcal{E}$ With these assumptions the internal energy can be differentiated to give

$$\frac{De}{Dt} = c_v\frac{DT}{Dt} + \frac{D\mathcal{E}}{Dt}. \tag{4.10}$$

Using 4.2, 4.3, 4.7, and 4.10, along with continuity and the ideal gas law, the definition of $q(x,t)$ can be shown to be

$$q(x,t) = \frac{\gamma-1}{P}\left\{ \underbrace{\nabla\cdot(k\nabla T)}_{\text{change in entropy following the fluid}} + \underbrace{\dot{q}}_{\text{change due to conduction}} + \underbrace{\Phi}_{\text{change due to heat generation}} - \underbrace{\rho\frac{D\mathcal{E}}{Dt}}_{\text{change due to chemical composition}} \right\}. \tag{4.11}$$

The physical contributions to the entropy are evident from 4.11. The mathematical expediency of using entropy does not obscure the physical clarity of each of the processes in 4.11. It is clear from 4.11 that, in the absence of conduction and dissipation, the heat generation and chemical change due to combustion both contribute to the change in entropy.

Typical flow situations in combustion chambers are such that the mean flow is relatively low (although not necessarily zero) and it is reasonable to neglect viscous effects and dissipation. This assumption is carried throughout this work. The nonlinear equations of motion can be rewritten to obtain

$$\frac{DP}{Dt} + \gamma P \nabla \cdot \vec{v} = \frac{\gamma P}{\rho} w + \frac{P}{c_v \gamma} \frac{Ds}{Dt}, \tag{4.12}$$

$$\frac{D\vec{v}}{Dt} + \frac{a^2}{\gamma P} \nabla P = \vec{b}_f, \tag{4.13}$$

$$\frac{Ds}{Dt} = c_v q. \tag{4.14}$$

Since the longitudinal modes are to be studied the equations of motion will be treated in one-dimension only. The one-dimensional equations become

$$P_t + u P_x + \gamma P u_x = a_0 w + \frac{Pq}{\gamma}, \tag{4.15}$$

$$u_t + u u_x + \frac{a^2}{\gamma P} P_x = b_f, \tag{4.16}$$

$$s_t + u s_x = q. \tag{4.17}$$

4.1.1 Perturbation Equations

The nonlinear equations of combined acoustics and entropy will be obtained by writing the dependent variables as sums of mean and fluctuating values,

$$u(x,t) = u_0(x) + u'(x,t), \tag{4.18}$$

$$P(x,t) = P_0(x) + P'(x,t), \tag{4.19}$$

$$s(x,t) = s_0(x) + s'(x,t), \tag{4.20}$$

where $(\ )_0$ (which is equivalent to $\bar{(\ )}$) denotes the steady state mean quantities and $(\ )'$ (which is equivalent to $(\ )_1$) denotes the perturbation quantities. The substitution of 4.18 through 4.20 into 4.15 through 4.17 is not an approximation. It is not until some of these terms are neglected that this expansion yields an approximate equation for the motion. This expansion is chosen since it is expected that there will exist a steady state condition from which the perturbation is to be performed.

4.1.2 Steady State

The steady state (or time independent) problem can be found by letting all the primed terms go to zero along with the time derivative terms to get

$$u_0 P_{0x} + \gamma P_0 u_{0x} = a_0^2 w_0 + \frac{P_0 q_0}{\gamma} \tag{4.21}$$

$$u_0 u_{0x} + \frac{a_0^2}{\gamma P_{0x}} = b_f \tag{4.22}$$

$$u_0 s_{0x} = c_v q_0 \tag{4.23}$$

where $(\ )_x$ stands for the partial differentiation of $(\ )$ with respect to x, and similarly for t. These are ordinary differential equations for functions of position only and are assumed to have known solutions subject to given boundary conditions.

4.1.3 Linear Perturbation Equations

By treating the source terms as having mean and fluctuating parts and dropping terms that are second order or higher in perturbation quantities, obtain the first order linear equations to be

$$u_{1t} + \frac{a_0^2}{\gamma P_0} P_{1x} = B^* \tag{4.24}$$

$$P_{1t} + \gamma P_0 u_{1x} = A^* \tag{4.25}$$

$$s_{1t} + u_0 s_{1x} = C^* \tag{4.26}$$

where

$$A^* = \underbrace{a_0^2\left(w_1 + \frac{T_1}{T_2}w_0\right)}_{\text{mass source terms}} + \underbrace{\frac{1}{\gamma}(P_1 q_0 + P_0 q_1)}_{\text{entropy source terms}} - \underbrace{u_1 P_{0x} - \gamma P_1 u_{0x}}_{\text{non-uniform field terms}} - \underbrace{u_0 P_{1x}}_{\text{mean flow term}} \tag{4.27}$$

and

$$B^* = \underbrace{b_f{}'}_{\substack{\text{forces on} \\ \text{element of} \\ \text{fluid}}} - \underbrace{\frac{a_0^2}{\gamma P_0}\left(\frac{1}{2} + \frac{T_1}{T_0} - \frac{P_1}{P_0}\right)P_{0x}}_{\substack{\text{non-uniform} \\ \text{mean field}}} - \underbrace{u_0 u_{1x}}_{\substack{\text{mean} \\ \text{flow}}} \tag{4.28}$$

and

$$C^* = \underbrace{c_v q_1}_{\substack{\text{entropy} \\ \text{fluctuations}}} - \underbrace{u_1 s_{0x}}_{\substack{\text{non-uniform} \\ \text{entropy} \\ \text{field}}} . \tag{4.29}$$

Note that 4.26 is in characteristic form and hence it is often useful to use the method of characteristics when entropy terms q_0 and q_1 are involved. With partial differentiation, 4.24 and 4.25 can be written in the standard form of non-homogeneous wave equations

$$u_{1tt} - a_0^2 u_{1xx} = -g_0{}'' \tag{4.30}$$

$$P_{1tt} - a_0^2 P_{1xx} = -h_0'' . \tag{4.31}$$

T_1/T_0, which is contained in 4.30 and 4.31, can be determined from 4.5 and 4.6 with logarithmic differentiation and linearization to get

$$\frac{T_1}{T_0} = \underbrace{\frac{\gamma - 1}{\gamma}\frac{P_1}{P_0}}_{\substack{\text{isentropic} \\ \text{contribution}}} + \underbrace{\frac{s_1}{c_p}}_{\substack{\text{entropy} \\ \text{contribution}}} . \tag{4.32}$$

The boundary conditions must be set to provide well-posed problems. Define f and l such that

$$\vec{n} \cdot \nabla P_1 = -f' \tag{4.33}$$

$$\vec{n} \cdot \nabla u_1 = -l' . \tag{4.34}$$

In the one-dimensional case, $\vec{n} = \pm\vec{i}$ where $\vec{i}$ is the unit vector in the x-direction. Take the dot product of 4.16 with the unit surface normal to find

$$-f' = \frac{\gamma P_0}{a_0^2}\left\{ {b_f}' - \frac{a_0^2}{\gamma P_0}\left(\frac{1}{2}\frac{T_1}{T_0} - \frac{P_1}{P_0}\right) P_{0x} - u_0 u_{1x} + u_1 t \right\}\Bigg|_{x=0}^{x=L_C} . \tag{4.35}$$

For the one-dimensional acoustics problem from $x = 0$ to $x = L_C$, 4.35 is the proper boundary condition.

4.2 Separation of Variables: Approximate Methods

Section 4.2 presents the details for solving the linear equations of acoustics by separation of variables. The method of Green's Functions is applicable in three dimensions but is quoted here in one dimension. After presenting the solution technique, four specific cases are solved to provide insight into the effects on stability of different types of sources.

The linear equations of acoustics and entropy can be solved approximately using a separation of time and space variables to obtain a system of ordinary differential equations in space variables which may then be solved by the approximate integral method of Green's Functions. Separation of variables is accomplished by substituting solutions that are periodic in time of the form

$$u_1(x,t) = u_1(x)e^{-i\Omega t} \tag{4.36}$$

to get

$$u_{1xx} + k^2 u_1 = g' \tag{4.37}$$

$$P_{1xx} + k^2 P_1 = h' \tag{4.38}$$

where

$$h' = \frac{h''}{a_0^2} = \frac{-1}{a_0^2}\left\{A_t^* - \gamma P_0 B_x^* + \gamma P_0 \left(\frac{a_0^2}{\gamma P_0}\right)_x P_{1x}\right\} \tag{4.39}$$

$$g' = \frac{g''}{a_0^2} = \frac{-1}{a_0^2}\left\{B_t^* - \frac{a_0^2}{\gamma P_0} A_x^* + \frac{a_0^2}{\gamma P_0}\gamma P_{0x} u_{1x}\right\} \tag{4.40}$$

$$k = \frac{\Omega}{a_0} \qquad \text{and} \qquad \Omega = w + i\alpha\,. \tag{4.41}$$

The procedure involves expanding the perturbation pressure (and velocity) in a series which satisfies the homogeneous equations. The integral averaging corrects the homogeneous solutions by successive approximations but due to the averaging often yields good results within one or just a few iterations. Consider the homogeneous equation

$$\Psi_{nxx} + k_n^2 \Psi_n = 0 \tag{4.42}$$

with boundary condition

$$\Psi_{nx}\Big|_1^2 = 0\,. \tag{4.43}$$

An explicit solution to 4.42 and 4.43 can be given as

$$\Psi_n = \cos(k_n x)\,, \qquad k_n = \frac{n\pi}{L_C}\,. \tag{4.44}$$

The functions Ψ_n can be used as the basis for an expansion of 4.38. The number of successive iterations required to get satisfactory results depends upon the magnitude of the inhomogeneity h and the desired accuracy. From the theory of Green's Functions the solution for P_1 is given by

$$P_1(x) = \sum_{n=1}^{\infty} \frac{\Psi_n(x)}{(k^2 - k_n^2)E_n^2} \left\{ \iiint \Psi_n h' dV + \oint \Psi_n f' dS \right\}. \tag{4.45}$$

Let

$$R_n = \iiint \Psi_n h' dV + \oint \Psi_n f' dS \tag{4.46}$$

so that

$$P_1(x) = \Psi_m(x) \frac{R_m}{(k^2 - k_m^2)E_m^2} + \sum_{n=1}^{\infty} \frac{\Psi_n(x) R_n}{(k^2 - k_n^2)E_n^2}. \tag{4.47}$$

Since the equations are linear, a normalization factor can be chosen so that in the limit of vanishing h and f , P reduces to Ψ_m. Choose

$$\frac{R_m}{(k^2 - k_m^2)E_m^2} = 1 \tag{4.48}$$

from which

$$k^2 = k_m^2 + \frac{R_m}{E_m^2}. \tag{4.49}$$

Equation 4.49 can be solved for vanishingly small values of the damping coefficient, α, to get

$$w^2 \approx a_0^2 (k_m^2 + R_{eal}(\frac{R_m}{E_m^2})) \tag{4.50}$$

and

$$\alpha \approx \frac{a_0^2}{2w} \left(I_{mag} \left(\frac{R_m}{E_m^2} \right) \right). \tag{4.51}$$

The linear characteristics of the system are provided in 4.50 and 4.51. The frequency of oscillation can be determined by a frequency shift term that modifies the frequency of the assumed form w_m. Stability can be determined by the sign of α since t is always greater than zero. The linear stability criterion is

$$\text{Stable System} \qquad \alpha < 0 \tag{4.52}$$

$$\text{Unstable System} \qquad \alpha > 0 \tag{4.53}$$

4.2.1 Simple Problems in Linear Acoustics

The goal here is to gain insight into some basic elements that can drive an acoustic system. Four examples are chosen, each of which could be a fundamental driving mechanism in a combustion chamber. Case 1 studies a mass source which is motivated by two physical processes. First, liquid fuel is usually spray-injected into the flow in the form of small droplets. The evaporation of these droplets acts as a volumetric mass source. Second, the fuels used are generally complex hydrocarbons, such as RJ-4, which when oxidized form a greater quantity of simpler molecules. For perfect gases, this change acts as a volumetric mass source. Case 2 studies a point force and is motivated as a result of Case 1 (see Case 2). Case 3 studies a point entropy source, the motivation for which has already been discussed. Case 4 studies a point heat source. Heat release is the driving force in Rayleigh's Criterion as well as in most combustion instabilities.

The modeled system is a combustor that has given boundary conditions. For the inlet end of the combustor the boundary condition is assumed to be an ideal acoustic wall for which the fluctuating velocity must vanish. This is a simplification that can be generalized if needed. The exit is terminated by a choked nozzle that is acoustically compact, i.e., the length of the nozzle is negligible in comparison to the wavelength of the oscillation. The exit condition is given by

$$A_N = \rho_o a_o \frac{u'}{P'} = \frac{\gamma - 1}{2} M_o \,. \tag{4.54}$$

Understanding these acoustic driving mechanisms is essential to determining how to control more complicated driving mechanisms that arise from the turbulent combustion in chambers. Four cases will be shown to illustrate the method and some simpler driving mechanisms. Since the interest here is to study the driving, the mean flow will be neglected. This is not precise because the

energy loss through the choked nozzle is a direct consequence of the mean flow. However, the mean flow is a minor correction to the acoustics and can be included.

Case 1.

Consider a small sinusoidally fluctuating point mass source located at x^*. Pick the mass source to be of the form

$$w_1 = \hat{m}\,\delta(x - x^*)e^{-i\Omega t} \tag{4.55}$$

where $\hat{m}$ is small, the flow is isentropic, and there are no forces acting on the fluid. Use 4.46 through 4.51 to find

$$R_n = \frac{1}{a_0^2}\cos\left(\frac{n\pi x^*}{L_C}\right) i\Omega\hat{m} - ikSA_N \tag{4.56}$$

from which the frequency and damping coefficient can be calculated as

$$w^2 \approx a_0^2\left(\left(\frac{m\pi}{L_C}\right)^2 - \alpha\frac{a_0^2}{Vol}(\kappa)\right) \tag{4.57}$$

$$\alpha \approx \frac{a_0^2}{Vol}(-\kappa) \tag{4.58}$$

where

$$\kappa = \left\{-\frac{\hat{m}}{a_0^2}\cos\left(\frac{m\pi x^*}{L_C}\right) + \frac{1}{a_0^2}SA_N\right\}^{1+\delta_{m0}} \tag{4.59}$$

and

$$\delta_{m0} = \left\{\begin{array}{ll} 0 & m \neq 0 \\ 1 & m = 0 \end{array}\right\}. \tag{4.60}$$

The stability of the system can be quickly determined by examining κ,

$$\text{Stable System} \qquad \kappa > 0 \tag{4.61}$$

$$\text{Unstable System} \qquad \kappa < 0 \tag{4.62}$$

$$\text{Stability Limit} \qquad \kappa = 0. \tag{4.63}$$

Hence it is shown that

$$\cos\left(\frac{m\pi x^*}{L_C}\right) > \frac{a_0 S A_N}{\hat{m}} \tag{4.64}$$

is the condition for instability.

In conclusion, a choked nozzle (where $A_n > 0$) always tends to stabilize the system just as expected since acoustic energy is lost through the nozzle due to the non-zero admittance function at the nozzle. This is true in all of the cases that are terminated by a choked nozzle. The mass source has two aspects effecting stability: position and magnitude. As expected, the system tends toward instability when m is increased. The position is also important. Actually, the phase between the mass source and pressure is the important issue. This is seen by letting the constant m be complex, i.e., letting the phase of the source be different from the local pressure. This is the mass addition equivalent of Rayleigh's criterion for heat addition (which is recovered in Case 4). For instability the source should be located so as to be in phase with a pressure antinode; for stability the source should be located 180 degrees out of phase with a pressure antinode. The mass source is neutralized if located at a pressure node.

Case 2.

Consider a small sinusoidally fluctuating point force located at x^*. This problem is prompted by the fact that a force is required to fix a point mass source in a uniform flow field. Neglect entropy fluctuations, mass sources, mean flow, and assume

$$b'_f = -\hat{b}_f \delta(x - x^*) e^{-i\omega t} \tag{4.65}$$

The magnitude of the force, $\hat{b}_f$, is considered to be complex. This allows the fluctuating force to be "out of phase" with the local pressure fluctuation. Use R_n

to determine the frequency and damping to get

$$\omega^2 \approx a_0^2 \left(\left(\frac{m\pi}{L_C}\right)^2 - \frac{2m\pi}{L_C Vol} \sin\left(\frac{m\pi x^*}{L_C}\right) \frac{\gamma P_0}{a_0^2} R_{eal}(\hat{b}_f) - \frac{\alpha}{a_0} S A_N \right) \tag{4.66}$$

and

$$\alpha \approx \frac{a_0^2}{2w} \left(S A_N \frac{w}{a_0} - \frac{n\pi}{L_C} \sin\left(\frac{n\pi x^*}{L_C}\right) \frac{\gamma P_0}{a_0^2} I_{mag}(\hat{b}_f) \right) \tag{4.67}$$

where the case of $m = 0$ is the degenerate case of zero frequency and is not very interesting since the influence of the force vanishes.

From 4.67 it is evident that the energy dissipation (or growth) is determined by the imaginary part of $\hat{b}_f$ and the nozzle. The frequency is also altered due to the point force. These results were found by Aaron [49] in a case where the major driving was the result of a point force created by vortices impinging on a barrier in the acoustic field. The imaginary part of $\hat{b}_f$ produces energy input because it represents a component of force in phase with the velocity. Hence a non-zero power input proportional to force times velocity.

Case 3.

Consider the case of a fluctuating point entropy source in a uniform flow field where the mean flow is negligible except with respect to the nozzle losses. Assume we are primarily interested in the pressure oscillations resulting from the entropy source and the choked nozzle. (The production of pressure waves by entropy waves incident upon a nozzle is not considered here. This case is examined in section 4.3.) The entropy source term is represented as

$$q_1 = \hat{q}_1 \, \delta(x - x^*) e^{i\phi(x)} e^{-i\Omega t} \, . \tag{4.68}$$

(The case of a step jump in the mean flow temperature at $x = x^*$ is easily solved by the use of an upstream and downstream region where the homogeneous wave

solution is valid in each region and coupled across the discontinuity at $x = x^*$.) Following the same procedure as before gives

$$R_n = (i\omega - \alpha)\left[\frac{P_0}{a_0^2}\left\{\frac{\hat{q}_1}{\gamma}\cos\left(\frac{n\pi x^*}{LC}\right) + (-1)^{(n+m)}\frac{a_0 S A_N}{P_0}\right\}\right] \tag{4.69}$$

from which the frequency can be calculated and the condition for ***instability*** is determined from

$$\cos\left(\frac{n\pi x^*}{LC}\right) \geq \frac{\gamma a_0}{\hat{q}_1 P_0} S A_N \,. \tag{4.70}$$

As expected, increasing $\hat{q}_1$ decreases stability and increasing A_N increases stability. Since damping is contained in this model, sufficiently small values of $\hat{q}_1$ will always be stable. However, the position (or phase) of $\hat{q}_1$ is also important. In the above calculation $\hat{q}_1$ is real but can be complex to allow for a phase shift between the entropy source and the pressure. (The nature of this phenomenon is similar to case 1.) This is actually a version of Rayleigh's criterion which is given in case 4.

Case 4.

A sinusoidally fluctuating point heat source is located at x^*. Also assume a uniform mean flow field and isentropic conditions. It is clear from reviewing 4.11 that a pure heat source is only one term in the equation for entropy. When conduction, dissipation, and chemical bonding energy is neglected the fluctuating heat source is proportional and in phase to a fluctuating entropy source. As mentioned earlier, this is the Rayleigh Criterion which is stated at the beginning of Chapter 3. The physical principle is generally applicable to any acoustic system that is driven and it is recognition of this that can lead to active or passive control of driven pressure oscillations.

4.3 Linear Acoustic and Entropy Waves

The second method (presented herein) for solving the linearized equations of acoustics and entropy is treated in this section. This method is the classical Sturm-Liouville eigenvalue problem and produces all of the eigenfrequencies for the boundary value acoustics with entropy problem. This section provides the linear solution techniques for determining the entropy modes in section 4.4 as well as all of Chapter 6. While the boundary conditions are discussed in general, the choked exit nozzle boundary condition is discussed in detail. The inlet boundary conditions are discussed in more detail in section 6.1 . A new exit reflectance and admittance are defined which incorporate both acoustic and entropy reflectance at a choked exit nozzle.

The previous section dealt with a method of approximating solutions to problems of quite general complexity containing all types of sources. The method is very useful when considering problems containing volumetric contributions such as distributed sources. Another class of problems, however, are those which are predominantly boundary value problems such as organ pipes, ducts, and horns [50]. The oscillations in combustion chambers are very often dominated by the duct characteristics of the chamber. The case of low frequency longitudinal modes can often be treated in this way since the elements of the combustor such as the exit nozzle, inlet, and dump plane are approximately acoustically compact. That is, the wavelength of oscillation is long compared to the length of the element. Hence, these elements can be treated as boundary conditions. This issue of modeling is dealt with in greater detail in section 6.1.

The linearized equations of motion can be reduced from 4.24 through 4.26. (Recall that the major assumptions already made are that the viscosity, heat conduction, and dissipation can be neglected.) These derivations follow those of

Culick and Rogers [51] and Yang and Culick [9]. In the one-dimensional case of ducts and combustors it is assumed that the flow is in a constant cross section region. Variable area can be accounted for in some cases when necessary. Since the flow has constant area and distributed losses are neglected, the mean flow quantities are assumed to be constant. Finally, neglecting sources, the linearized equations become

$$\rho u'_t + \rho u u'_x + p'_x = 0, \tag{4.71}$$

$$P'_t + u P'_x + \gamma P u'_x = 0, \tag{4.72}$$

$$s'_t + u s'_x = 0. \tag{4.73}$$

One major feature of ramjet combustion chambers and inlets is the significant mean flow. The mean flow is very important for two reasons. First, the loss of acoustic energy at the choked nozzle is a result of the mean flow entering the nozzle. Second, from 4.73 it is clear that the mean flow is crucial to the issue of entropy when entropy source terms are neglected. Of lesser importance is the modification of the spatial structure of the acoustic field due to mean flow. The solutions can be determined by assuming a periodic time dependence to get

$$P'(x,t) = P_0\Big[P^+ e^{iKx} + P^- e^{-iKx}\Big] e^{-iM_0 Kx} e^{-i\Omega t}, \tag{4.74}$$

$$u'(x,t) = \frac{P_0}{\rho_0 a_0}\Big[U^+ e^{iKx} + U^- e^{-iKx}\Big] e^{-iM_0 Kx} e^{-i\Omega t}, \tag{4.75}$$

$$s'(x,t) = A e^{i\frac{\Omega}{u_0}x} e^{-i\Omega t}, \tag{4.76}$$

where

$$K = \frac{k}{1-M_0^2} \quad , \quad M_0 = \frac{u_0}{a_0} \quad , \quad k = \frac{\Omega}{a_0} \quad , \quad \Omega = \omega + i\alpha, \tag{4.77}$$

and

$$U^+ = P^+ \quad , \qquad U^- = -P^-. \tag{4.78}$$

The solution to the acoustic pressure and velocity is the superposition of two waves; one wave propagating upstream (leftward) and one downstream (rightward) where the $-$ $(+)$ indicates the upstream (downstream) traveling wave. The propagation velocity is $a_0 + M_0$ downstream and $a_0 - M_0$ upstream. As the mean flow approaches zero the solution reduces to the classical sonic velocity. The solution for the entropy has only one wave that propagates with the mean flow velocity. This does not require the entropy to be constant throughout the combustor. The entropy of different particles in the flow can be different but the entropy of each particle is constant as it moves through the duct with the mean flow. These solutions can be written in several different forms depending on the application. The above form will be used in these studies.

The next phase of the linear problem is to determine the boundary conditions. One boundary condition is required for each of the upstream and downstream ends of the duct. The entropy boundary condition at the entrance is also required. The boundary conditions most often used for acoustics are reflectances and admittances. The admittance is defined as

$$A = \rho_0 u_0 \frac{u'}{P'} \tag{4.79}$$

at a specific position. The reflectance, β, is simply the ratio of the reflected wave to the incident wave. It is not difficult to relate the admittance to the reflectance but care must be taken when applying these conditions that are defined at $x = 0$ to positions where x is not at the origin. The more traditional mathematical boundary condition given by 4.35 can be calculated from the admittance or reflectance if desired.

Choked Exit Nozzle Boundary Conditions

The exit boundary conditions require special mention. Often, combustion chambers are terminated by choked nozzles. Marble and Candel [44] showed that incident entropy waves impinging on a choked nozzle would reflect a pressure wave. Hence, a choked exit nozzle has an entropy reflectance as well as an acoustic reflectance. By defining an acoustic entropy reflectance, β_{EE}, the reflected pressure wave can be given by

$$\text{Reflected Pressure Wave } = \beta_{EE}\frac{\gamma P_0}{c_p}Ae^{i\frac{\Omega}{u_0}L} \tag{4.80}$$

where

$$\beta_{EE} = \frac{-M_0}{2+(\gamma-1)M_0}. \tag{4.81}$$

This result is similar to the acoustic reflectance, β_E, where

$$\beta_E = \frac{2-(\gamma-1)M_0}{2+(\gamma-1)M_0}. \tag{4.82}$$

These results are linear and thus it is proper simply to add the reflected acoustic pressure wave and the reflected entropy pressure wave. Therefore,

$$P_0P^-e^{-iKL}e^{-iM_0KL} = \beta_E P_0P^+e^{iKL}e^{-iM_0KL} + \beta_{EE}\frac{\gamma P_0}{c_p}Ae^{i\frac{\Omega}{u_0}L} \tag{4.83}$$

where P_0 is dimensional and P^+ and P^- are nondimensional terms. The following manipulations with 4.83 were not the obvious choice until the end of work on the following chapters. It is presented here since it is convenient to use these definitions in later derivations as well as here. In modeling the linear acoustics, it is useful to define the linear reflectance as the ratio of the reflected wave to the incident wave. That is, given the incident wave, the reflected wave is simply the product of the reflectance and the incident wave. (It should be observed that this definition results in a slightly different form for the inlet and exit.) Often the reflectance is given for the case where the boundary is chosen to be at the origin,

(i.e., $x = 0$) and care must be taken when applying reflectances at locations other than the origin. Define an exit reflectance, β_{EXIT}, such that

$$\beta_{EXIT} = \frac{P^-}{P+}. \tag{4.84}$$

As a direct consequence of 4.83 and 4.84

$$\beta_{EXIT} = \frac{\beta_E e^{iKL}}{e^{-iKL} - \beta_{EE}\frac{\gamma}{c_p}\frac{A}{P^-}e^{i\frac{\Omega}{u_o}L}e^{iM_0KL}}. \tag{4.85}$$

It is also common to define the admittance as

$$A_N = \rho_0 a_0 \frac{u'}{P'}. \tag{4.86}$$

Using 4.85 with 4.74 and 4.75, 4.86 becomes

$$A_{NEXIT} = \frac{K - \beta_E}{K + \beta_E} \tag{4.87}$$

where

$$K = 1 - \beta_{EE}\frac{\gamma}{c_p}\frac{A}{P^-}e^{i\frac{\Omega}{u_o}L}e^{iKL}e^{iM_0KL}. \tag{4.88}$$

It should be emphasized that these definitions assume that the acoustic exit reflectance (defined at $x = L$), β_E, does not vanish. When the acoustic exit reflectance vanishes, P^+ is undetermined in 4.83. In this case, the reflectance β_{EXIT} should be defined in terms of A/P^-. Another convenient way to write the reflectance is

$$\beta = |\beta| e^{i2\Phi}. \tag{4.89}$$

Returning to 4.74-4.76 with 4.78, there are four unknowns P^+, P^-, A, and Ω. The inlet boundary condition on entropy can be of two forms. If the inlet entropy is a function of the local pressure then $A = A(P^+, P^-)$. If not, then A/P^- is an input parameter. Use the inlet and exit reflectances (or admittances) to eliminate P^+ and P^- from 4.74-4.76. If $A = A(P^+, P^-)$, then A can also be eliminated to give a transcendental equation for the eigenfrequencies, Ω,

$$F(\Omega) = 0. \tag{4.90}$$

If A is an input parameter, then $F(\Omega) = 0$ contains the parameter A/P^- and is solved for the eigenfrequencies subject to the input parameter.

4.4 Simple Entropy and Acoustic Modes

To illustrate the modes of oscillation in simple problems of acoustics and entropy-induced acoustics, consider a constant area burner that is initiated by an acoustic wall with leakage and terminated by a choked nozzle. The acoustic wall with leakage condition does not restrict the generality of this analysis which will be clear from the derivation. It is desired to find the fundamental acoustic modes with and without entropy. The acoustic equations are 4.71 and 4.72 while the entropy is given by

$$s'_t + u_0 s'_x + \sigma s' = 0 \tag{4.91}$$

where σ has been included for generality. The geometry for this case is shown in Figure 4.1. The solutions to 4.71 and 4.72 are given in 4.74 and 4.75. The solution to 4.91 is

$$s'(x,t) = Se^{-\frac{\sigma}{u_0}} e^{i\frac{\Omega}{u_0}x} e^{-i\Omega t}. \tag{4.92}$$

The boundary conditions to accompany the equations require some explanation. At the inlet, the entropy fluctuation is assumed to be pressure-induced. For example, the case of an oscillating shock wave in an inlet diffuser is a pressure-induced fluctuating entropy source. The entropy fluctuation at the inlet, $x = 0$, is related to the pressure fluctuation at $x = 0$ by a constant A_0. A_0 can be complex to allow for a phase shift between the pressure and the resultant entropy. The inlet acoustic boundary condition is the reflectance, β_I , such that

$$\beta_I = \frac{P^+}{P^-}. \tag{4.93}$$

The exit reflectance is given by 4.85.

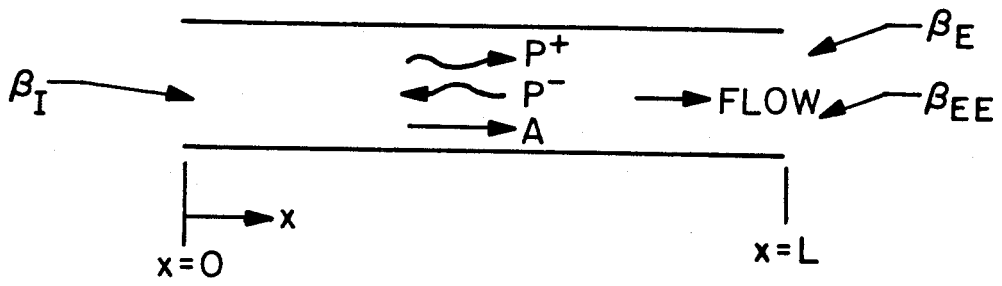

Figure 4.1: Geometry for Illustration of Entropy and Acoustic Modes in a Constant Area Burner.

It cannot be overemphasized that this acoustic problem is a boundary value problem and that as a result the application of the boundary conditions is extremely important. This is especially true when mean flow is considered. To illustrate, consider the condition for a rigid wall,

$$u' = 0\,. \tag{4.94}$$

Without mean flow it is equivalent to require

$$\frac{dP'}{dx} = 0\,. \tag{4.95}$$

However, with mean flow, these two conditions are not equivalent. In fact, to pick 4.95 requires that energy be added at the boundary. In other words, an active boundary is required to satisfy 4.95. An acoustic wall, on the other hand, neither generates nor absorbs energy.

4.4.1 Application of Boundary Conditions

The boundary conditions β_I, β_E, and β_{EE} can be used with 4.74-4.78 to eliminate the linear constants P^+ and P^-. The resulting equation is

$$\beta_I \beta_E e^{i2KL} - 1 + \beta_{EE} \frac{\gamma}{c_p} \frac{A}{P^-} e^{i\frac{\Omega}{u_0}L} e^{iKL} e^{-iM_0KL} = 0 . \tag{4.96}$$

This is a transcendental equation for the eigenfrequencies or resonant modes of the acoustic-entropy system. This is a very useful form of 4.96 for studying the oscillatory modes of the system. The solutions of 4.96 are for the linearized (or infinitesimal) pressure oscillations and in this sense are acoustic pressure oscillations. However, it is convenient to reserve the use of the term acoustic modes to mean the classical acoustic modes in the absence of entropy fluctuation. The term entropy-induced modes will be used to describe the modes in which pressure oscillations are a result of the presence of entropy waves. Also, these entropy waves are not entirely arbitrary; rather they are a consequence of existing pressure fluctuations (through the inlet coupling) and are of the same frequency (not necessarily same phase) as the linear eigenfrequency found by solving 4.96.

The reason that equation 4.96 is in a convenient form is that the two modes can be seen directly in the absence of the other. The purely classical acoustics mode can be seen by letting $\beta_{EE} = 0$, and is simply a balance of the first two terms in 4.96. A pure entropy-induced oscillation can be generated by setting $\beta_I = 0$, that is to say that the only waves present are the entropy wave moving downstream and the reflected upstream moving pressure wave from the entropy wave impinging on the choked exit nozzle at $x = L$. The entropy-induced modes can be obtained by neglecting 1 with respect to the first and third terms in 4.96. For typical values of the reflectances and very small entropy coupling, this is the correct balance of terms.

4.4.2 Limiting Cases

Three limiting cases are presented here to illustrate first the procedure of solution and second the physical significance of the modes of oscillation. The first case neglects entropy and recovers the pure classical acoustics as it should. The second case neglects the acoustic reflectances of the inlet and exit to obtain a series of oscillatory modes resulting from entropy. These modes are due to the entropy-acoustic coupling at the exit and the acoustic-entropy coupling at the inlet. This case also illustrates the dependence of the mode on the combustor length, the upstream traveling acoustic velocity, and the mean flow velocity. The third case is the most interesting since it retains the acoustic reflectances and entropy to determine a series of oscillatory modes herein defined as the entropy modes of the acoustic system. Typical values for each case are given in the calculations section following the three cases. The interpretation of these cases is given in the Summary of Acoustics and Entropy Modes which follows the calculations.

Case 1 – No Entropy

The case of no entropy is treated in two parts. The first illustrates the case of no entropy and no acoustic losses. The second illustrates no entropy but retains acoustic losses (or gains) at the inlet and exit boundaries.

Case 1a. No Acoustic Losses

This is the case where there is no entropy and no acoustic energy loss at the boundary conditions. When there is no energy loss the magnitude of the reflectance is unity. With these assumptions, 4.96 is the balancing of the first two terms to give

$$e^{i2(KL+\Phi_I+\Phi_E)} = 1 \tag{4.97}$$

where

$$\beta_I = |\beta_I| e^{i2\Phi_I} \qquad \text{and} \qquad \beta_E = |\beta_E| e^{i2\Phi_E} . \tag{4.98}$$

Solving yields $\Omega = \omega + i\alpha$ to be

$$\omega = \frac{a_0(1 - M_0^2)}{L}(m\pi - \Phi_I - \Phi_E) \tag{4.99}$$

where by definition ω is greater than zero and by the calculation

$$\alpha = 0 . \tag{4.100}$$

It is natural to find $\alpha = 0$ in the absence of damping and driving. The frequencies, ω_m, are simply the classical acoustics organ pipe modes of a one-dimensional chamber with mean flow.

Case 1b. Acoustic Losses (Gains) at the Boundary

Case 1b relaxes the constraint in 1a that the reflectances have magnitude unity, so that

$$|\beta_I||\beta_E| e^{i2(kL + \Phi_I + \Phi_E)} = 1 . \tag{4.101}$$

Hence,

$$\omega = \frac{a_0(1 - M_0^2)}{2\pi L}(m\pi - \Phi_I - \Phi_E) \qquad (H_z) \tag{4.102}$$

$$\alpha = \frac{a_0(1 - M_0^2)}{4\pi L} \ln(|\beta_I||\beta_E|) \qquad (H_z) . \tag{4.103}$$

The frequencies are the organ pipe modes while the damping, α, can be greater than, less than, or equal to zero depending on whether the product of $|\beta_I||\beta_E|$ is greater than, less than, or equal to *one* respectively.

Case 2 $|\beta_I|$ Vanishes

Choosing $|\beta_I| = 0$ will generate pure entropy-induced oscillations and balance the last two terms in 4.96, giving

$$\beta_{EE}\frac{\gamma}{c_p}\frac{A}{P^-}e^{i\frac{\Omega}{u_o}L}e^{ikL}e^{-iM_0kL} = 1\,. \tag{4.104}$$

Let

$$\frac{A}{P^-} = \frac{|A|}{P^-}e^{i2\Phi_A} \qquad \text{and} \qquad \beta_{EE} = |\beta_{EE}|e^{i2\Phi_{EE}} \tag{4.105}$$

so

$$\alpha = \frac{a_0M_0(1-M_0)}{2\pi L}\left(\ln\left(|\beta_{EE}||\frac{A}{P^-}|\frac{\gamma}{c_p}\right)\right) \tag{4.106}$$

and

$$\omega = \frac{2a_0M_0(1-M_0)}{\pi L}(m\pi - \Phi_A - \Phi_{EE})\,. \tag{4.107}$$

Several important observations can be made. Since the inlet reflectance is zero, the only important times are the convective transport time from the inlet to exit and the acoustic travel time from the exit to the inlet. This is directly apparent in the above calculations from the term

$$\left(\frac{1}{u_o} + \frac{1+M_0}{a_0(1-M_0^2)}\right)L \tag{4.108}$$

in the exponential of 4.104. Also, as the term A/P^- is diminished, the entropy induced oscillation never reduces to the acoustics mode. These modes are separate and distinct in the limiting cases. As A/P^- is reduced to zero the entropy induced oscillation simply becomes so highly damped as to vanish and *does not* approach classical acoustics.

It is also clear in this derivation that the frequency of the pure entropy-induced oscillation is inversely proportional to the chamber length L.

Case 3 $|A|/P^-$ Small and $|\beta_I| \neq 0$

This case is more interesting than case 2 since β_I is seldom identically zero as in the case of an inlet shock and dump plane and will be referred to as the entropy-induced mode throughout the remainder of the text. In this limiting case, neglect the second term, 1, and balance the first and third terms in 4.96. Then, to check the validity of the balance, the magnitude of the first term is compared to one and should be very much greater than one. Balancing the first and third terms gives

$$\frac{|\beta_I||\beta_E|e^{i2m\pi}}{|\beta_{EE}||\frac{A}{P^-}|\frac{\gamma}{c_p}} = e^{\frac{-\alpha L}{a_0 M_0(1+M_0)}} e^{i\frac{\omega L}{a_0 M_0(1+M_0)}} e^{i2(\Phi_{EE}+\Phi_A-\Phi_E-\Phi_I+\frac{\pi}{2})} \tag{4.109}$$

from which

$$\omega = \frac{2a_0 M_0(1+M_0)}{\pi L}(m\pi + \Phi_I + \Phi_E - \Phi_{EE} - \Phi_A - \frac{\pi}{2}) \tag{4.110}$$

$$\alpha = \frac{-a_0 M_0(1+M_0)}{2\pi L}\left(\ln\left(\frac{|\beta_I||\beta_E|}{|\beta_{EE}||\frac{A}{P^-}|\frac{\gamma}{c_p}}\right)\right) \tag{4.111}$$

and m is any integer which keeps ω greater than 0.

The magnitude of the first term is

$$|\beta_I||\beta_E|e^{\frac{-2\alpha L}{a_0(1-M_0^2)}} \tag{4.112}$$

and should be checked when calculations are made with 4.110 and 4.111 to verify that one is negligible compared to the first term.

4.4.3 Calculations

The following calculations illustrate the three limiting cases and are based upon typical parameters for a ramjet combustor. Case 1 has $\beta_I = 1$ with $\frac{\|A\|}{P_1^-} = 0$. Case 2 has $\beta_I = 0$ with $\frac{\|A\|}{P_1^-} = 10^{-2}$ and Case 3 has $\beta_I = 1$ with $\frac{\|A\|}{P_1^-} = 10^{-7}$. The equations used were 4.102, 4.103, 4.106, 4.107, 4.110, 4.111, and 4.112.

$$\text{Based on} \begin{cases} a_0 = 3000\, ft/sec & c_p = .3\, BTU/lbm\ ^\circ R \\ M_0 = .3 & \gamma = 1.28 \\ L = 4.0\, ft & \Phi_A = 0 \\ \beta_E = .9194 & \Phi_I = \Phi_E = 0 \\ |\beta_{EE}| = .144 & \Phi_{EE} = \frac{\pi}{2} \end{cases}$$

Case 1b $|\beta_I| = 1\,, \quad \frac{\|A\|}{P^-} = 0$

$\omega \approx 0,\ 341.25,\ 682.5,\ 1024,\ \ldots$ Hz

$\alpha \approx$ -4.564 Hz

Case 2 $|\beta_I| = 0\,, \quad \frac{\|A\|}{P^-} = 10^{-2}$

$\omega \approx 78.8,\ 236,\ 394,\ 551,\ \ldots$ Hz

$\alpha \approx$ -416.24 Hz

Case 3 $|\beta_I| = 1\,, \quad \frac{\|A\|}{P^-} = 10^{-7}$

$\omega \approx 0,\ 292.5,\ 585,\ 877,\ \ldots$ Hz

$\alpha \approx$ -769.1 Hz

By calculation the first term in 4.96 is of order 10^5, which is much greater than 1 for verification of the initial assumption.

To illustrate the acoustic modes (Case 1) relative to the entropy-induced modes (Case 3), the eigenfrequencies are plotted relative to each other in Figure 4.2.

4.4.4 Summary of Acoustic and Entropy Modes

Several important observations can be made from this section. Case 1 recovers classical acoustics from the acoustics with entropy formulation. These modes are

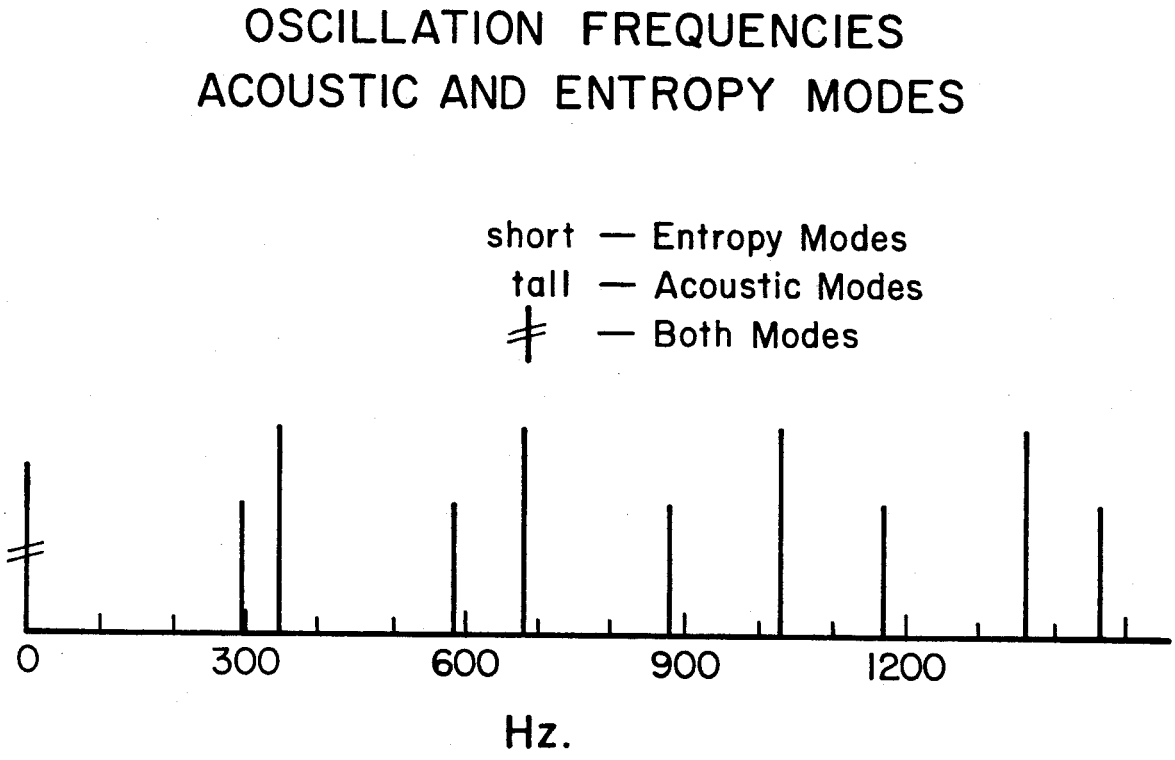

Figure 4.2: Eigenfrequencies for the Acoustic Modes (Case 1) and the Entropy-induced Modes (Case 3).

called the classical acoustic modes or acoustic modes of the system. Case 3 is solved to give a new mode of oscillation which is called the *entropy-induced mode* of acoustic pressure oscillations. When 4.96 is solved with sufficiently small entropy fluctuations the classical acoustic modes are only slightly modified by the entropy, and likewise the entropy mode is only slightly modified by the acoustic mode. As long as the entropy is small enough that the entropy mode damping, α, is more negative than approximately – 200 radians per second, then the interactions between the two modes is less than about one percent. For larger values of entropy, the eigenfrequencies of 4.96 can be solved numerically to show the level of interaction between the two modes. This procedure is used in Chapter 6. Both modes will continue to coexist even for very strong interactions between the modes.

Chapter 5

Acoustic Response of a Plane Flame

In this chapter we study the response of a plane flame in a general combustor, specifically, the response of the flame to impinging pressure and entropy waves is determined in the limit of infinitesimally small disturbances. The general issues are (1) conditions for the stable location of a flame, (2) the response to forward and rearward running acoustic waves, (3) the response to incident fluctuating entropy waves, (4) the resulting motion of the flame sheet due to these perturbations, and (5) the effect on the stability of pressure oscillations in a combustion chamber containing a planar flame sheet. The last two of these are addressed in Chapter 6.

The response of the plane flame is determined by treating the flame as a matching condition in a flow field in the same manner as Chu [41]. The use of a plane flame is a crude approximation to the actual flame contained in the combustor. In the low frequency limit the wavelengths are often much longer than the combustion zone even though the combustion zone may have finite thickness. In these cases it can be useful to consider the approximate case of an infinitesimal

flame sheet.

5.1 Problem and Geometry

The goal of studying the plane flame is to obtain a modeling unit to use in combustion chambers. The issues of boundary conditions at the ends of the combustor will be discussed in later sections of Chapter 5 and in Chapter 6. Consider a plane flame that is situated in a combustor (or duct, for that matter) where the area, S, is an arbitrary function of position, x,as in Figure 5.1. The incoming flow is also given an imposed fluctuating entropy such that at $x = 0$ the entropy consists of a steady state term and a given small periodic fluctuation term, so that

$$s(x,t) = s_0 + Ae^{-i\Omega t} \tag{5.1}$$

where A may be a complex constant (and possibly a function of frequency ω).

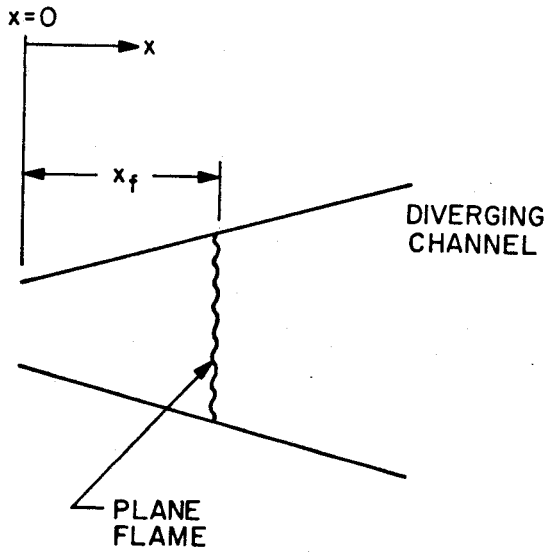

Figure 5.1: Variable Area Combustor – $S = S(x)$.

It is assumed that certain characteristics of the flame are known. Typically, these are determined from experimental data from the literature. The important

characteristics are the dependence of flame speed, S_t, on changes in pressure and temperature, or rather the partial derivatives of the flame speed with respect to the pressure and temperature of the incoming mixture. The mixture is assumed to be thoroughly mixed fuel and oxidizer, and any equivalence ratio dependence is assumed to be contained in the flame speed, its derivatives, and the heat of combustion.

Two issues are critically important in developing this model which determine whether or not the model can have any practical importance. The first is stability. The geometry of many combustion chambers consists of slightly diverging cross-sectional areas. It needs to be shown that, with the introduction of fluctuations, a plane flame will reach a stable location. Certainly it is unacceptable to have a non-stationary or unstable mean flame position. This issue of stability will be addressed in the next section. The second concern is whether or not it is possible to generate a periodic oscillation that is neutrally stable. Should it be that the position of the flame is self-accelerating, that is, if the flame is perturbed it tends to move and its fluctuation further accelerates the flame, then the model would be useless. This motion is determined by both the flame response and the boundary conditions and is discussed later in this chapter.

5.2 Stability of a Flat Laminar Flame

This section will show the condition for which an idealized flat laminar flame will be stable in a changing area duct. Consider a changing area duct with a stationary laminar flame having infinitesimal thickness. Assume that the ideal gas law holds and that the fluid properties, γ, c_p, and R are constant throughout. For a typical low speed deflagration, the flow everywhere in the duct has low Mach number and thus the $O(M^2)$ contributions to the equations of motion are negligible. The

flame is regarded as an infinitesimally thin heat addition zone. The pressure is essentially constant (to $O(M^2)$) and the heat addition causes primarily a temperature and thus density discontinuity at the flame. From continuity, the velocity must suffer a discontinuity at the flame to accommodate the density discontinuity. The steady state equations of motion give the following matching conditions across the flame

$$\rho_1 u_1 = \rho_2 u_2 , \tag{5.2}$$

$$P_1 = P_2 , \tag{5.3}$$

$$c_p T_1 = c_p T_2 - Q . \tag{5.4}$$

Define a constant, λ, to be temperature ratio so that

$$\lambda^2 = \frac{T_1}{T_2} = 1 + \frac{Q}{T_1 c_p} = (\frac{{M_2}^2}{M_1}) = \frac{u_2}{u_1} \tag{5.5}$$

where the speed of sound is $a_i = \sqrt{\gamma R T_i}$.

Suppose that the flame is subjected to a disturbance of velocity, u_{2e}^2, incident from the downstream direction. In response the flame moves x' from its average position positive in the downstream direction, with a fluctuation of velocity $v_f' = dx'/dt$, also positive in the downstream direction. In subsonic flow the motion will produce a disturbance, u_{1e}', upstream of the flame. In the presence of a nonuniform mean flow, the flame is also exposed to fluctuations due to its motion along the gradients of the mean flow proportional to $x' d\bar{u}_1/dx$, etc. Hence, the fluctuations to which the flame is exposed are

$$u_1' = -v_f' + x' \left(\frac{d\bar{u}_1}{dx}\right) + u_{1e}' \tag{5.6}$$

$$P_1' = x' \left(\frac{d\bar{P}_1}{dx}\right) + P_{1e}' \tag{5.7}$$

and

$$u_2' = -v_f' + x' \left(\frac{d\bar{u}_2}{dx}\right) + u_{2e}' \tag{5.8}$$

$$P_2' = x'\left(\frac{d\bar{P}_2}{dx}\right) + P_{2e}' \tag{5.9}$$

where the bar denotes mean quantities.

It is assumed that the flame responds quasi-statically to a small disturbance so that 5.2 through 5.4 will apply at all times in a reference frame attached to the flame. Substituting the mean quantities plus the fluctuating quantities 5.7 and 5.9 into 5.3 gives

$$P_1' + x'\left(\frac{d\bar{P}_1}{dx}\right) + P_{1e}') = P_2' + x'\left(\frac{d\bar{P}_2}{dx}\right) + P_{2e}'. \tag{5.10}$$

In steady flow, $\bar{P}_1 = \bar{P}_2$ and $d\bar{P}_1/dx = d\bar{P}_2/dx$ so that 5.10 becomes

$$P_{1e}' = P_{2e}'. \tag{5.11}$$

From 5.5, after dropping the steady terms, we find

$$-v_f' + x'\left(\frac{d\bar{u}_2}{dx}\right) + u_{2e}' = \lambda^2(-v_f' + x'\left(\frac{d\bar{u}_1}{dx}\right) + u_{1e}'). \tag{5.12}$$

Use $v_f = dx'/dt$ and $d\bar{u}_1/dx = d\bar{u}_2/dx$ to find

$$\frac{dx'}{dt} - x'\left(\frac{d\bar{u}}{dx}\right) = \frac{1}{(\lambda^2-1)}(\lambda^2 u_{1e}' - u_{2e}'). \tag{5.13}$$

Let $\tau = -1/(d\bar{u}/dx)$. Then the solution to the position of the flame can be written as

$$x'(t) = \frac{1}{\tau(\lambda^2-1)} e^{\frac{-t}{\tau}} \int_0^t e^{\frac{t'}{\tau}}(\lambda^2 u_{1e}' - u_{2e}')dt'. \tag{5.14}$$

This result is analogous to the case of stability of a shock wave in a supercritical diffuser [52]. In the case of the shock wave, stability occurs when supersonic flow downstream of the choked throat in a diverging flow undergoes a shock.

Whatever the form of the imposed disturbance, as long as it lasts for a finite time, the transient motion will decay only if $\tau > 0$. Hence stability requires that

$$\frac{d\bar{u}}{dx} < 0 \qquad or \qquad \frac{dS}{dx} > 0 \tag{5.15}$$

where S is the cross-sectional area. Thus the flame is stable in a diverging duct in which the speed decreases in the flow direction.

5.3 Matching Conditions for a Plane Flame in General Combustor

In this section three matching conditions of continuity, momentum, and energy are derived for matching two acoustic regions across an acoustically compact plane flame. These matching conditions form the basis from which the acoustic and entropy response of a plane flame are determined in the next three sections. these matching conditions are also used to study the oscillating flame inside a combustor system in Chapter 6.

The combustor given has two boundary conditions. These are set at the inlet and exit of the combustor. In addition the two regions are matched at $x = x^*$ across a plane flame. The matching at the flame is carried out in the spirit of Chu's work [46] [47] on plane flames from region 1 to region 2. (Chu's work did not include divergent flows nor considerations of stability.) The method is also similar to that used by Culick and Rogers [10] on shock waves in diffusers.

Actually, this is an extension of Chu's work to a diverging duct and then a specific application. The arguments presented by Culick and Rogers on the quasi-steady behavior of the flow can be applied to the flame case just as they are in the shock case; hence, we treat the flow as quasi-steady and one-dimensional. The constant area case will be presented along with the divergent flow case at the beginning. Then not all of the constant area case will be shown. This is because it can be recovered from the divergent flow case when the change in area with respect to position vanishes (just as it should).

The procedure is to treat each of the flow quantities as a time independent

mean term (indicated by subscript 0) and a fluctuating term (superscript prime). Place these into the equations of motion to recover the mean flow conditions and the first order perturbation equations. The equations to be used are continuity, momentum, energy, and the ideal gas equation of state. In both cases the flame is located at $x = x^* + x'$.

Constant Area Duct	Divergent Duct	
$\rho = \bar{\rho} + \rho'$	$\rho = \bar{\rho} + x'\frac{d\bar{\rho}}{dx} + \rho'$	(5.16)
$u = \bar{u} + u' + S_a'$	$u = \bar{u} + x'\frac{d\bar{u}}{dx} + u' + S_a'$	(5.17)
$S_t = \bar{S}_t + S_t'$	$S_t = \bar{S}_t + S_t'$	(5.18)
$Q = \bar{Q} + Q'$	$Q = \bar{Q} + Q'$	(5.19)
$P = \bar{P} + P'$	$P = \bar{P} + x'\frac{d\bar{P}}{dx} + P'$	(5.20)
$T = \bar{T} + T'$	$T = \bar{T} + x'\frac{d\bar{T}}{dx} + T'$	(5.21)
$S_a = -u_1' + S_t'$	$S_a = -u_1' + S_t'$	(5.22)

All of these equations have been corrected to allow the flame speed to change. The apparent flame speed, S_a, has been introduced to correct the steady state equations. Terms that correct for the changes in the flow quantities due to the change in area are contained in the divergent case. This allows the use of the 1-dimensional steady equations of motion which are

$$\rho_1 u_1 = \rho_2 u_2, \tag{5.23}$$

$$P_1 + \rho_1 u_1^2 = P_2 + \rho_2 u_2^2, \tag{5.24}$$

$$Q_1 = c_{p2}T_2 + \frac{1}{2}u_2^2 - c_{p1}T_1 - \frac{1}{2}u_1^2 \tag{5.25}$$

for continuity, momentum, and energy respectively with Q defined as the heat of combustion per mass burned. After substitution of 5.16-5.22 into 5.23 and

elimination of the steady state terms the equation of continuity becomes

$$\begin{aligned}\frac{\rho_1'}{\bar{\rho}_1}\left(1+\frac{S_t'}{\bar{u}_1}\right) \quad + \quad & \frac{S_t'}{\bar{u}_1}-\frac{\rho_2'}{\bar{\rho}_2}\left(1+\frac{\bar{u}_1}{\bar{u}_2}\left(G+\frac{S_t'}{\bar{u}_1}\right)\right)-\frac{\bar{u}_1}{\bar{u}_2}\left(G+\frac{S_t'}{\bar{u}_1}\right)= \\ & +x'\frac{d\ln(S)}{dx}\left[-\left(\frac{\rho_1'}{\bar{\rho}_1}+1\right)\frac{d\ln(\bar{u}_1)}{d\ln(S)}+\left(\frac{\rho_2'}{\bar{\rho}_2}+1\right)\frac{d\ln(\bar{u}2)}{d\ln(S)}\right] \\ & +x'\frac{d\ln(S)}{dx}\left[-\frac{d\ln(\bar{\rho}_1)}{d\ln(S)}\left(1+x'\frac{d\ln(\bar{u}_1)}{dx}+\frac{S_t'}{\bar{u}_1}\right)\right] \\ & +x'\frac{d\ln(S)}{dx}\left[+\frac{d\ln(\bar{\rho}_2)}{d\ln(S)}\left(1+x'\frac{d\ln(\bar{u}_2)}{dx}+\frac{\bar{u}_1}{\bar{u}_2}\left(G+\frac{S_t'}{\bar{u}_1}\right)\right)\right]\end{aligned} \tag{5.26}$$

where G is defined for convenience to be

$$G=\frac{u_2'-u_1'}{\bar{u}_1}, \tag{5.27}$$

and S is the duct area.

Continue with the same procedure for the momentum equation and invoke low mean Mach number of the flow. This is not required but significantly reduces the algebra. This is to say that we will neglect terms of $O(M^2)$. (It is worthwhile to point out that this is not always the case and care must be taken later in neglecting higher order terms to realize that certain assumptions have already been imposed.) Assume that the flame is infinitesimally thin and subtract the mean flow terms to get the equation for conservation of momentum

$$(\bar{P}_1+x'\frac{d\bar{P}_1}{dx}+P_1')=(\bar{P}_2+x'\frac{d\bar{P}_2}{dx}+P_2'). \tag{5.28}$$

Since $\bar{P}_1/\bar{P}_2=1$ (neglecting $O(M^2)$ terms) the mean flow terms vanish to give the simple relation

$$\frac{P_2'}{\bar{P}_2}=\frac{P_1'}{\bar{P}_1}. \tag{5.29}$$

This is a nice result since there is no difference between the constant area case and the divergent case (to $O(M^2)$).

Repeat these manipulations on the energy equation, neglect the $O(M^2)$ terms, and neglect second order terms involving c'_{p1} and c'_{p2} to find

$$\begin{aligned}\frac{Q'}{c_{p1}T_1} &= \left(\frac{c_{p2}}{c_{p1}}\frac{c'_{p2}}{c_{p2}}\frac{T_2}{T_1} - \frac{c'_{p1}}{c_{p1}}\right) + \left(\frac{c_{p2}}{c_{p1}}\frac{T_2}{T_1}\frac{T'_2}{T_2} - \frac{T'_1}{T_1}\right) + \\ &\quad + x'\frac{d\ln S}{dx}\left(\frac{c_{p2}}{c_{p1}}\frac{T_2}{T_1}\frac{d\ln T_2}{d\ln S} - \frac{d\ln T_1}{d\ln S}\right). \end{aligned} \tag{5.30}$$

The above equation was written with the mean flow bar dropped but assumed nonetheless wherever there is no prime. This notation is continued throughout.

The perfect gas law $P = \rho RT$ becomes, to first order

$$\frac{P'}{P} = \frac{T'}{T} + \frac{\rho'}{\rho} + x'\frac{d}{dx}(\ln T + \ln\rho - \ln P). \tag{5.31}$$

The mean flow terms in 5.31 can be written as

$$\frac{d}{dx}(\ln T + \ln\rho - \ln P) = \frac{d}{dx}(\ln\frac{1}{R}) = 0 \tag{5.32}$$

to give the familiar first order result

$$\frac{P'}{P} = \frac{T'}{T} + \frac{\rho'}{\rho}. \tag{5.33}$$

For a polytropic gas

$$\frac{T'}{T} = \frac{s'}{c_p} + \frac{\gamma-1}{\gamma}\frac{P'}{P} \tag{5.34}$$

and

$$\frac{\rho'}{\rho} = \frac{1}{\gamma}\frac{P'}{P} - \frac{s'}{c_p}. \tag{5.35}$$

To simplify some of the equations define C_s and E_s as

$$\begin{aligned} C_s &= -\left(\frac{\rho'_1}{\bar\rho_1}+1\right)\frac{d\ln\bar u_1}{d\ln S} + \left(\frac{\rho'_2}{\bar\rho_2}+1\right)\frac{d\ln(\bar u_2)}{d\ln(S)} \\ &\quad -\frac{d\ln(\bar\rho_1)}{d\ln(S)}\left(1 + x'\frac{d\ln(\bar u_1)}{dx} + \frac{S'_t}{u_1}\right) \\ &\quad +\frac{d\ln(\bar\rho_2)}{d\ln(S)}\left(1 + x'\frac{d\ln(\bar u_2)}{dx} + \frac{\bar u_1}{\bar u_2}\left(G + \frac{S'_t}{u_1}\right)\right) \end{aligned} \tag{5.36}$$

and

$$E_s = \frac{c_{p2}}{c_{p1}}\frac{T_2}{T_1}\frac{d\ln T_2}{d\ln S} - \frac{d\ln T_1}{d\ln S}\,. \tag{5.37}$$

These terms, C_s and E_s, contain the area change contributions that will enter the general matching condition.

5.4 Summary of Equations

This section summarizes the equations of matching in the previous section and introduces specific simplifications used to solve examples presented later. These simplifications include a consistent Taylor series expansion of denominator terms; distinction between constant area and divergent area contributions; harmonic motion of the flame; consideration of all terms to $O(M^2)$; elimination of S_t' and Q' in favor of acoustic terms; and small flame speed fluctuation with respect to the mean flow velocity.

In summary, the equations of motion are

Continuity

$$A_2 + \frac{\rho_1'}{\rho_1}A_1 - A_4 - \frac{\rho_2'}{\rho_2}A_3 = x'\frac{1}{S}\frac{dS}{dx}C_s\,, \tag{5.38}$$

Momentum

$$\frac{P_1'}{P_1} = \frac{P_2'}{P_2}\,, \tag{5.39}$$

and **Energy**

$$\frac{Q'}{c_{p1}T_1} = \left(\frac{c_{p2}}{c_{p1}}\frac{c_{p2}'}{c_{p2}}\frac{T_2}{T_1} - \frac{c_p'}{c_{p1}}\right) + \left(\frac{c_{p2}}{c_{p1}}\frac{T_2}{T_1}\frac{T_2'}{T_2} - \frac{T_1'}{T_1}\right) + x'\frac{1}{S}\frac{dS}{dx}E_S\,. \tag{5.40}$$

The gas law gives

$$\frac{P_1'}{P_1} - \frac{\rho_1'}{\rho_1} - \frac{T_1'}{T_1} = 0 \quad \text{and} \quad \frac{P_2'}{P_2} - \frac{\rho_2'}{\rho_2} - \frac{T_2'}{T_2} = 0\,. \tag{5.41}$$

The following definitions are used in 5.38

$$A_1 = 1 + \frac{S_t'}{u_1}\,, \tag{5.42}$$

$$A_2 = \frac{S_t'}{u_1}, \tag{5.43}$$

$$A_3 = 1 + \frac{u_1}{u_2}\left(G + \frac{S_t'}{\bar{u}_1}\right), \tag{5.44}$$

and

$$A_4 = \frac{u_1}{u_2}\left(G + \frac{S_t'}{\bar{u}_1}\right). \tag{5.45}$$

Also,

$$\frac{T_1'}{T_1} = \frac{s_1'}{c_{p1}} + \frac{\gamma_1 - 1}{\gamma_1}\frac{P_1'}{P_1} \tag{5.46}$$

and

$$\frac{\rho_1'}{\rho_1} = \frac{1}{\gamma}\frac{P_1'}{P_1} - \frac{s_1'}{c_{p1}}. \tag{5.47}$$

5.4.1 Solving for G

This section simplifies some of the terms in 5.38 in order to solve for G. When considering linear acoustics, the following terms are small:

$$\frac{P_1'}{P_1}, \quad \frac{s_1'}{c_{p1}}, \quad \frac{T_1'}{T_1}, \quad \frac{T_2'}{T_2}, \quad \frac{u_1'}{a_1}, \quad \frac{u_2'}{a_2} << 1, \tag{5.48}$$

while no restrictions are placed on G, S_t'/u_1, and x'. More will be said about these terms later. Using a Taylor expansion, define D such that

$$\frac{1}{\left(1 + \frac{1}{\gamma_1}\frac{P_1'}{P_1} - \frac{s_1'}{c_{p1}} + \frac{T_1'}{T_1} - \frac{T_2'}{T_2}\right)} \approx 1 - \frac{1}{\gamma_1}\frac{P_1'}{P_1} + \frac{s_1'}{c_{p1}} - \frac{T_1'}{T_1} + \frac{T_2'}{T_2} = D. \tag{5.49}$$

With higher order acoustics terms neglected, and after considerable manipulations, G can be found to be

$$\begin{aligned} G \approx & \left(\frac{u_2}{u_1} - 1\right)\frac{S_t'}{u_1} + \frac{u_2}{u_1}\left(1 + \frac{S_t'}{u_1}\right)\left(\frac{T_2'}{T_2} - \frac{T_1'}{T_1}\right) + \\ & x'\frac{1}{S}\frac{dS}{dx}C_s D. \end{aligned} \tag{5.50}$$

Define $\tilde{G}$ to be the value of G in the absence of area change to get

$$G = \tilde{G} + H \tag{5.51}$$

where $\tilde{G}$ is the same term that would have been found by substituting the constant area version of 5.16-5.22 into 5.25. (Verified by actual calculation.) Use equations 5.50 and 5.51 to show

$$H \approx x' \left(\frac{1}{S}\frac{dS}{dx}\right)\left(C_s D - E_s \frac{u_2}{u_1}\frac{T_1}{T_2}\frac{c_{p1}}{c_{p2}}\left(1+\frac{S_t'}{u_1}\right)\right). \tag{5.52}$$

For the motion of the flame to be harmonic it is assumed that

$$S_a' = -i\Omega x' \tag{5.53}$$

and

$$S_t' - u_1' = -i\Omega x' \tag{5.54}$$

which gives

$$x' = \frac{S_t' - u_1'}{-i\Omega}. \tag{5.55}$$

This gives a relation to eliminate x' in favor of S_t' and u_1'.

Steady State Equations of Motion: Divergent Channel

The divergent channel contributions have been lumped into the terms C_s and E_s. The evaluation of the terms C_s and E_s requires an analysis of the steady state quantities in a divergent combustion chamber. Start with the control volume given in Figure 5.2. In the limit that $\Delta x \rightarrow$ infinitesimal, we find that

Continuity gives

$$\frac{d\rho}{\rho} + \frac{du}{u} + \frac{dA}{A} = 0, \tag{5.56}$$

Momentum gives

$$\frac{d(P+\rho u^2)}{(P+\rho u^2)} + \frac{dA}{A} = 0, \tag{5.57}$$

and Energy gives

$$\frac{d\left(\left(e+\frac{P}{\rho}\right)\rho u\right)}{\left(\left(e+\frac{P}{\rho}\right)\rho u\right)} + \frac{dA}{A} = \frac{\Delta h_c}{\left(e+\frac{P}{\rho}\right)\rho u} \tag{5.58}$$

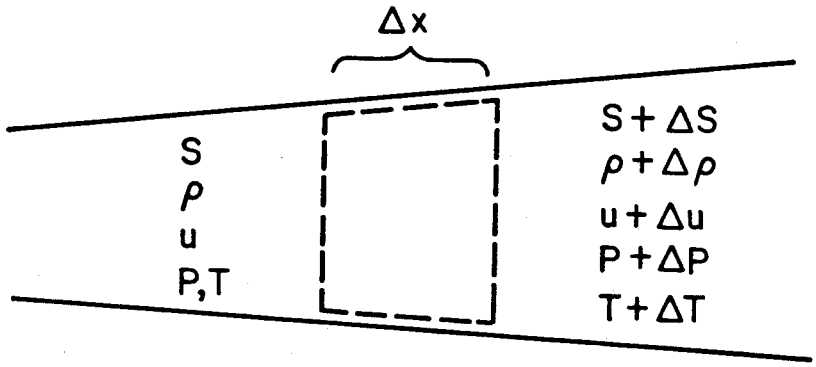

Figure 5.2: Control Volume for Flame in Changing Area Channel.

where Δh_c is the heat release inside the control volume.

Neglect terms of $O(M^2)$ and treat c_p as constant to find

$$d\ln(\rho) + d\ln(u) + d\ln(A) = 0\,, \tag{5.59}$$

$$d\ln(P) + d\ln(A) = 0\,, \tag{5.60}$$

and

$$d\ln(T) - \frac{\Delta h_c}{c_p T} = 0\,. \tag{5.61}$$

The gas law yields

$$d\ln(P) - d\ln(\rho) - d\ln(T) = 0\,. \tag{5.62}$$

Using equations 5.59 and 5.62 to eliminate P with 5.60 and 5.61 we find

$$d\ln(u) = d\ln(T) = \frac{\Delta h_c}{c_p T}\,. \tag{5.63}$$

To evaluate E_s, consider region 1 and 2 separately. In each case $\Delta h_c = 0$ and hence

$$d\ln(T_1) = d\ln(T_2) = 0 \tag{5.64}$$

from which it follows that

$$E_s = O + O(M^2)\,. \tag{5.65}$$

From 5.63 it follows that

$$d\ln(u) = 0 + O(M^2) \tag{5.66}$$

and

$$d\ln(\rho) = -d\ln(A)\,. \tag{5.67}$$

Evaluate C_s to get

$$C_s = -\frac{u_1}{u_2}\left(G + \left(1 - \frac{u_2}{u_1}\right)\frac{S_t'}{u_1}\right) + O(M^2)\,. \tag{5.68}$$

Then use 5.65 and 5.52 with C_s to find

$$H \approx \frac{1}{S}\frac{dS}{dx}\left(\frac{S_t' - u_1'}{-\Omega}\right) i\frac{u_1}{u_2}\left(G + \left(1 - \frac{u_2}{u_1}\right)\frac{S_t'}{u_1}\right) D\,. \tag{5.69}$$

Define a reduced (or dimensionless) frequency such that

$$\hat{\Omega} = \frac{\Omega}{a_1 \frac{1}{S}\frac{dS}{dx}} \tag{5.70}$$

in the same manner as Culick and Rogers [10]. It is also convenient to define

$$\mathcal{R} = -\left(\frac{S_t' - u_1'}{-a_1}\right) i\frac{u_1}{u_2} D\,. \tag{5.71}$$

Incorporate 5.70 and 5.71 into 5.69 to get

$$H \approx \frac{1}{\hat{\Omega}}\left(G + \left(1 - \frac{u_2}{u_1}\right)\frac{S_t'}{u_1}\right)\mathcal{R}\,. \tag{5.72}$$

Evaluation of the Constant Area Contribution — $\tilde{G}$

Now that the term H in G that contains the contributions due to area change has been considered, return to 5.51 to find

$$G \approx \tilde{G} + \frac{1}{\hat{\Omega}}\left(G + \left(1 - \frac{u_2}{u_1}\right)\frac{S_t'}{u_1}\right)\mathcal{R}\,. \tag{5.73}$$

Rewrite 5.73 to get

$$G \approx \left(\frac{\hat{\Omega}}{\hat{\Omega}-\mathcal{R}}\right)\left\{\tilde{G}+\frac{\mathcal{R}}{\hat{\Omega}}\left(1-\frac{u_2}{u_1}\right)\frac{S_t'}{u_1}\right\}. \tag{5.74}$$

Clearly, if $dS/dx = 0$, then $\Omega \to \infty$ while R remains finite, and G reduces to $\tilde{G}$. Consider $\tilde{G}$. From equation 5.40 where $E_s = 0$ it can be shown that

$$\frac{T_2'}{T_2} = \frac{c_{p1}}{c_{p2}}\frac{T_1}{T_2}\frac{T_1'}{T_1} + \left(\frac{c_{p1}}{c_{p2}}\frac{T_1}{T_2}\frac{c_{P1}'}{c_{P1}} - \frac{c_{P2}'}{c_{P2}}\right) + \frac{c_{p1}}{c_{p2}}\frac{T_1}{T_2}\frac{Q_1'}{c_{p1}T_1}. \tag{5.75}$$

Eliminate T_2' from $\tilde{G}$ and after several rearrangements it can be shown that

$$\begin{aligned}
\tilde{G} \;=\; & \left(\frac{R_2}{R_1}\lambda - 1\right)\frac{S_t'}{u_1} + \frac{R_2}{R_1}\left(\frac{S_t'}{u_1}+1\right)\frac{Q'}{c_{p2}T_1} \\
& -\frac{R_2}{R_1}\left(\frac{S_t'}{u_1}+1\right)\left(\frac{c_{p2}}{c_{p1}}\lambda - 1\right)\frac{s_1'}{c_{p2}} \\
& -\frac{\gamma_2-1}{\gamma_2}\left(\frac{S_t'}{u_1}+1\right)\left(\frac{c_{p2}}{c_{p1}}\lambda - 1\right)\frac{P_1'}{P_1} \\
& +\frac{\gamma_2-1}{\gamma_2}\left(\frac{S_t'}{u_1}+1\right)\left(\frac{R_2}{R_1}\lambda\frac{\gamma_2'}{(\gamma_2+1)^2} - \frac{\gamma_1'}{(\gamma_1+1)^2}\right).
\end{aligned} \tag{5.76}$$

This result is equivalent to that found by Chu [53] When $S_t'/u_1 << 1$ then

$$\begin{aligned}
\tilde{G} \;=\; & \left(\frac{R_2}{R_1}\lambda - 1\right)\frac{S_t'}{u_1} + \frac{R_2}{R_1}\frac{Q'}{c_{p2}T_1} - \frac{R_2}{R_1}\left(\frac{c_{p2}}{c_{p1}}\lambda - 1\right)\frac{s_1'}{c_{p2}} \\
& -\frac{\gamma_2-1}{\gamma_2}\left(\frac{c_{p2}}{c_{p1}}\lambda - 1\right)\frac{P_1'}{P_1} + \frac{\gamma_2-1}{\gamma_2}\left[\frac{R_2}{R_1}\lambda\frac{\gamma_2'}{(\gamma_2+1)^2} - \frac{\gamma_1'}{(\gamma_1+1)^2}\right].
\end{aligned} \tag{5.77}$$

Evaluating the Magnitude of H

In order to evaluate the importance of the area changes, it is convenient to study the magnitude of H. From 5.74

$$H \propto \frac{\mathcal{R}}{\hat{\Omega}}\frac{S_t'}{u_1} \tag{5.78}$$

and

$$\mathcal{R} \propto \frac{S_t' - u_1'}{a_1}\frac{u_1}{u_2} \tag{5.79}$$

from which

$$H \propto \left(\frac{S_t'}{a_1} - \frac{u_1'}{a_1}\right)\left(\frac{S_t'}{u_1}\right)\left(\frac{a_1}{\Omega}\right)\left(\frac{1}{S}\frac{dS}{dx}\right)\left(\frac{u_1}{u_2}\right). \tag{5.80}$$

In the case that S_t'/u_1 is $<< 1$ then H becomes second order for typical values of the mean parameters. For these cases it is consistent to neglect H.

5.4.2 Steady State Conditions to $O(M^2)$

To keep the expansions consistent to $O(M^2)$, the steady state terms are evaluated. The steady state of the flame is given in a coordinate system where the flame is stationary. For the flame to remain stationary, then $u_1 = S_t$ where S_t is the mean flame speed. The equations of motion are given in 5.23-5.25. When neglecting $O(M^2)$ terms these equations can be solved to give

$$\frac{P_2}{P_1} = 1 + O(M_1^2), \tag{5.81}$$

$$\frac{\rho_2}{\rho_1} = \frac{R_1}{R_2\lambda} + O(M_1^2), \tag{5.82}$$

$$\frac{T_2}{T_1} = \lambda + O(M_1^2), \tag{5.83}$$

$$\frac{u_2}{u_1} = \frac{R_2}{R_1}\lambda + O(M_1^2), \tag{5.84}$$

and

$$\frac{M_2^2}{M_1^2} = \frac{\gamma_1}{\gamma_2}\frac{R_2}{R_1}\lambda + O(M_1^2). \tag{5.85}$$

Elimination of S_t' and Q'

The acoustic field is described in terms of u', P', and s'. The matching condition for G contains S_t' and Q'. It is preferable to express S_t' and Q' in terms of the acoustic field quantities. The flame speed, S_t, can be written as

$$S_t = S_t(P_1, T_1) \tag{5.86}$$

where P_1 and T_1 refer to the incoming (or upstream) quantities. Differentiate 5.86 to find

$$S_t' = \frac{\partial S_t}{\partial P_1} P_1' + \frac{\partial S_t}{\partial T_1} T_1', \tag{5.87}$$

and eliminate T_1' with 5.34 to find

$$S_t' = \left[\frac{\partial S_t}{\partial P_1} + \frac{\partial S_t}{\partial T_1}\frac{T_1}{P_1}\frac{\gamma_1 - 1}{\gamma_1}\right] P_1' + \left[\frac{\partial S_t}{\partial T_1}\frac{T_1}{c_{p1}}\right] s_1' . \tag{5.88}$$

Define

$$W_1 = \frac{\partial S_t}{\partial P_1} + \frac{\partial S_t}{\partial T_1}\frac{T_1}{P_1}\frac{\gamma_1 - 1}{\gamma_1} \tag{5.89}$$

and

$$W_2 = \frac{\partial S_t}{\partial T_1}\frac{T_1}{c_{p1}} \tag{5.90}$$

to get

$$S_t' = W_1 P_1' + W_2 s_1' . \tag{5.91}$$

The term Q' in this formulation is identical to $\Delta h_c'$. (Q was used to conform to Chu's formulation.) It is possible to work on a model for fuel mixture or composition fluctuation. It is here that such considerations would be included. Just as for W_1 and W_2, another two constants can be defined as W_3 and W_4. In this study, the fuel mixture is considered ideal; hence $\Delta h_c'$ is zero as well as W_3 and W_4.

Case of S_t'/u_1 Small in G

When S_t'/u_1 is sufficiently small then G is given by 5.77. Neglect for now γ_2' and γ_1'. Using 5.91 in 5.77 results in

$$\begin{aligned}\tilde{G} \;=\; & \left(\frac{R_2}{R_1}\lambda - 1\right)\frac{1}{u_1}(W_1 P_1' + W_2 s_1') + \frac{R_2}{R_1}\frac{1}{c_{p2}T_1}(W_3 P_1' + W_4 s_1') \\ & - \frac{R_2}{R_1}\left(\frac{c_{p2}}{c_{p1}}\lambda - 1\right)\frac{1}{c_{p2}} s_1' - \frac{\gamma_2 - 1}{\gamma_2}\left(\frac{c_{p2}}{c_{p1}}\lambda - 1\right)\frac{1}{P_1} P_1' .\end{aligned} \tag{5.92}$$

Define

$$W_5 = \left(\frac{R_2}{R_1}\lambda - 1\right)\frac{W_1}{u_1} + \frac{R_2}{R_1}\frac{W_3}{c_{p2}T_1} - \frac{\gamma_2 - 1}{\gamma_2}\left(\frac{c_{p2}}{c_{p1}}\lambda - 1\right)\frac{1}{P_1} \tag{5.93}$$

and

$$W_6 = \left(\frac{R_2}{R_1}\lambda - 1\right)\frac{W_2}{u_1} + \frac{R_2}{R_1}\frac{W_4}{c_{p2}T_1} - \frac{R_2}{R_2}\left(\frac{c_{p2}}{c_{p1}}\lambda - 1\right)\frac{1}{c_{p2}} \tag{5.94}$$

to get

$$\tilde{G} \approx W_5 P_1' + W_6 s_1' \ . \tag{5.95}$$

5.4.3 Combustor Considerations

The combustor consists of two regions which are matched across the flame as in Figure 5.3. Each of the two regions ($0 < x < x_f$ and $x_f < x < L$) are linearly acoustic and governed by 4.71-4.73. To determine the response of the flame in the combustor one has only to match the acoustic regions 1 and 2 across the flame.

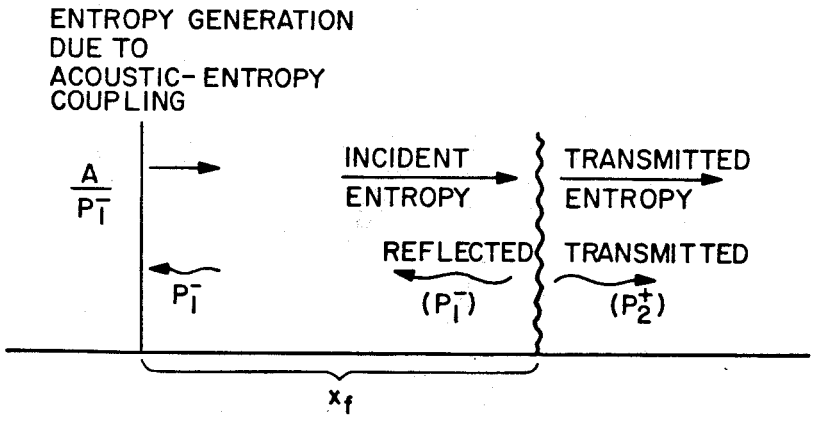

Figure 5.3: Combustor Containing a Plane Flame.

Matching Conditions

The matching conditions at the flame are continuity, momentum, and energy across the flame sheet. Hence, apply 5.39, 5.40, and 5.95 at $x = x^* + x'$ with the definitions of W_i. Define

$$W_7 = \frac{c_{p1}}{c_{p2}\lambda}\left(\frac{\gamma_1 - 1}{\gamma_1}\frac{1}{P_1} + \frac{W_3}{c_{p1}T_1}\right) \tag{5.96}$$

and

$$W_8 = \frac{c_{p1}}{c_{p2}\lambda}\left(\frac{1}{c_{p1}} + \frac{W_4}{c_{p1}T_1}\right) \tag{5.97}$$

to get (from 5.40)

$$\frac{T_2'}{T_2} = W_7 P_1' + W_8 s_1' . \tag{5.98}$$

There is no contribution from change of area in 5.98. There are two reasons for this: neglecting $O(M^2)$ terms, and treating the divergence of the duct to be small. Then T_2' in 5.98 can be eliminated in favor of P_2' and s_2'. Define

$$W_9 = c_{p1}\left(W_7 - \frac{\gamma_2 - 1}{\gamma_2}\frac{1}{P_1}\right) \tag{5.99}$$

and

$$W_{10} = c_{p2} W_8 \tag{5.100}$$

to get (from 5.98)

$$s_2' = W_9 P_1' + W_{10} s_1' . \tag{5.101}$$

The solution of the governing equations in regions 1 and 2 can be solved directly to get

$$P_1'(x,t) = P_{10}\left[P_1^+ e^{iK_1 x} + P_1^- e^{-iK_1 x}\right] e^{-iM_{10}K_1 x} e^{-i\Omega t} , \tag{5.102}$$

$$u_1'(x,t) = \frac{P_{10}}{\rho_{10} a_{10}}\left[P_1^+ e^{iK_1 x} + U_1^- e^{-iK_1 x}\right] e^{-iM_{10}K_1 x} e^{-i\Omega t} , \tag{5.103}$$

$$s_1'(x,t) = A e^{i\frac{\Omega}{u_{10}}x} e^{-i\Omega t} , \tag{5.104}$$

and

$$P_2'(x,t) = P_{20}\Big[P_2^+ e^{iK_2 x} + P_2^- e^{-iK_2 x}\Big] e^{-iM_{20}K_2 x} e^{-i\Omega t}\,, \tag{5.105}$$

$$u_2'(x,t) = \frac{P_{20}}{\rho_{20} a_{20}}\Big[P_2^+ e^{iK_2 x} + U_2^- e^{-iK_2 x}\Big] e^{-iM_{20}K_2 x} e^{-i\Omega t}\,, \tag{5.106}$$

$$s_2'(x,t) = B e^{i\frac{\Omega}{u_{20}}x} e^{-i\Omega t}\,, \tag{5.107}$$

where

$$K_n = \frac{k_n}{1 - M_{n0}^2}\,, \quad k_n = \frac{\Omega_n}{a_{n0}}\,, \quad \Omega_n = \omega_n + i\alpha_n \tag{5.108}$$

and the constant for the magnitude of the upstream entropy is A and for the downstream entropy is B. The unknowns constants are P_1^+, P_1^-, P_2^+, P_2^-, B, Ω. Use the inlet and exit boundary conditions along with 5.39, 5.95, and 5.101 at $x = x^* + x'$ to eliminate the first five of these constants to give

$$F(\Omega) = 0\,, \tag{5.109}$$

a transcendental equation for the eigenvalues Ω_n .

In the elimination, it is necessary to point out that the ratio of A/P_1^- is required. This is due to the lack of a boundary condition thus far for the entropy. If a model for the entropy generation is chosen (such as the fluctuating shock in the inlet diffuser) then A/P^- can be eliminated. This will be discussed in Chapter 6. Here, the term A/P_1^- is simply treated as a given parameter.

Summary of Section 5.4

In summary, Section 5.3 developed the equations of matching for an acoustically compact plane flame in an acoustic medium. Section 5.4 simplified these results as applied to a typical ramjet combustor environment. In addition, the general procedure for solving the linear eigenfrequencies is outlined. This analysis will be used in the next two sections of this chapter and in the modeling of Chapter 6.

5.5 Response to Acoustic Waves

Before showing the mathematics of the complete combustor, it is important to verify that the process of pressure wave interaction with the flame sheet can in fact produce a periodic process. Consider two cases where only the pressure waves and downstream entropy are included and no boundaries.

The equations are first given for Case 1 and Case 2. Then these are used and discussed in an example. The results are generalized in the Results of Acoustic Response, Section 5.5.3.

5.5.1 Case 1. Incident Pressure Wave from Downstream

Consider a flame, Figure 5.4, situated at $x^* = 0$ with no upstream incident entropy and constant area combustor located in an infinite duct. The matching conditions at $x = x^* = 0$ become

$$P_1' = P_2', \tag{5.110}$$

$$\tilde{G} = W_5 P_1', \tag{5.111}$$

and

$$s_2' = W_9 P_1'. \tag{5.112}$$

Substitute the linear acoustic solutions from 5.102-5.107 and 5.110-5.112 along with $P_1^+ = 0$ to get

$$P_1^- = P_2^+ + P_2^-, \tag{5.113}$$

$$P_2^+ - P_2^- - \frac{\rho_2 a_2}{\rho_1 a_1}(-P_1^-) = \rho_2 a_2 u_1 W_5 P_1^-, \tag{5.114}$$

and

$$B = W_9 P_1^- P_0. \tag{5.115}$$

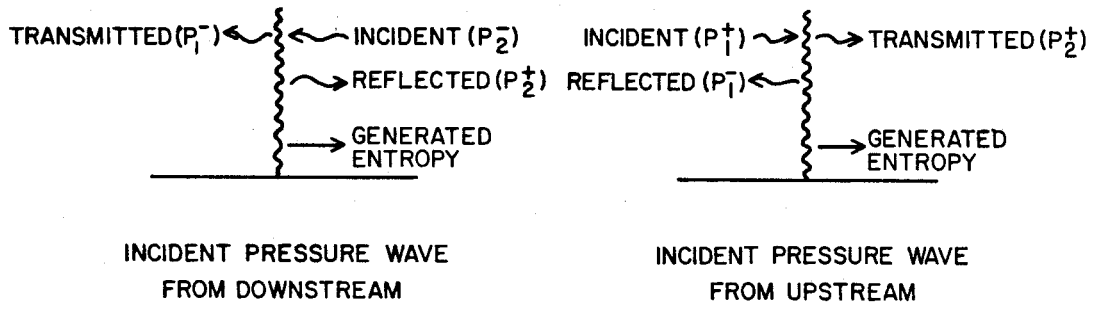

Figure 5.4: Flame Geometry for Case 1 and Case 2.

Solve P_2^+ to find

$$P_2^+ = \left(\frac{W_{30}+1}{W_{30}-1}\right) P_2^- \tag{5.116}$$

where

$$W_{30} = \left(\rho_2 a_2 u_1 W_5 - \frac{\rho_2 a_2}{\rho_1 a_1}\right)^{-1} . \tag{5.117}$$

Then P_1^- becomes

$$P_1^- = \left(\frac{2W_{30}}{W_{30}-1}\right) P_2^- \tag{5.118}$$

and B becomes

$$B = P_0 W_9 \left(\frac{2W_{30}}{W_{30}-1}\right) P_2^- . \tag{5.119}$$

Hence, the reflected and transmitted waves along with the generated entropy wave can be calculated from the mean conditions and the magnitude of the incident wave.

5.5.2 Case 2. Incident Pressure Wave from Upstream

Similar to Case 1 the case of an incident pressure wave from upstream is considered in Figure 5.4 . Then with $P_2^- = 0$ and solving in the same manner as before

find

$$P_1^- = W_{31} P_1^+ , \tag{5.120}$$

$$P_2^+ = W_{32} P_1^+ , \tag{5.121}$$

and

$$B = W_{33} P_1^+ , \tag{5.122}$$

where

$$W_{31} = -\left(\frac{1 - \frac{\rho_2 a_2}{\rho_1 a_1} - \rho_2 a_2 u_1 W_5}{1 + \frac{\rho_2 a_2}{\rho_1 a_1} - \rho_2 a_2 u_1 W_5} \right) , \tag{5.123}$$

$$W_{32} = \frac{\rho_2 a_2}{\rho_1 a_1} + \rho_2 a_2 u_1 W_5 + \left(-\frac{\rho_2 a_2}{\rho_1 a_1} + \rho_2 a_2 u_1 W_5 \right) W_{31} , \tag{5.124}$$

and

$$W_{33} = P_0 W_9 (1 + W_{31}) . \tag{5.125}$$

Example

Now we are in a position to determine the reflected and transmitted pressure waves from a plane flame given an incident pressure wave from either upstream (cold region) or downstream (hot region). Assume, for example, that $\gamma_1 = \gamma_2$ and $c_{p1} = c_{p2}$ are placed into the relations. Then relations for P_1^- and P_2^+ can be found as a function of λ. Assume that $M_1 \approx .2$, $\lambda = 4$, $\gamma = 1.3$, and $P_0 = 75 psi$.

Case I

$$P_1^- \approx \frac{6}{5} P_2^- \tag{5.126}$$

$$P_2^+ \approx \frac{1}{5} P_2^- \tag{5.127}$$

$$\frac{B}{c_{p1}} \approx -\frac{1}{5} P_2^- \tag{5.128}$$

Case II

$$P_2^+ \approx \frac{3}{5} P_1^+ \tag{5.129}$$

$$P_1^- \approx -\frac{2}{5}P_1^+ \tag{5.130}$$

$$\frac{B}{c_{p1}} \approx -\frac{1}{10}P_1^+ \tag{5.131}$$

5.5.3 Results of Acoustic Response

The results of these calculations summarized as follows where λ is the temperature ratio (to paraphrase Chu's comments):

Case I

A compression (or expansion) wave approaching the flame from downstream (the hot region) is transmitted as another compression (expansion) wave and is amplified. The reflected wave has the same sign as the incident wave and is always weaker in strength.

When $\lambda = 1$ the amplification of the transmitted wave is 1 ; if $\lambda \to \infty$ the amplification never exceeds a maximum of 2. For $\lambda = 1$ the reflected wave vanishes and as $\lambda \to \infty$ it reaches a strength of 1.

Case II

A compression (expansion) wave approaching the flame from upstream (the cold region) is transmitted as another compression (expansion) wave that is weaker. The reflected wave is a weak expansion (compression) wave.

When $\lambda = 1$ the amplitude of the transmitted wave is 1 and as $\lambda \to \infty$ the transmitted wave vanishes. Hence there exists an optimum λ for maximum transmitted amplitude. The amplitude of the reflected wave is 1 for $\lambda = 1$ and -1 for $\lambda \to \infty$.

The entropy term, B, is nonzero when $\gamma_1 = \gamma_2$ and $\Delta h_c' = 0$ as long as $\lambda \neq 1$. Hence, the entropy generation at the flame has three contributions:

1. the contribution due to the temperature discontinuity and constant specific heats (considered above),
2. the contribution due to the nonisentropic changes in specific heats, and
3. the contribution due to the fluctuations in the flame speed.

The dominant influence is from the first contribution, the temperature discontinuity.

5.5.4 Application of Acoustic Response in a Chamber

Here, the conceptual possibility of an oscillatory flame in the combustor with boundaries is examined. It is convenient to consider the combustor in the $x-t$ coordinate system. For this purpose, we will assume that both ends of the combustor are ideal closed ends, (i.e., no energy loss). The goal is to determine whether or not a disturbance can configure itself in the combustor to produce periodic oscillations. Starting with an unperturbed combustor, a pressure pulse from downstream is introduced externally (upstream works just as well). Consider the special case where the flame is in the combustor so that the acoustic path is identical in each the cold and hot regions. Using Case I and Case II at each interaction of the flame with a pulse as necessary, see if the pulse will reach a periodic existence.

The $x-t$ diagram in Figure 5.5 shows how the process is initiated in time and progresses through successive interactions. Figure 5.6 shows the steady state that occurs after approximately 25 interactions. Any acoustic pulse will settle out to this periodic oscillation.

The same pattern results regardless of whether P is incident from upstream or downstream. Certainly, the computation is more lengthy when S_t', Q', S_1', γ_1', and γ_2' and boundary conditions are included but the concept is the same.

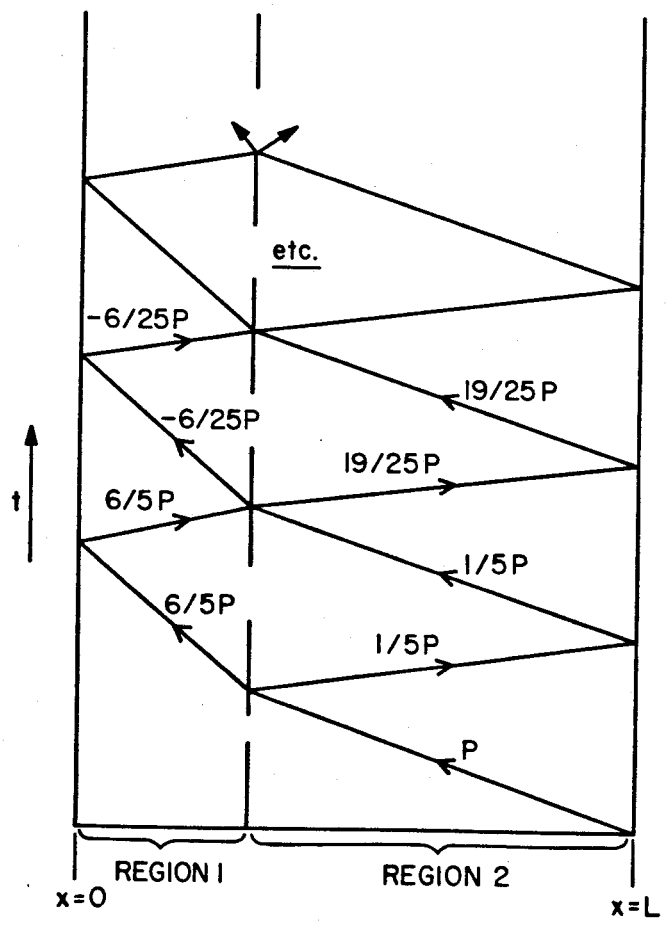

Figure 5.5: Initial $x-t$ Diagram for Pressure Pulse Initiation in a Chamber.

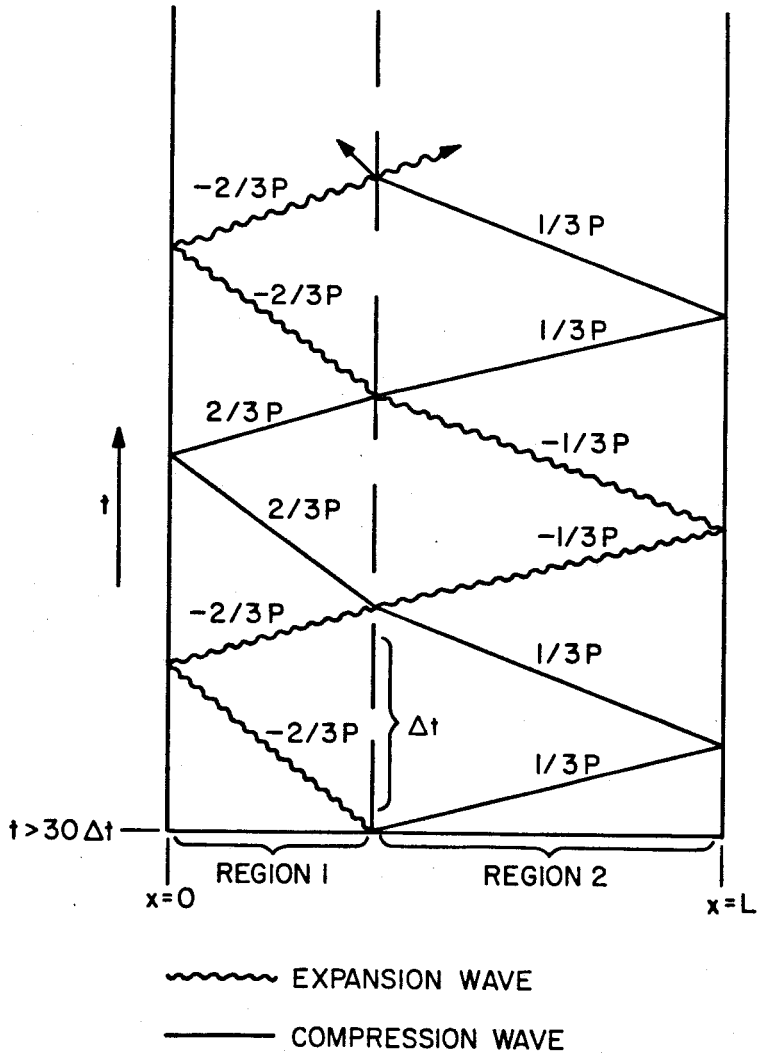

Figure 5.6: Steady State $x-t$ Diagram for Pressure Oscillation in a Chamber.

Actually, when these are considered, it is possible to have growth or decay but the periodicity should remain if the pulse is not damped out too rapidly.

In conclusion, placing a plane flame in a combustor and introducing acoustic fluctuations can produce an oscillatory configuration. This is applied in the next chapter to determine the stability of several combustor configurations. These calculations show that without boundary losses and in the absence of entropy reflection at the exit the acoustic response is neutrally stable. Including the entropy reflectance at the exit nozzle can either add or remove energy from the oscillation to cause decay or growth. It is this energy source that provides a source of driving in the combustor and is studied in Chapter 6.

5.6 Response to Entropy Waves

This section examines the response of the plane flame to a fluctuating entropy source upstream. This is of interest because an oscillating upstream shock will produce a fluctuating entropy source.

It is of practical interest to determine the response of a plane flame to incident entropy waves (obviously from upstream). This case is illustrated in Figure 5.7. Again the matching conditions can be used with $P_1^+ = P_2^- = 0$ to find

$$P_1^- = W_{40} A \,, \tag{5.132}$$

$$P_2^+ = W_{40} A \,, \tag{5.133}$$

$$B = (W_9 P_0 W_{40} + W_{10}) A \,, \tag{5.134}$$

and

$$W_{40} = \frac{\rho_2 a_2 u_1 W_6}{P_0} \left(1 + \frac{\rho_2 a_2}{\rho_1 a_1} - \rho_2 a_2 u_1 W_5 \right)^{-1} . \tag{5.135}$$

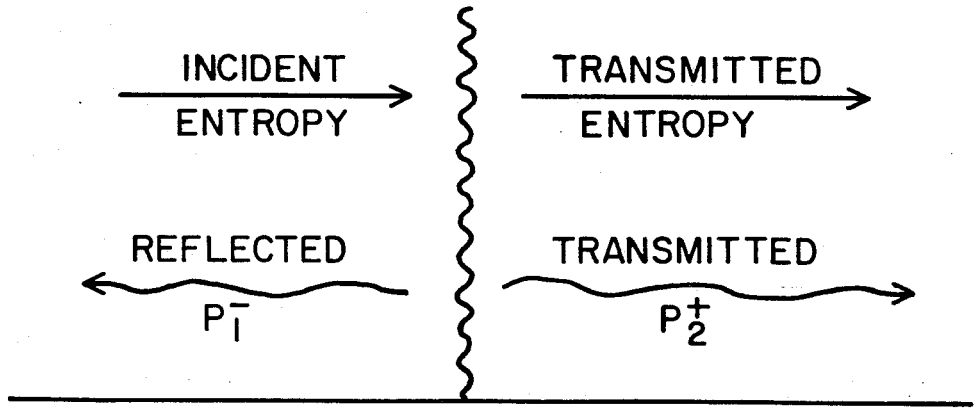

Figure 5.7: Illustration of Incident Upstream Entropy on a Plane Flame.

To illustrate, let $\gamma_1 = \gamma_2$, $c_{p1} = c_{p2}$ and $\lambda = 4$, $\gamma_1 = 1.3$, $M_1 = .2$, $P_0 = 75$ psi and $a_1 = 1500$ ft/sec. Consider also an input fluctuating entropy that is 1% of the mean specific heat. Hence, $A = .01 c_{p1}$. By calculation, we find

$$P_1^- \approx -.00274\,, \tag{5.136}$$

$$P_2^+ \approx -.00274\,, \tag{5.137}$$

and

$$B \approx (.003)(.3)\frac{BTU}{\text{lbm deg}\,R}\,. \tag{5.138}$$

From these results it is obvious that some of the energy contained in the incoming entropy wave is converted into acoustic energy in the form of pressure waves. For this example a 1% fluctuation in incoming entropy will transmit through the flame .3% downstream entropy fluctuation. A 1% incident entropy fluctuation will produce .27% fluctuation transmitted pressure wave and reflected pressure wave each of which are 180 degrees out of phase with the local entropy. The real issue of phase is whether the pressure generated by entropy is in phase

with the classical acoustics pressure. If so, then a significant driving can occur. Conversely, if out of phase with the pressure, then damping is the result.

In conclusion, an upstream entropy fluctuation incident on a plane flame will transfer some of the energy in the entropy fluctuation to acoustic energy while transmitting the remainder of energy as downstream fluctuating entropy. Whether or not this transfer tends to drive the system is dependent on the phase relationship of the pressure and entropy which is determined from the geometry and mean conditions.

5.7 Summary

The general matching conditions for a thin flame are formulated for a diverging duct. These are simplified for the case of a slightly diverging combustion chamber. Two cases are treated which illustrate the processes occurring at the flame in a constant area chamber. Case I illustrates the response of the flame as a result of incident pressure oscillations. This process produces entropy oscillations that are convected downstream. Physically, the fluctuating entropy is produced by the fluctuating heat release or more fundamentally the fluctuating mass flux across the flame [46]. Case II illustrates how energy can be transferred from the entropy field to the acoustic field at the flame when there exists upstream entropy fluctuations.

Physically, the dominant flame response can be divided into two parts: the flame response to acoustic excitation and the flame response to entropy excitation. The flame response to acoustic excitation is dominated not by the flame characteristics but by a simple step discontinuity in temperature without mean flow. This is analogous to the simple duct acoustics problem where a step temperature change occurs in the medium. The acoustic flame response to entropy disturbances (that is, the acoustic waves generated at the flame due to incident

entropy) is a direct consequence and proportional to the mean flow Mach number into the flame. (This dependence on the Mach number will become more significant in the combustor modeling of Chapter 6.) The entropy disturbance generation or transmission at the flame is determined by the local pressure and entropy field.

The plane flame can be used as a tool in the modeling of heat release in combustors with low frequency oscillations. The previous work on this topic has been expanded to include conditions of stability in a channel flow, divergent channel flows, and specific application to chamber acoustics with reflectance and arbitrary inlet thermodynamic fluctuations.

Chapter 6

Acoustics with Nonuniform Entropy Models

Chapter Six incorporates the previous two chapters along with boundary conditions to begin modeling combustors linearly. Chapter Four dealt with the methods of solving the linear boundary value acoustics with entropy problems. Chapter Five developed the conditions of a plane flame in the combustor. Here we combine these to determine the conditions of stability of combustors and inlets with entropy. Stability will be shown to be dependent on the phase of the entropy relative to pressure at each of the three coupling points. The three coupling points are the inlet shock, the flame, and the exit nozzle. When the geometry produces "in phase" coupling, then driving will occur which can sometimes overcome losses and result in linear instability. Similarly, "out of phase" coupling will remove energy from the oscillation. The phase relationships are discussed in the Section 6.2, Linear Results. The first section deals with modeling while the second presents some results of the modeling.

6.1 Linear Modeling of Combustion Chambers

The mathematical tools developed can be assembled in many ways. The goal is to find a suitable combination which will contain the most important features of the actual problem. When successful, the model will contain the major features and predict with reasonable accuracy the results when the problems parameters are changed.

As stated earlier, the acoustic chamber problem is predominantly a boundary value problem. That is not to say that the combustion processes are not important. The combustion processes are, however, a function of the acoustic field in which they take place despite how complex and poorly understood the functional relationship might be. In addition, any acoustic disturbances generated by the combustion processes are themselves subject to the boundary conditions. For these reasons it is essential that the boundary conditions be carefully applied.

The advantage of the importance of boundary conditions is that a large class of problems can be treated in a similar way even though the geometry is significantly different. It is more precise to refer to the problem as a *system.* The acoustics of the *system* is the critical issue *not* the combustor. The combustor alone without the inlet and exit boundary conditions is not a system. The exit boundary condition is usually a choked exit nozzle for high-performance propulsion systems such as rockets and ramjets. The boundary condition for a choked exit nozzle for both acoustics and entropy were discussed in detail in Section 4.3. Section 6.1.2 deals with the inlet boundary conditions.

In order to add some continuity to the following sections, the goals of each section is outlined here.

§ **6.1.1** — The linearized equations of acoustics are discussed in cases where the channel has area change. This is applicable to the inlet diffuser section

where flow through a sonic throat expands supersonically, undergoes a normal shock, and then expands subsonically to the area of the inlet duct. It is the region downstream of the shock and prior to the constant area inlet that is of interest in this section.

§ **6.1.2** — The application of the inlet boundary conditions is treated in both a general methodology and in a specific application for the ramjet combustor problem. The specific inlet details addressed are:

- Details of the different geometries considered.
- Calculation of the reflection of acoustic waves from an inlet shock.
- Shock, diffuser, and inlet duct considerations.
- Dump plane considerations.
- Calculation of entropy generation at shock.

§ **6.1.3** — The combustor modeling section treats the combustor as five distinct elements: a compact inlet, a cold flow constant area combustor section, a compact plane flame, a hot flow constant area combustor section, and a compact exit nozzle. These elements are combined to make the combustor model.

§ **6.1.4** — The linear solution combines the above model elements to obtain the characteristic equation for the eigenvalues of the linear system. The determination of the eigenvalues essentially solves the linear problem since the pressure magnitude mode shapes and phase distributions can be calculated from the eigenfunctions once the eigenfrequencies are known. These eigenfrequencies are the resonant modes of the system (like the tones from an organ pipe).

6.1.1 Consideration of P^+ and P^- with Area Change

In one-dimensional linear acoustics, three constants (possibly a function of x) are required to specify the acoustic field in one region: P^+, P^-, and A. This section discusses the linearized equations of acoustics with area change. The values of P^+ and P^- are constant in the case of a constant area duct (actually for uniform mean flow). In the case of a duct with nonuniform area, however, these constants are functions of x. With area change the differential equations of acoustics are modified and are, in general, difficult to solve. (Ref. Morse, Vibration and Sound, Section 24 : Propagation of sound in horns [54].) However, there are some simple results for the case of no mean flow and either conical or hyperbolic horns. In the case of a conical horn (axisymmetric) then we can simply replace

$$P^+ \rightarrow \frac{P^+}{\hat{x}} \quad \textit{and} \quad P^- \rightarrow \frac{P^-}{\hat{x}} \tag{6.1}$$

where $\hat{x}$ is the axial position (x-position) measured from the apex of the cone.

The entropy constants A and B from 5.102 and 5.107 will remain constant as long as the expansion is isentropic. This is typically the case for gradual area changes. Gradual area changes are also required to keep the flow essentially one-dimensional. It is not the intent to consider flow separation, recirculation, etc. in the model treated here.

The variable $\hat{x}$ in 6.1 can be replaced with

$$\hat{x} = x + x_0 \tag{6.2}$$

where x_0 is the distance to the apex of the cone from $x = 0$. (If $x_0 >> L$ then we can neglect the area change effects in P^+ and P^-.)

Rewrite equations 5.102 and 5.103 with $M_0 \rightarrow 0$ and a conical area change to get

$$P_1'(x,t) = \left(\frac{1}{x + x_0}\right) \left\{P_1^+ e^{ik_1 x} + P_1^- e^{-ik_1 x}\right\} e^{-i\Omega t} \tag{6.3}$$

$$u_1'(x,t) = \frac{1}{\rho_1 a_1}\left(\frac{1}{x+x_0}\right)\left\{P_1^+ e^{ik_1 x} - P_1^- e^{-ik_1 x}\right\} e^{-i\Omega t} \tag{6.4}$$

while 5.105 and 5.106 become

$$P_2'(x,t) = \left(\frac{1}{x+x_0}\right)\left\{P_2^+ e^{ik_2 x} + P_2^- e^{-ik_2 x}\right\} e^{-i\Omega t} \tag{6.5}$$

$$u_2'(x,t) = \frac{1}{\rho_2 a_2}\left(\frac{1}{x+x_0}\right)\left\{P_2^+ e^{ik_2 x} - P_2^- e^{-ik_2 x}\right\} e^{-i\Omega t} \tag{6.6}$$

and 5.104 and 5.107 for entropy are unchanged.

In the case of negligible area change $x_0 >> x$ and $1/(x+x_0) \rightarrow 1/x_0$. which can be incorporated into P^+ and P^- to recover the equations for constant area.

The area of the opening of a cone is given by

$$S = S_0\left(\frac{x+x_0}{x_0}\right) \tag{6.7}$$

which may be differentiated to get

$$\frac{1}{S}\frac{dS}{dx} = \frac{2}{x+x_0}. \tag{6.8}$$

Recall that $x = 0$ at a distance x_0 from the apex. When the area change becomes negligible it is equivalent to stating that x_0 becomes large and $1/S\ dS/dx$ becomes 0.

6.1.2 Inlet Boundary Conditions

This section investigates the application of the inlet boundary conditions. There are two components of the inlet boundary condition: an acoustic reflectance and an acoustic-entropy coupling relation. The treatment of the inlet boundary condition is the way in which many systems can be studied. If the inlet reflectance (that is, the reflectance of a leftward traveling acoustic wave in the combustor at the inlet end of the combustor) is known, then it can simply be used. The inlet,

however, may be a dump plane, which is then connected to an inlet duct. The inlet duct may in turn be terminated with a choked inlet diffuser as in a missile application. In a connected pipe experiment, however, the inlet duct may be connected by another dump plane to a plenum chamber and so on back upstream. Since this flow is subsonic, it is not decoupled and is part of the acoustic system. It is the resonance of this system which is important.

The inlet duct is treated as an acoustic region and is coupled to the combustor acoustic region by matching conditions. Typically the matching condition at a dump plane is given to be continuity of mass and pressure, while the expansion is treated as nearly isentropic. Thus the inlet boundary condition is replaced by matching conditions and an upstream inlet duct boundary condition. This process can be repeated until each acoustic element has been accounted for with matching conditions and a new boundary condition.

The specific geometries of interest are shown in Figure 6.1. The first two are useful in analyzing experimental tests that are not terminated by an inlet diffuser shock. The third geometry is useful in analyzing actual applications as well as experimental tests which have inlet shock waves. The shock wave plays an important role in defining the acoustic system because it clearly defines the upstream boundary. No acoustic waves can penetrate a shock wave since the acoustic velocity is less than the flow entering the shock.

The shock wave also has characteristics which are significantly different from the geometry shown in Figure 6.1 (Geometry 1). The acoustic energy is not dissipated by the acoustic wall, plenum, plenum-inlet dump, inlet duct, and inlet-combustor dump of Geometry 1. Also, no significant entropy fluctuation is generated upstream of the combustor in this geometry. The inlet shock on the other hand, absorbs about ninety percent of the incident acoustic energy and generates an upstream fluctuating entropy. As a result, the *system* acoustics are

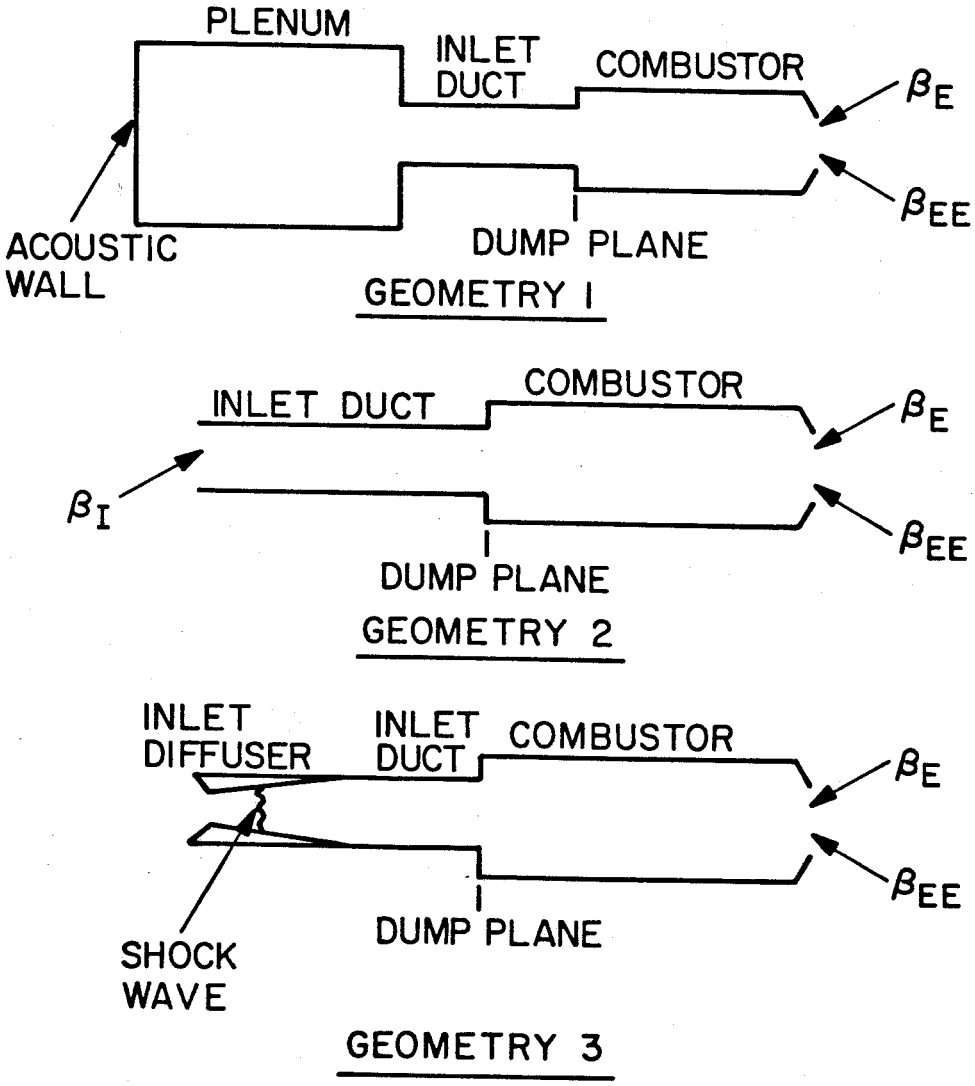

Figure 6.1: Three Modeling Geometries for One-Dimensional Ramjets.

significantly different.

Since the equations are linear, it is possible to define a reflectance at the combustor inlet that contains all of the upstream conditions. This is the procedure adopted here. The following sections develop the inlet conditions required for Geometry 3 in Figure 6.1, which will be used in the combustor modeling.

Calculation of Reflectance

Calculate $\beta_I = P_1^+/P_1^-$ and A/P_1^- for the geometry shown in Figure 6.2. The inlet shock, diffuser, inlet duct, and inlet-combustor dump plane are used to determine the combustor inlet reflectance β_I and entropy A/P_1^-.

Region D

$$P_d'(x,t) = \quad P_0 \left\{ P_d^+ e^{ik_1 x} + P_d^- e^{-ik_1 x} \right\} e^{-i\Omega t} \tag{6.9}$$

$$u_d'(x,t) = \frac{P_0}{\rho_1 a_1} \left\{ P_d^+ e^{ik_1 x} - P_d^- e^{-ik_1 x} \right\} e^{-i\Omega t} \tag{6.10}$$

Region C

$$P_c'(x,t) = \quad P_0 \frac{1}{x + x_v} \left\{ P_c^+ e^{ik_1 x} + P_c^- e^{-ik_1 x} \right\} e^{-i\Omega t} \tag{6.11}$$

$$u_c'(x,t) = \frac{P_0}{\rho_1 a_1} \frac{1}{x + x_v} \left\{ P_c^+ e^{ik_1 x} - P_c^- e^{-ik_1 x} \right\} e^{-i\Omega t} \tag{6.12}$$

The shock reflectance can be calculated from the shock admittance which is calculated from the linear results of Culick and Rogers:

$$\beta_{ISH}^0 = \frac{1 + A_{SH}^0}{1 - A_{SH}^0} = \frac{P_c^+ e^{-ik_1 x_s}}{P_c^- e^{ik_1 x_s}}. \tag{6.13}$$

The shock reflectance is given for the shock location at $x = 0$. The exponential terms in (above) contain the correction for the shock located at $x = -x_s$ rather than $x = 0$.

The matching at $x = -L_I$ is simply

$$P_d^+ = \frac{P_c^+}{x_v - L_I} \tag{6.14}$$

and

$$P_d^- = \frac{P_c^-}{x_v - L_I}. \tag{6.15}$$

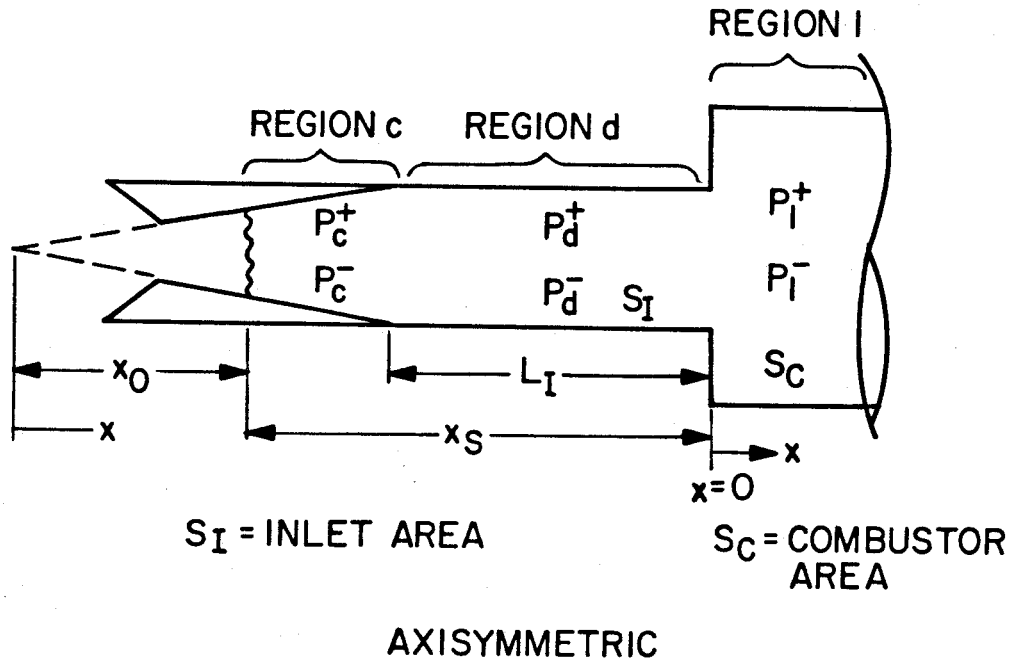

Figure 6.2: Geometry of Inlet Diffuser and Inlet with Shock.

Dump Plane

One of the advantageous features of ramjet combustors is the abrupt area change between the inlet and the combustor. In the coaxial dump plane version of ramjet configurations, the sudden area change will produce a recirculation zone in the flow field. In combustion flows this region fills with hot burned exhaust gases and acts as a strong flame holder at the inlet to the combustor. Although there are losses associated with sudden expansions, the total pressure loss for the dump plane is less than for conventional wedge-type flame holders often employed in gas turbine afterburners.

A simple dump plane area change is a nonisentropic process unless the areas are equal, $S_I = S_C$. However, for a first approximation, an isentropic area change is assumed even though $S_I \neq S_C$. More important than the assumption that the expansion be isentropic is that entropy generation be non-fluctuating. This is generally a good assumption since the geometry is fixed. Matching across the dump plane involves mass and pressure continuity. Pressure continuity gives

$$P_1^+ + P_1^- = P_d^+ + P_d^- . \tag{6.16}$$

The mass continuity is

$$u_d' = u_1' \frac{\rho_1}{\rho_d} \frac{S_C}{S_I} \tag{6.17}$$

or

$$P_d^+ - P_d^- = (P_1^+ - P_1^-) \frac{a_d}{a_l} \frac{S_C}{S_I} \tag{6.18}$$

where this form of mass continuity requires that the fluctuating entropy not change across the dump plane. (This is the same approximation as used in the above paragraph.) Let

$$\beta_{ISH} = \beta_{ISH}^{\circ} e^{i2k_1 x_s} \tag{6.19}$$

and then

$$\beta_{ISH} = \frac{P_c^+}{P_c^-} = \frac{P_d^+}{P_d^-} . \tag{6.20}$$

Define

$$A_{ISH} = \frac{\beta_{ISH} - 1}{\beta_{ISH} + 1} \tag{6.21}$$

to find

$$\beta_I = \beta_{ICALC} = \frac{P_1^+}{P_1^-} = \frac{\frac{a_d}{a_1}\frac{S_C}{S_I} + A_{ISH}}{\frac{a_d}{a_1}\frac{S_C}{S_I} - A_{ISH}} . \tag{6.22}$$

Substitute $\frac{a_d}{a_1}$ from the isentropic expansion equations to get

$$\left(\frac{a_d}{a_1}^2\right) = \frac{1 + \frac{\gamma-1}{2} M_1^2}{1 + \frac{\gamma-1}{2} M_d^2} \tag{6.23}$$

and

$$\frac{\rho_1}{\rho_d} = \left(\frac{1+\frac{\gamma-1}{2}M_d^2}{1+\frac{\gamma-1}{2}M_1^2}\right)^{\frac{1}{\gamma-1}} . \tag{6.24}$$

From continuity find

$$\frac{u_d}{u_1} = \left(\frac{1+\frac{\gamma-1}{2}M_d^2}{1+\frac{\gamma-1}{2}M_1^2}\right)^{\frac{1}{\gamma-1}} \frac{S_C}{S_I} \tag{6.25}$$

and hence,

$$\frac{M_d}{M_1} = \left(\frac{1+\frac{\gamma-1}{2}M_d^2}{1+\frac{\gamma-1}{2}M_1^2}\right)^{\frac{\gamma+1}{2(\gamma-1)}} \frac{S_C}{S_I} . \tag{6.26}$$

Calculation of Entropy Generation at Shock

The presence of an acoustic disturbance downstream of the inlet shock will change the equilibrium position of shock in the diffuser. This adjustment in the shock position changes the shock conditions and thus the entropy generation across the shock. For a stationary shock, the entropy generation is constant, but, if the shock wave oscillates then there is generation of a fluctuating entropy also. In this section we will calculate the fluctuating entropy source.

The linear shock position is given by $x_s = -\bar{x}_s + x_s'$, and from Culick and Rogers [10]

$$x_s' = \left(\frac{C}{1-i\omega\tau}\right) P_c'(-\bar{x}_s) \tag{6.27}$$

$$C = \frac{-1}{P_{upst}} \left(\frac{1}{S}\frac{dS}{dx}\right)^{-1} \frac{(\gamma+1)^2}{2\gamma(\gamma-1)} \left(1+\frac{\gamma^2+1}{\gamma-1}\bar{M}_{1s}^2\right)^{-1} \tag{6.28}$$

$$\tau = \frac{1}{a_{1s}} \left(\frac{1}{S}\frac{dS}{dx}\right)^{-1} \frac{2(\gamma+1)\bar{M}_{1s}}{(\gamma-1)} \left(1+\frac{\gamma^2+1}{\gamma-1}\bar{M}_{1s}^2\right)^{-1} \tag{6.29}$$

where all terms are calculated at the mean shock location. Here, S represents the area at the shock. Also, from 6.11-6.26 we find

$$\frac{P_c'(-\bar{x}_s)}{P_1^-} = \left(\frac{x_v - L_I}{x_v - \bar{x}_s}\right) \left(\frac{1}{1+\beta_{ISH}}\right) (\beta_I + 1)(\beta_{ISH} e^{-ik_1\bar{x}_s} + e^{ik_1\bar{x}_s}) P_0 . \tag{6.30}$$

To determine the fluctuating entropy wave generated at the oscillating shock in a polytropic gas (i.e. $s = c_v \ln(P/\rho^\gamma)$), look at the shock wave in terms

of the strength parameter Z (Ref. Whitham "Linear and Nonlinear Waves" [38])

$$Z = \frac{P_2 - P_1}{P_1} = \frac{2\gamma(M^2 - 1)}{\gamma + 1}, \tag{6.31}$$

$$M = \frac{U - u_1}{a_1}, \tag{6.32}$$

and

$$\frac{s_2 - s_1}{c_v} = \ln\left\{(1+Z)\left(1 + \frac{\gamma - 1}{2\gamma}Z\right)^{\gamma}\left(1 + \frac{\gamma+1}{2\gamma}Z\right)^{-\gamma}\right\} \tag{6.33}$$

where the subscript 1 is for entering the shock wave and 2 is for leaving the shock. M is the mach number of the flow ahead of the shock relative to the shock.

Consider the shock strength, Z, where P_1 is the mean pressure upstream of the shock and P_2 is the mean pressure downstream of the shock. When the inlet flow is uniform (i.e. $P_1 = P_{1_0}$) then

$$Z = \frac{P_2'(x,t) + P_2(x) - P_1(x)}{P_1(x)} \tag{6.34}$$

and for longer wavelengths treat $P(x,t) \approx P(\bar{x},t)$ where $x = \bar{x} + x'$ to give

$$Z = \frac{P_2'(\bar{x},t) + P_2(\bar{x}+x') - P_1(\bar{x}+x')}{P_1(\bar{x}+x')}. \tag{6.35}$$

As long as x' is small then

$$P_i(\bar{x}+x') = P_i(\bar{x}) + \frac{dP_i(\bar{x})}{dx}x' + H.O.T. \ . \tag{6.36}$$

In steady state,

$$\bar{Z} = \frac{P_{2_0}(\bar{x}) - P_{1_0}(\bar{x})}{P_{1_0}(\bar{x})}. \tag{6.37}$$

If x' is small then

$$1 >> \frac{1}{P_{1_0}(\bar{x})}\frac{dP_{1_0}(\bar{x})}{dx}x' \tag{6.38}$$

Define Z' so

$$Z = \bar{Z} + Z' \tag{6.39}$$

and

$$Z' = \frac{1}{P_{1_0}(\bar{x})}\left\{P_2'(\bar{x},t) + \left(\frac{dP_{2_0}(\bar{x})}{dx} - (1+\bar{Z})\frac{dP_{1_0}(\bar{x})}{dx}\right)x'\right\}. \tag{6.40}$$

Return to the inlet notation to get

$$Z' = \frac{P_c'(-\bar{x}_s)}{P_{upst}}\left\{1 + Q_1 P_{upst}\frac{1}{S}\frac{dS}{dx}\left(\frac{C}{1-i\omega\tau}\right)\right\} \tag{6.41}$$

where

$$Q_1 = \left(\frac{\gamma M_{2S}^2}{1-M_{2S}^2}\right)\frac{P_{2S}}{P_{1S}} - (1+\bar{Z})\left(\frac{\gamma M_{1S}^2}{1-M_{1S}^2}\right). \tag{6.42}$$

After rearrangement and the expansion of $ln(1+x)$ for small x

$$\frac{s_c'}{c_v} = Z' \cdot Z_{BAR1} \tag{6.43}$$

where

$$Z_{BAR1} = \frac{1}{1+\bar{Z}} + \frac{\gamma}{\frac{2\gamma}{\gamma-1}+\bar{Z}} - \frac{\gamma}{\frac{2\gamma}{\gamma+1}+\bar{Z}}. \tag{6.44}$$

Then, assuming the expansion in the diffuser from the shock to the inlet duct is isentropic, it can be shown that

$$\frac{A}{P_1^-} = c_v\frac{P_c'(\bar{x}_s)}{P_1^-}\frac{1}{P_{upst}}Q_2\, Z_{BAR1}\, e^{i\frac{\Omega}{u_d}(\bar{x}_s)} \tag{6.45}$$

where

$$Q_2 = \left\{1 + Q_1 P_{upst}\frac{1}{S}\frac{dS}{dx}\left(\frac{C}{1-i\omega\tau}\right)\right\}. \tag{6.46}$$

To calculate this, use

$$\bar{Z} = \frac{P_{2_0} - P_{1_0}}{P_{1_0}}, \tag{6.47}$$

$$\frac{P_c(-\bar{x}_s)}{P_{upst}(-\bar{x}_s)} = \bar{Z} + 1 = \frac{P_{1S}}{P_{2S}}, \tag{6.48}$$

$$M = \frac{U - u_1}{a_1}, \tag{6.49}$$

and

$$\bar{Z} = \frac{2\gamma}{\gamma+1}(M_{1S}^2 - 1). \tag{6.50}$$

The result here is that an inlet shock, inlet duct, and dump plane have been reduced to boundary conditions applied at the upstream end of the combustor channel. The boundary conditions are given by 6.22 and 6.45. Reducing these components of the inlet to combustor boundary conditions simplifies the characteristic equation for the eigenfrequencies.

6.1.3 Combustor Modeling

This section formulates a five element combustor that uses as one element the compact inlet information developed in the previous sections. The combustor is modeled as two acoustic regions divided by the plane flame of Chapter 5 as shown in Figure 6.2. The inlet and exit boundary conditions are used to terminate the acoustic regions upstream and downstream of the flame. The only available experimental data [6] [15] are for constant area, so that is the case treated here.

The reflectance, β_I, can be coupled with the combustor region from $x = 0$ to $x = x_f$ and the flame matching conditions to determine a new reflectance β_{Iflame} at $x = x_f$. The procedure is similar to defining the inlet reflectance. Also recall that A is the entropy constant in region 1 (the acoustic region upstream of the flame) and B for region 2 (the acoustic region downstream of the flame). It is assumed that β and A/P^- are known from 6.1.1. The equations of P, u, and s in regions 1 and 2 are

$$P_1 = P_0 \left(P_1^+ e^{ik_1 x} + P_1^- e^{-ik_1 x} \right) e^{-i\Omega t}, \tag{6.51}$$

$$u_1 = \frac{P_0}{\rho_1 a_1} \left(P_1^+ e^{ik_1 x} + P_1^- e^{-ik_1 x} \right) e^{-i\Omega t}, \tag{6.52}$$

$$s_1 = A e^{i\Omega/(u_1)x} e^{-i\Omega t}; \tag{6.53}$$

and

$$P_2 = P_0 \left(P_2^+ e^{ik_2 x} + P_2^- e^{-ik_2 x} \right) e^{-i\Omega t}, \tag{6.54}$$

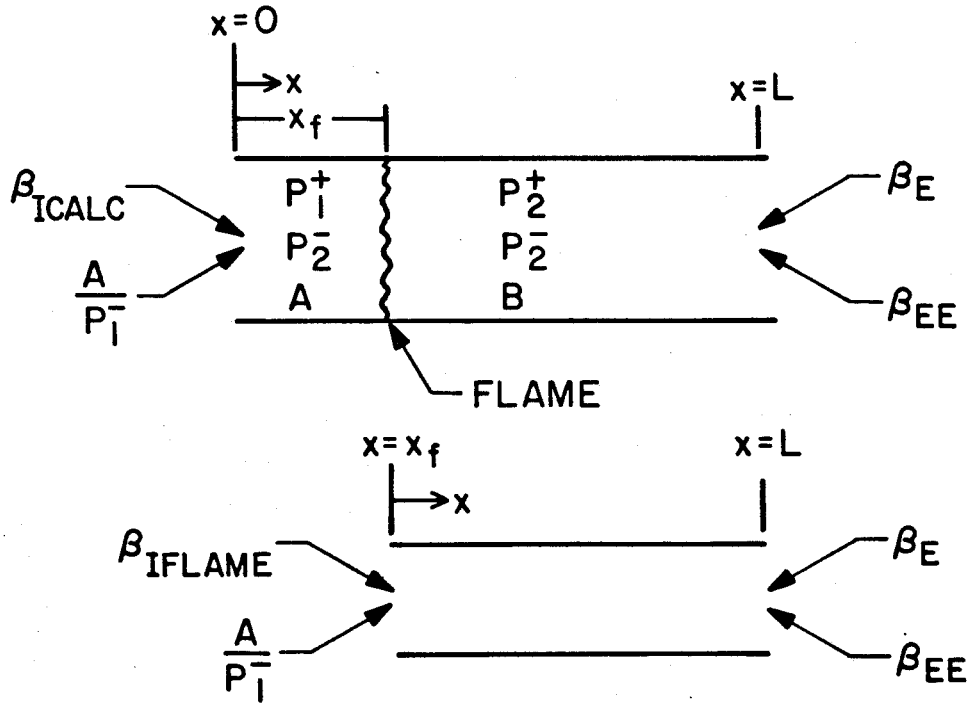

Figure 6.3: Combustor Model Geometry.

$$u_2 = \frac{P_0}{\rho_2 a_2}\left(P_2^+ e^{ik_1 x} + P_2^- e^{-ik_2 x}\right) e^{-i\Omega t}\,, \tag{6.55}$$

$$s_2 = B e^{i\Omega/(u_2)x} e^{-i\Omega t} \tag{6.56}$$

where A and B are the constants which specify the magnitude of the entropy in regions 1 and 2 respectively. Define β_{Iflame} such that

$$\beta_{Iflame} = \frac{P_2^+}{P_2^-}\,. \tag{6.57}$$

The flame matching conditions at $x = x_f$ are

$$P_1' = P_2'\,, \tag{6.58}$$

$$\tilde{G} = W_5 P_1' + W_6 s_1'\,, \tag{6.59}$$

$$s_2' = W_9 P_1' + W_{10} s_1'\,, \tag{6.60}$$

and $P_{10} = P_{20}$ since the flame is flat and not curved. Define Γ_i to be :

$$\Gamma_1 = \beta_I e^{ik_1 x_f} + e^{-ik_1 x_f}\,, \tag{6.61}$$

$$\Gamma_2 = \beta_I e^{ik_1 x_f} - e^{-ik_1 x_f}\,, \tag{6.62}$$

$$\Gamma_3 = \left(\Gamma_1(1 - \rho_2 a_2 u_1 W_5) - \Gamma_2 \frac{\rho_2 a_2}{\rho_1 a_1}\right) e^{ik_2 x_f}\,, \tag{6.63}$$

$$\Gamma_4 = \left(\Gamma_1(1 + \rho_2 a_2 u_1 W_5) + \Gamma_2 \frac{\rho_2 a_2}{\rho_1 a_1}\right) e^{-ik_2 x_f}\,, \tag{6.64}$$

$$\Gamma_5 = \rho_2 a_2 u_1 \Gamma_1 \frac{W_6}{P_{20}} e^{i\frac{\Omega}{u_1}x_f} \frac{A}{P_1^-}\,, \tag{6.65}$$

$$\Gamma_6 = \Gamma_3 \Gamma_1 - \Gamma_5 e^{ik_2 x_f}\,, \tag{6.66}$$

$$\Gamma_7 = \Gamma_4 \Gamma_1 + \Gamma_5 e^{-ik_2 x_f}\,, \tag{6.67}$$

$$\Gamma_8 = W_9 P_{20}(\beta_{Iflame} e^{ik_2 x_f} + e^{-ik_2 x_f}) e^{-i\frac{\Omega}{u_2}x_f}\,, \tag{6.68}$$

and

$$\Gamma_9 = W_{10} e^{i\frac{\Omega}{u_1}x_f} e^{-i\frac{\Omega}{u_2}x_f}\,. \tag{6.69}$$

After some manipulation find

$$\frac{P_2^+}{P_2^-} = \beta_{Iflame} = \frac{\Gamma_7}{\Gamma_6} \tag{6.70}$$

and

$$\frac{B}{P_2^-} = \Gamma_8 + \Gamma_9 \frac{A}{P_1^-} \frac{P_1^-}{P_2^-} . \tag{6.71}$$

To avoid confusion we call the reflectance a condensed reflectance when it contains more than just a reflectance and is generally applied at a position other than where the original reflectance occurred. The procedure of this section compresses again the already condensed inlet reflectance at the upstream end of the combustor, β_{ICALC}, the section of the combustor upstream of the flame, and the flame matching conditions to a new combustor reflectance, β_{Iflame}, applied at $x = x_f$. This sets the boundaries for the combustor to be used in the frequency calculation of the next section. The application of the condensed reflectance does not influence the generality of the linear formulation.

6.1.4 Linear Frequency Calculation

The previous sections reduce the inlet with the inlet shock, the dump plane, and the plane flame to a single set of boundary conditions for the inlet to the combustor. With equations 6.54 and 6.56 and the boundary conditions β_{Iflame} and β_{EXIT}, eliminating P_2^+ and P_2^- gives

$$F(\Omega) = 1 - \beta_{Iflame}\beta_{EXIT} = 0 . \tag{6.72}$$

Equation 6.72 gives a transcendental equation for the linear eigenfrequencies which are the acoustic resonant modes of the *system*. Recall that B/P_2^- is required to calculate β_{EXIT} . The eigenfrequencies, Ω, are found by solving for the zeroes of 6.72. For simple cases this can be done analytically but for more typical geometries, 6.72 is solved numerically. Once the eigenfrequencies are known,

they can be used to calculate the eigenfunctions and hence the pressure and velocity mode shapes. These calculations are done in the following section for several different cases.

6.1.5 Summary of Linear Modeling

As shown in the previous sections, important aspects of a ramjet combustor (such as the inlet shock, dump plane, heat release across a flame sheet, and the choked exit nozzle) have been assembled into the linear model. Many of the actual processes can be accounted for in a simple and realistic way. Two important items that can be studied are the energy contributions due to entropy coupling and the compilation of both acoustic and entropy contributions into one stability model. Specific cases will be presented to assess stability as well as the physical consequences of the individual components in the next section.

6.2 Linear Results

The results of calculations using the analysis of this chapter are presented in this section for six cases. The six cases were chosen to either verify the procedure, or to illustrate physical processes. The six cases are called Runs 1 through 6. The first two cases, Runs 1 and 2 were chosen primarily to compare with other analytical solutions. Run 3 studies the response of the flame to incident entropy fluctuations (from upstream). Runs 3 through 5 all treat the upstream entropy magnitude and phase as an input parameter. The entropy magnitude is specified for the linear acoustic-entropy coupling upstream (that is, the upstream entropy is generated as a linear function of pressure). Run 4 studies the stability of a combustor with no flame but upstream fluctuating entropy and exit entropy reflectance. Run 5 combines the exit entropy reflectance and the plane flame. Again, the upstream

entropy coupling is parametrically varied in the stability study. Run 6 uses the linear inlet shock theory to determine the upstream acoustic-entropy coupling. It is convenient to define the notation

$$\mathcal{H} = \frac{A}{c_p P_1^-}, \tag{6.73}$$

where $\mathcal{H}$ is the nondimensional measure of the magnitude (and phase) of the acoustic-entropy coupling specified at the origin.

6.2.1 Run 1 – Verification

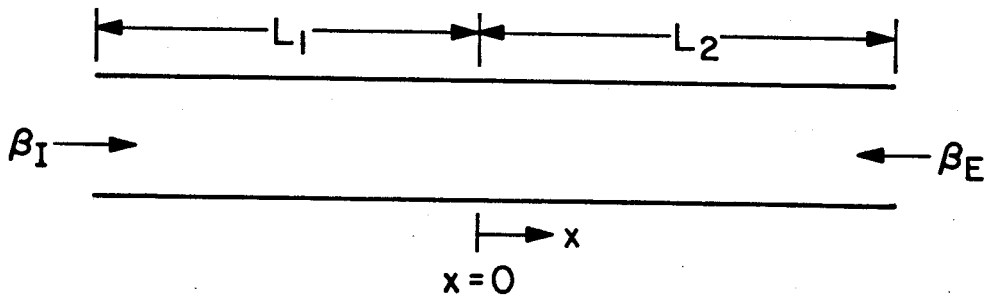

Figure 6.4: Geometry for Analytical Solution.

Run 1 is used to verify that the calculations match those of a previous linear acoustic eigenvalue code. The example contains a constant area duct, no flame, and complex boundary conditions of magnitude different from 1. An analytical solution was shown by Humphrey [11] to be

$$1 = \beta_I \beta_E e^{i2K(L_1+L_2)}. \tag{6.74}$$

The geometry is shown in Figure 6.4. The conditions used for Run 1 were:

- $a = 1500$ ft/sec
- $M_0 = .25$
- $L_1 + L_2 = 7.7$ ft
- $\beta_I = (.25, .25)$
- $\beta_E = (1, 6)$

The frequencies calculated from 6.72 are given in Table 6.1. The calculated results were identical to the analytical results obtained from 6.74. This is not too surprising since the calculated results are also analytical as opposed to numerical. Since the boundary conditions are independent of frequency and there is no entropy, the damping (or growth) is the same for all modes.

solution	ω	α
1	-31.84	11.129
2	59.47	11.129
3	150.79	11.129
4	242.10	11.129
5	333.42	11.129
6	424.73	11.129

Table 6.1: Run 1 – Calculated Eigenfrequencies (Hz).

The energy loss or gain is determined by the product of the magnitude of the inlet and exit reflectance. If the magnitude is greater than one, the oscillation grows exponentially due to the net flux of energy into the duct at the boundaries. When the magnitude is less than 1, the oscillation decays exponentially due to energy loss at the boundaries. If the magnitude is identically one, then the oscillation is neutrally stable.

6.2.2 Run 2 – Verification

Run 2 is an example of a simple organ pipe mode with one end open and one end closed with mean flow (hence $\beta_1 = 1$ and $\beta_E = -1$). The analytical frequencies are solved from 6.74 to be

$$\omega_n = \frac{a}{\lambda}(1 - M^2)^{-1}(2n + 1) \tag{6.75}$$

where a is the sonic velocity and λ is the first fundamental wave length. Hence, the frequency is approximately $(2n+1)\,87.89Hz$. The analytical damping coefficient is identically zero when both reflectances have magnitude 1. Table 6.2 summarizes the eigenvalues and contains the frequency and damping coefficient for both the analytical solution 6.75 and the calculated solution from 6.72 with $\beta_{flame} = \beta_I$ and $\beta_{EXIT} = \beta_E$. The analytical results were identical to the calculated results.

mode	n	analytical		calculated	
1	0	87.89	0	87.89	.000
2	1	263.67	0	263.67	.000
3	2	439.45	0	439.45	.000
4	3	615.23	0	615.23	.000
5	4	791.02	0	791.02	.000
6	5	966.80	0	966.80	.000

Table 6.2: Run 2 – Eigenfrequency Calculations.

6.2.3 Run 3 – Response of Flame to Entropy

Run 3 studies the response of a plane flame to incident entropy waves. The values for the flame conditions used to determine the response of the flame to incident

entropy fluctuations are:

- $T_{1_0} = 950\ ^\circ R$
- $P_{1_0} = 75psi$
- $\lambda = 4$
- $L = 4$ ft
- $\gamma = 1.4$
- $c_p = .3$ BTU/lbm R

Two cases are considered. Run 3a studies the flame response in the absence of inlet and exit reflectances. Run 3b studies the flame response with conditions similar to Run 3a with the addition of an acoustic wall at the exit plane. Run 3b will provide a comparison basis for Run 4.

Run 3a

Run 3a uses the given values for the flame conditions with all of the duct reflectances set to zero. This simulates a flame in an infinite medium where no boundary conditions are present. This is similar to the entropy response of the plane flame presented in Section 5.6. If a constant fluctuating entropy is applied from upstream, then the flame will respond so as to reflect and transmit a constant pressure wave as well as transmit an entropy wave. Thus, the only significant value of $\mathcal{H}$ (which is the ratio of the magnitude of the entropy wave over the reflected pressure wave, or coupling factor, in Table 6.3) is the one which produces a neutrally stable wave (growth rate, α, is zero).

The neutrally stable value of $\mathcal{H}$ can be calculated from the results of Chapter 5. Consider the response of a plane flame (with no reflec-

tions). Figure 6.5 shows the configuration of the flame. Solving (from momentum, energy, and mass conservation) the matching conditions 5.39, 5.95, and 5.101 across the flame from Section 5.4.3, it is possible to find

$$\mathcal{H} = \frac{\rho_1 a_1 + \rho_2 a_2 - \rho_1 \rho_2 a_1 a_2 u_1 W_5}{\rho_1 \rho_2 a_1 a_2 u_1 W_6 c_{p1}}. \tag{6.76}$$

Substitute the values of the known constants and proper unit conversions into 6.76 and nondimensionalize to get $\mathcal{H}^* \approx 3.202$, where the * represents the neutrally stable value. The value calculated from 6.72 was identical to the analytical value from 6.76.

$\mathcal{H}$	Ω_1		Ω_2		Ω_3		Ω_4	
	ω	α	ω	α	ω	α	ω	α
$2.5*10^{-5}$	141	-526	422	-526	703	-526	984	-526
$2.5*10^{-4}$	141	-423	422	-423	703	-423	984	-423
$2.5*10^{-3}$	141	-320	422	-320	703	-320	984	-320
$2.5*10^{-2}$	141	-217	422	-217	703	-217	984	-217
$2.5*10^{-1}$	141	-114	422	-114	703	-114	984	-114
2.5	141	-11	422	-11	703	-11	984	-11
$2.5*10^{1}$	141	92	422	92	703	92	984	92

Table 6.3: Run 3a – Dependence of Frequency, ω, and Damping, α, on Entropy.

The entropy, $\mathcal{H}$, is the only driving mechanism in this case. Thus, to get a neutrally stable reflected pressure wave of 1 psi then an entropy wave must be applied of magnitude $.0128 BTU/lbm/\,^\circ R$.

This example is convenient in terms of describing physically the processes which are occurring. When $\mathcal{H} \approx 3.202$, the upstream entropy can be treated as either supplied (arbitrary) or coupling generated.

$x(ft)$	Ω_1		Ω_2		Ω_3		Ω_4	
	ω	α	ω	α	ω	α	ω	α
1	141	.001	422	.001	703	.001	984	.001
2	70	.0004	211	.0004	352	.0004	492	.0004

Table 6.4: Run 3a – Flame Position Dependence for $\mathcal{H} = 3.202$.

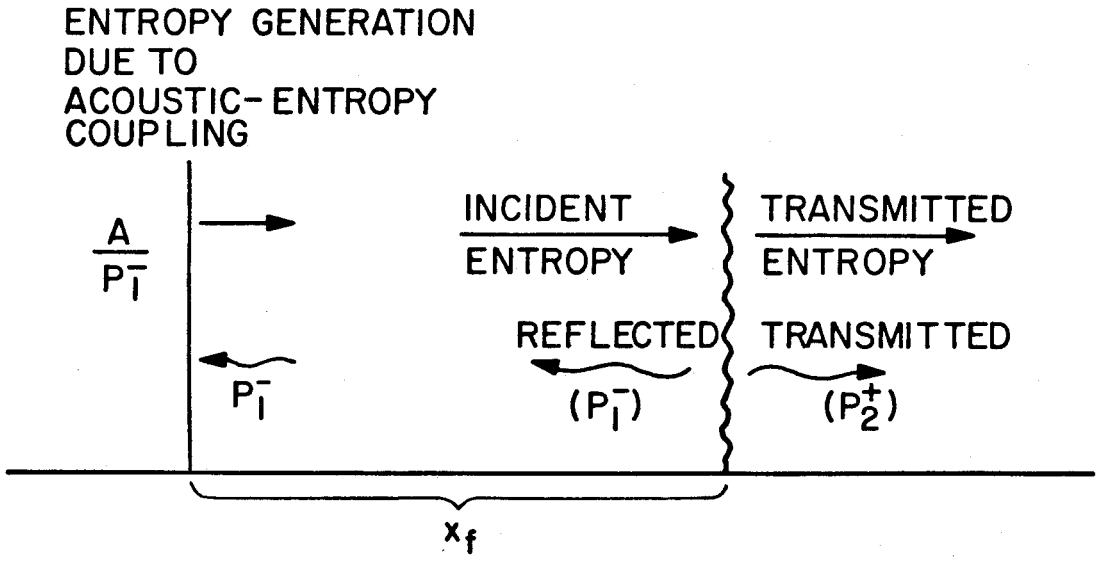

Figure 6.5: Run 3a – Flame and Inlet Configuration.

The transfer of energy from the entropy fluctuations to the acoustic fluctuations at the flame and from the acoustic field to entropy at the inlet produces a net energy into the acoustic field. This is obvious since the steady process generates two acoustic traveling waves which radiate acoustic energy out of the region upstream and downstream. The energy is supplied by the the response of the flame.

In this simple example it is easy to calculate the frequency from purely conceptual terms. The important time scales in this problem are the acoustic travel time from the flame to the inlet (at $x = 0$)

$$\tau_{acoustic} = \frac{x_f}{a_0(1 - M_0)}, \tag{6.77}$$

and the convective time for the entropy wave to travel from the inlet to the flame

$$\tau_{convective} = \frac{x_f}{a_0 M_0}. \tag{6.78}$$

There are phase relationships between the pressure and entropy at each of the coupling locations. These can be converted into equivalent time delays. At the inlet we let the phase between the pressure and generated entropy be ϕ_I so that the associated time delay is

$$\tau_{inlet} = \frac{\phi_I}{2\pi\omega} \tag{6.79}$$

where ω is in Hertz. Similarly, for the flame

$$\tau_{flame} = \frac{\phi_{flame}}{2\pi\omega}. \tag{6.80}$$

For this specific example, ϕ_I is zero and

$$\tau_{flame} = (1 - 2n)\pi. \tag{6.81}$$

For this choice of ϕ_{flame}, the reflected pressure wave is 180 degrees out of phase with the incident entropy wave as in the case of a choked

exit nozzle. The period for a cycle is given by the sum of these to be

$$\tau = \tau_{acoustic} + \tau_{convective} + \tau_{inlet} + \tau_{flame}. \tag{6.82}$$

The frequency can be solved to find

$$\omega_n = \frac{(1+2n)a_0(1-M_0)M_0}{2x_f}. \tag{6.83}$$

This precisely reproduces the frequencies calculated in Table 6.3.

Figure 6.6 is a plot of the magnitude and phase distribution for the pressure and entropy. The drop in entropy magnitude at $x/L_C = .25$ indicates a conversion of energy from the entropy to acoustics. The constant value in pressure magnitude indicate that the traveling pressure waves radiated from the flame travel without losses with changes in position and without interacting with other traveling waves to form standing wave patterns. The phase distribution has a positive slope downstream of the flame and negative slope upstream. Hence, two pressure waves are produced and travel in opposite directions. The difference in slope reflects that the acoustic velocity upstream is $a_0(1-M_0)$ and downstream is $a_0(1+M_0)$. The slope of the entropy is always positive since the mean flow (convective velocity) is positive. The change in the slope across the flame is due to the change in the mean flow due to the mean heat addition.

Although the flame oscillates about its mean position, the motion is very small. Typical magnitudes of flame displacement are of the order $10^{-5} ft$. This justifies the analytical approximation that the acoustic terms into and out of the flame can be evaluated at the mean flame position.

Run 3b

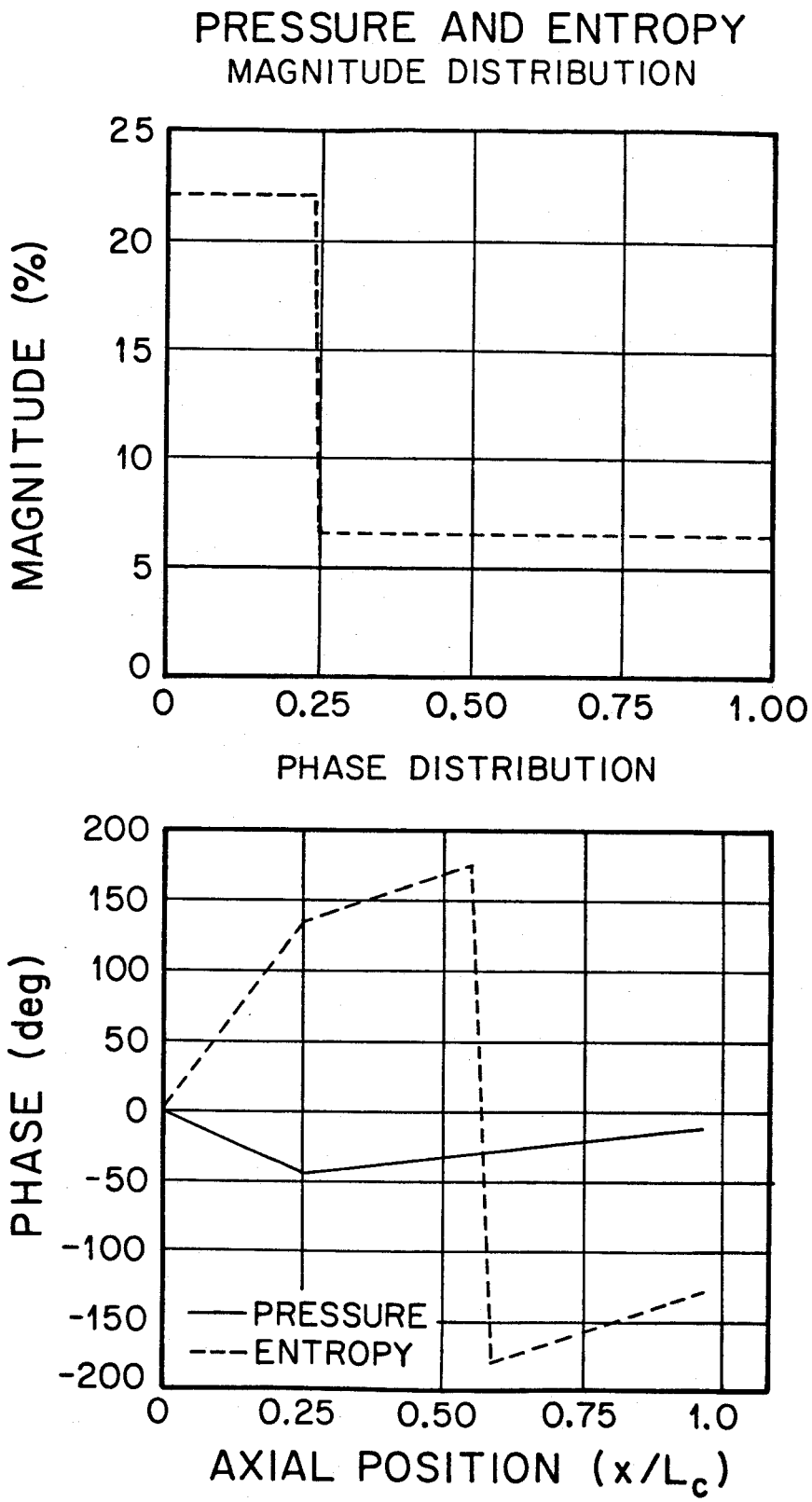

Figure 6.6: Run 3a – Magnitude and Phase Distribution for 141 Hz.

Run 3b is similar to 3b except that the exit acoustic reflectance is set to one. This would be the zeroth order approximation to the choked exit nozzle (without entropy reflectance). This simulates a flame in a chamber where there is acoustic reflectance at the exit but no entropy reflectance. The inlet with no reflectance looks similar to an inlet shock in that a shock usually absorbs most of the incident acoustic energy. The frequency will be dependent upon the distance from the flame to the inlet only because the phase of the entropy is set to zero at this position. Thus, adjusting the length between the inlet and the flame will change the phase of the entropy fluctuations into the flame. In this case we find that $\mathcal{H}^* \approx 1.35$ for neutrally stable oscillations. It is expected that when less acoustic energy is lost (compared to Run 3a) the required energy input from entropy is less to obtain a stable oscillation and hence a smaller value of $\mathcal{H}$. Table 6.5 summarizes the eigenfrequencies. We see that the frequencies are not all damped at the same rate. This is due to the contribution of both the reflected acoustic wave at the flame and the incident entropy wave and their relative phase in determining the stability.

6.2.4 Run 4 – Response of Exit Nozzle to Entropy

Run 4 studies the influence on the linear stability due to entropy waves impinging on a choked nozzle. This case is similar to Run 3b because the inlet acoustic reflectance is set to zero and the exit acoustic reflectance is set to one. Again, we solve 6.72 with $\beta_{flame} = \beta_I = 0$ and the acoustic contribution to β_{EXIT} is 1. The coupling interactions occur at the inlet and exit (none at the flame yet). The frequency results are summarized in Tables 6.6 and 6.7. There is a definite

n	Ω_n	
	ω	α
1	89.2	-15.6
2	232.8	-37.8
3	404.9	0.2
4	562.5	-47.4
5	720.1	0.2
6	892.2	-37.8

Table 6.5: Run 3b – Eigenfrequencies for $\mathcal{H}^* = 1.35$.

selection of frequencies that becomes unstable while others become more stable. The first unstable frequencies are 176, 527, 879 Hz and become unstable for $\mathcal{H} > .50$ (at $\mathcal{H} = .50$, $\alpha \approx -.26$).

When $\mathcal{H} \approx .5$, the energy input into the modes 176, 527, and 879 Hz from the entropy-acoustic coupling at the choked nozzle is offset by the acoustic energy loss through the nozzle (since the inlet neither adds nor absorbs energy in this case). The entropy-acoustic reflectance is real and less than zero so that driving will occur when the impinging entropy is 180 degrees out of phase with the local pressure (at the exit nozzle). Thus, the driving is "in phase" when the pressure and entropy are 180 out of phase. Similarly, the oscillation is discouraged when the entropy is in phase with the pressure.

The tendency of the entropy to drive or dampen the oscillation is determined by the phase of the entropy relative to the pressure. In this example the phase of the entropy relative to the pressure is dependent on two time scales and the phase of the acoustic-entropy coupling at the inlet. The time scales are the acoustic travel time upstream from the exit to the inlet and second the convective

$\mathcal{H}$	Ω_1		Ω_2		Ω_3		Ω_4		Ω_5		Ω_6	
	ω_1	α_1	ω_2	α_2	ω_3	α_3	ω_4	α_4	ω_5	α_5	ω_6	α_6
$2.5 * 10^{-4}$	0	-2.6	176	-2.6	352	-2.6	527	-2.6	703	-2.6	879	-2.6
$2.5 * 10^{-3}$	0	-2.6	176	-2.6	352	-2.6	527	-2.6	703	-2.6	879	-2.6
$2.5 * 10^{-2}$	0	-2.8	176	-2.5	352	-2.8	527	-2.5	703	-2.8	879	-2.5
$2.5 * 10^{-1}$	0	-4.3	176	-1.3	352	-4.3	527	-1.3	703	-4.3	879	-1.3
$1.0 * 10^{-0}$			176	1.6			527	1.6			879	1.6
$2.5 * 10^{-0}$			176	5.5			527	5.5			879	5.5

Table 6.6: Run 4 – Eigenfrequencies 1-6 for a Combustor with Entropy Reflectance at the exit and No Flame. $\mathcal{H}^* \approx .3$.

$\mathcal{H}$	Ω_7		Ω_8		Ω_9		Ω_{10}		Ω_{11}		Ω_{12}	
	ω_7	α_7	ω_8	α_8	ω_9	α_9	ω_{10}	α_{10}	ω_{11}	α_{11}	ω_{12}	α_{12}
$2.5 * 10^{-4}$	0	-187	117	-187	234	-187	352	-187	469	-187	586	-187
$2.5 * 10^{-3}$			117	-144	234	-144	352	-144	469	-144	586	-144
$2.5 * 10^{-2}$	0	-100	117	-101	235	-101	352	-100	468	-101	586	-101
$2.5 * 10^{-1}$	0	-55	115	-59	236	-59	352	-55	467	-59	588	-59
$1.0 * 10^{-0}$			113	-35	238	-35			465	-35	590	-35
$2.5 * 10^{-0}$			112	-21	240	-21			463	-21	591	-21

Table 6.7: Run 4 – Eigenfrequencies 7-12 for a Combustor with Entropy Reflectance at the exit and No Flame. $\mathcal{H}^* \approx .3$.

travel time for the entropy generated at the inlet to convect downstream to the exit. (This is identical to the case for Run 3b where the flame coupling is replaced by the exit coupling and the dimensions have changed.)

Based on the same physical arguments as Run 3b, the conditions for the incident entropy to be out of phase can be determined from the acoustic field. One important observation that can be made is that the exit nozzle seems to be more efficient in converting energy in the entropy wave to energy in the acoustics. The reason for this is quite important. The coupling at the exit and the flame are proportional to the mean Mach number, however, the mean Mach number is always higher in the hot region of the combustor. The mean Mach number into the flame is for cold flow and thus is less than the mean Mach number into the nozzle. It is for this reason that the values of $\mathcal{H}^*$ were less for Run 4 than for Run 3b.

6.2.5 Run 5 – Study of the Influence of $\mathcal{H}$ on Stability with a Flame

Run 5 models a typical combustor with an acoustic wall for an inlet, a plane flame with a temperature ratio of 4, and a choked exit nozzle to study the effects on stability of various values of $\mathcal{H}$. Here, the contributions of both the flame and exit coupling influence the stability. The equation solved is 6.72 where β_I in 6.61 and 6.62 is set to 1. A summary of the eigenvalues is given in Table 6.8. The first frequency that is observed to become unstable is 705 Hz for $\mathcal{H} > .475$. Other frequencies to become unstable for larger $\mathcal{H}$ are 977, 422, and 232 Hz.

It is not so easy to make general comments for Run 5 as it was for the simpler cases of Runs 3 and 4 due the contributions from several processes whose relative phases are frequency dependent. There are two classes of modes as de-

$\mathcal{H}$	Ω_1		Ω_2		Ω_3		Ω_4		Ω_5		Ω_6	
	ω_1	α_1	ω_2	α_2	ω_3	α_3	ω_4	α_4	ω_5	α_5	ω_6	α_6
$2.5 * 10^{-3}$	0	-11.0	256	-7.5	447	-8.8	706	-11.3	961	-6.5	323	-310
$2.5 * 10^{-2}$	0	-11.7	256	-7.4	446	-8.7	706	-10.6	961	-6.5	323	-251
$2.5 * 10^{-1}$	0	-19.9	256	-7.3	441	-7.7	706	-4.8	967	-5.6	327	-175
$4.7 * 10^{-1}$	0	-33.8	256	-6.4	437	-5.9	706	-.02	972	-3.4	336	-156
$7.5 * 10^{-1}$	31	-49	256	-4.7	432	-2.6	705	5.0	977	0.6	343	-146
$1.5 * 10^{-0}$	59	-30	256	0.1	422	8.2	705	15.0	880	-62	356	-137
$2.5 * 10^{-0}$	72	-16	256	5.7	417	21.0	705	26.0	876	-46	362	-134

Table 6.8: Run 5 – Eigenfrequencies 1-6 for a Combustor with Entropy Reflectance at the exit and Plane Flame. $\mathcal{H}^* \approx .475$.

scribed in Chapter 4 — the acoustic modes and the entropy-induced modes. The entropy-induced modes are very highly damped for small entropy fluctuations. The damping changes rapidly for the entropy-induced modes as the entropy fluctuations increase in magnitude. The frequency is a stronger function of entropy for the entropy-induced modes than for the acoustic modes. The stability of the acoustic modes is strongly dependent upon the entropy. The frequency of the acoustic modes is only slightly dependent upon the entropy.

Figure 6.7 is a plot of the magnitude and phase distribution for the pressure and entropy. The leftward and rightward running acoustic waves superimpose to form a standing wave pattern that is distorted due to the effects of entropy and mean flow. The phase distribution has the characteristic 180 degree phase shift across pressure nodes; the linear variation of phase between nodes is due to the mean flow. Larger values of the mean flow Mach number will increase the tilt of the phase distribution. The entropy has little effect on the magnitude, mode

shape, or frequency but does influence the damping coefficient.

6.2.6 Run 6 – Study of the Influence of $\frac{A}{P_1}$ on Stability with an Inlet Shock.

Run 6 uses the linear shock theory applied to an inlet duct terminated by an inlet shock to determine the value of the combustor reflectance at $x = 0$. Recall that $\frac{A}{P_1}$ is the coupling factor which gives the magnitude of entropy generation at the inlet relative to the pressure oscillation. The equation solved is 6.72 where the inlet shock is used to calculate $\beta_{ICALC} = \beta_I$ from 6.22. The intent is to approximate a realistic combustor inlet configuration. The results are tabulated in Table 6.9.

Frequency		Reflectance β_I		$\mathcal{H}^*$	
ω	α	Real	Imag	Real	Imag
0	-14.0	.6577	.0000	-.0006068	.0000000
315	-23.5	.6157	.0209	-.0006004	.0003414
612	-28.9	.5967	.0111	.0004766	.0003502
925	-21.7	.5943	.0096	.0002163	-.0001738
377	-64.3	.6045	-.0044	.0063566	.0002277

Table 6.9: Run 6 – Frequency Dependence of the Inlet Reflectance and Entropy of an Oscillating Shock.

From Runs 4 and 5, we see that the magnitude of $\mathcal{H}$ is sufficient to drive the system more vigorously than the decay rates in Table 6.9 would imply. This suggests that the driving is "out-of-phase" in this case. However, the inlet acoustic reflectance is $\approx 2/3$ where in Runs 4 and 5 it was 1. This implies much stronger acoustic damping. A study of $\mathcal{H}$ and β_I (at $x = 0$) might prove useful in

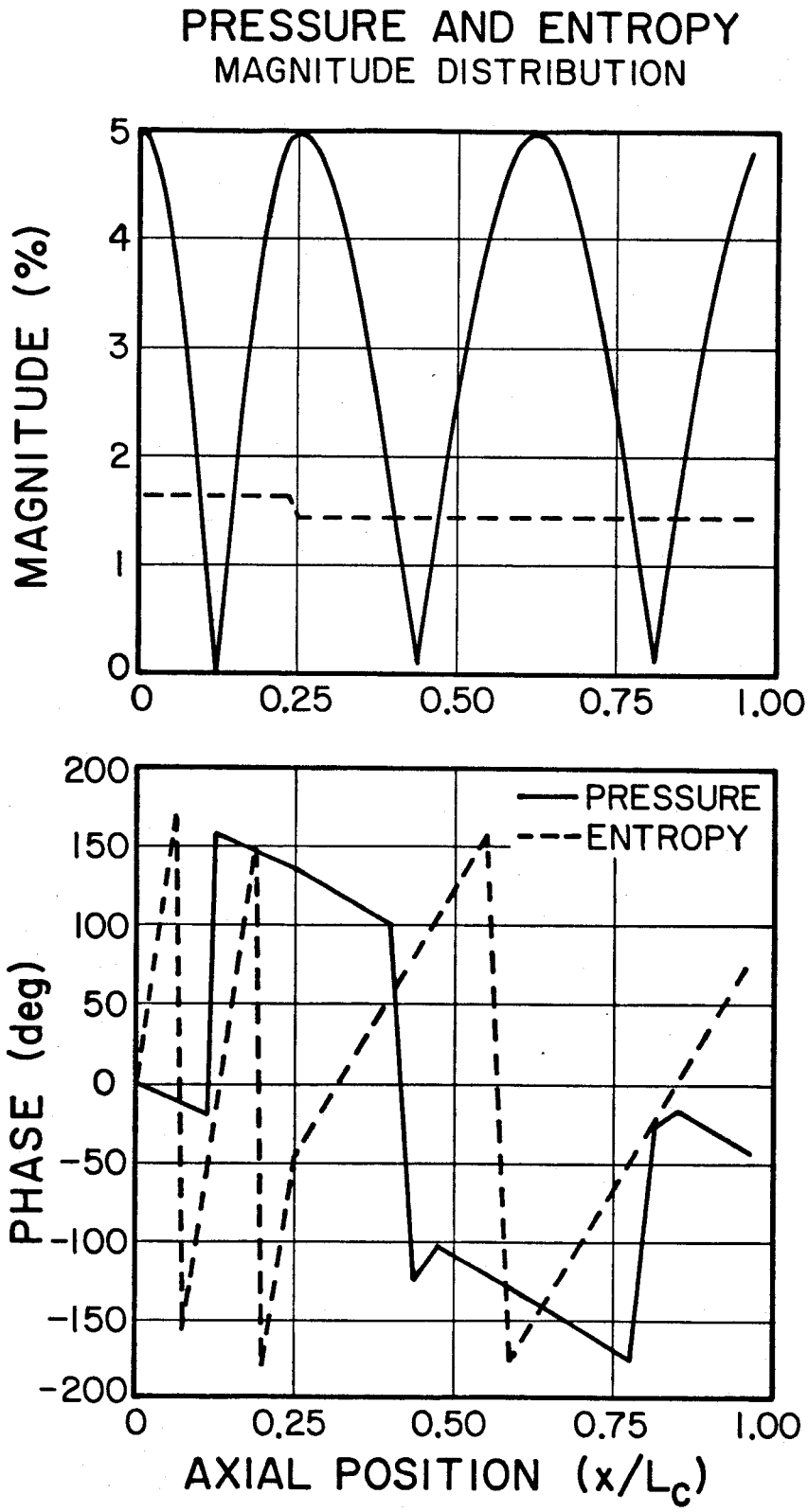

Figure 6.7: Run 5 – Magnitude and Phase Distribution for 705 Hz

determining the stability of this system. Another way to study this is to change the inlet length. The results of changing the inlet length are given in Table 6.10.

Inlet Duct	Ω_1		Ω_2		Ω_3		Ω_4		Ω_5	
Length	ω_1	α_1	ω_2	α_2	ω_3	α_3	ω_4	α_4	ω_5	α_5
1.0	0	-15	204	-113	317	-30	607	-29	923	-22
2.5	0	-14			315	-24	612	-29	925	-22
4.0	0	-13	228	-59	303	-28	594	-35	925	-20

Inlet Duct	Ω_6		Ω_7	
Length	ω_6	α_6	ω_7	α_7
1.0			736	-129
2.5	377	-64		
4.0				

Table 6.10: Run 6 – Frequency Dependence on Inlet Duct Length Length (ft).

This particular choice of inlet lengths shows that the eigenvalues are dependent on geometry and frequency. But the driving is never sufficient to push the system into instability. This implies that the linear oscillating shock does not produce a sufficiently large entropy fluctuation to force instability.

Figures 6.8 and 6.9 are plots of the magnitude and phase distribution for the pressure and entropy. These two plots show the differences between the acoustic mode and the entropy-induced mode. The leftward and rightward running acoustic waves superimpose to form a standing wave pattern that is distorted due to the effects of entropy and mean flow. In Figure 6.8, the pressure phase distribution has the characteristic 180 degree phase shift across pressure nodes

and the tilt is due to the mean flow. Larger values of the mean flow Mach number will increase the linear variation of the phase distribution. The entropy has little effect on the magnitude, mode shape, or frequency but does influence the damping coefficient. In Figure 6.9, the entropy can strongly change the mode shape as seen by the change in slope of the pressure magnitude at the flame ($x/L_C = .025$). The larger damping also modifies the mode shape and can be seen by the different value of the pressure magnitude peak between $x/L_C \approx .1$ and $x/L_C \approx .9$. This is the spatial exponential decay that is a part of the linear solution.

6.3 Summary

The linear stability of acoustics with entropy is strongly a function of the entropy for geometries with sufficient coupling at the boundaries. This is true even for cases where the frequencies are only slightly affected, as the case is for the acoustic modes. The boundary conditions are extremely important, as expected, and can significantly alter both the stability and the frequencies of oscillation. The application of an inlet shock to the entropy coupling at the inlet is derived and shown to be insufficient to produce instabilities in the system having the geometry assumed here. This is probably due to an underestimation of the oscillating heat release at the plane flame. It is suggested that the plane flame matching condition be used to develop a variable area multi-dimensional flame sheet. This could greatly enhance the driving at the flame. Then the results with enhanced heat release can be applied to the one-dimensional acoustics.

The differences between acoustic and entropy-induced modes are significant and in general, the entropy alters the growth rate more than the frequency. The dependence of frequency and mode shape upon entropy is more pronounced for the entropy-induced modes than for the acoustic modes. The primary differ-

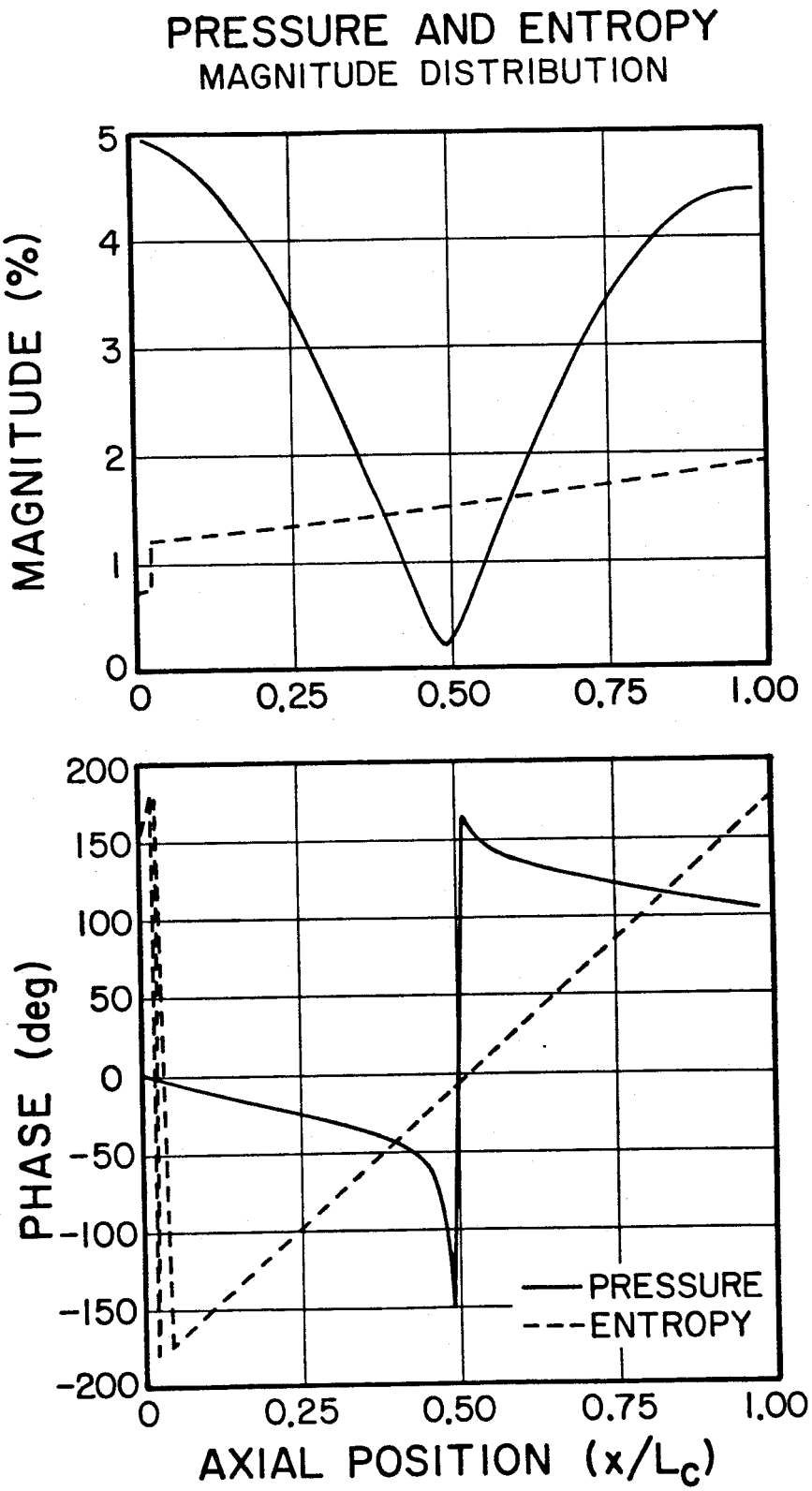

Figure 6.8: Run 6 – Magnitude and Phase Distribution for 315 Hz and Damping of -24 Hz. (This is the acoustic mode.)

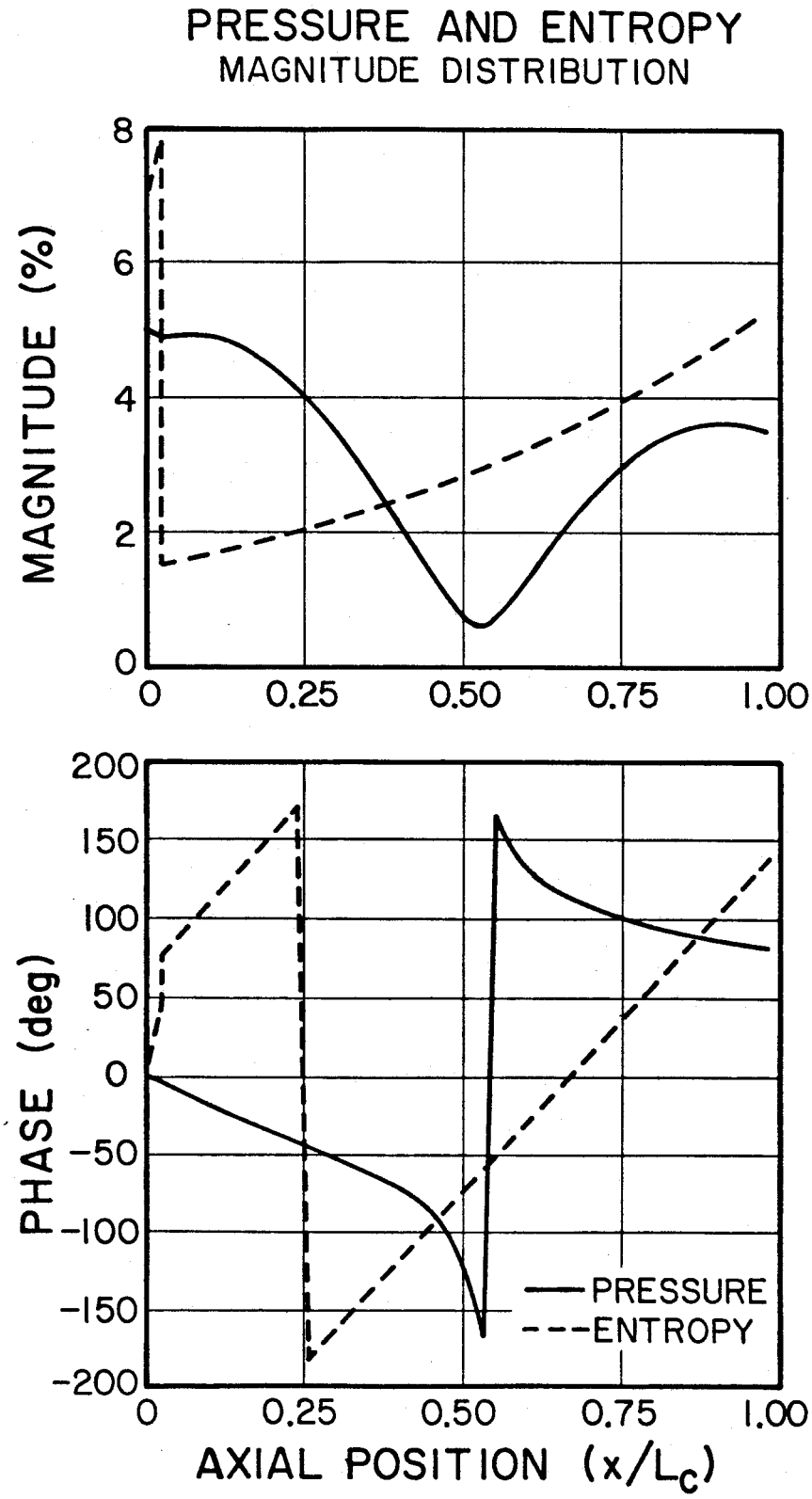

Figure 6.9: Run 6 – Magnitude and Phase Distribution for 377 Hz and Damping of -64 Hz. (This is the entropy-induced mode.)

ences (other than the physics) between the acoustic modes and entropy-induced modes are the frequencies and the mode shapes.

Chapter 7

Nonlinear Acoustics with Nonuniform Entropy

In this chapter we investigate the nonlinear aspects of acoustics with entropy. The main reason to extend the work to nonlinear effects is to capture the characteristics of the limit cycles that are seen experimentally and the transition from the linear growth and decay to the nonlinear limit cycle. The procedure that follows is based on the model developed in Chapter 6, the general equations of Chapter 4, and the solution techniques outlined below. In general, the procedure is similar to that used by Culick to study solid propellant rocket motors [26] [27].

The nonlinear fluid-mechanic interactions were discussed in Section 3.4. The quadratic nonlinearity is investigated with respect to acoustic-acoustic and acoustic-entropy interactions for the case of acoustic mode interactions. The goal is to gain insight into the nonlinear acoustic-entropy interactions, to study stability of the system, and to find nonlinear steady limit cycles. It is not sufficient to consider only acoustic-entropy interactions because as shown in this chapter, the acoustic-entropy interaction terms are less than one percent of the acoustic-acoustic terms for the acoustic mode interactions. Hence, it is shown that the

nonlinearities are dominated by the acoustic-acoustic interactions and not by the acoustic-entropy interactions.

The solution techniques involve a Galerkin expansion in normal modes to obtain a spatial approximation through spatial averaging. Then, time averaging is used to reduce the second order equations to first order equations. The resulting time averaged equations govern the time evolution and stability of the solution. The linear solutions are determined and used as input information in the nonlinear analysis.

7.1 Formulation and Approximate Methods of Solution

The general formalism is presented and described before applying the simplifying assumptions required to work through an actual example. The example was chosen to obtain basic physical insight into the problem.

The problem studied is a one-dimensional (constant area) combustor that contains a plane flame at $x = x_f$ and specified boundary conditions at $x = 0$ and $x = L$. The influence of mean flow is retained and is discussed in detail later. The upstream mean flow in the one-dimensional case must match the mean steady flame speed for the steady plane flame to remain at a fixed mean position, $x = x_f$. This limitation can be relaxed in the limit of low frequencies. The crucial issue is that the flame zone be acoustically compact. Hence, it would be possible to formulate an oblique flame in the framework of the one-dimensional analysis subject to the low frequency considerations and some type of spatial averaging of the mean flow (such as suggested by Yang [37]). In addition, the position of x_f must be given. (In many cases, flame holders may be present to fix x_f.)

The general equations are given by 4.13 - 4.14. In one-dimension, the

equations of motion can be summarized as

$$P_t + uP_x + \gamma P u_x = Q_1 \tag{7.1}$$

$$u_t + uu_x + \frac{a^2}{\gamma P} P_x = \vec{Q}_2 \tag{7.2}$$

$$s_t + us_x = Q_3 \tag{7.3}$$

where

$$Q_1 = a^2 w(x,t) + \frac{Pq(x,t)}{\gamma} \tag{7.4}$$

$$\vec{Q}_2 = b_f(x,t) \tag{7.5}$$

$$Q_3 = c_v q(x,t) \tag{7.6}$$

and $q(x,t)$ is the entropy term defined in Chapter 4. Often, when acoustic dominated phenomena are studied, it is convenient to write the governing equations in a second order wave equation form. Performing the second partial derivatives and rearranging in one-dimension, the acoustic equations become

$$P_{tt} - a^2 P_{xx} = H_\mu + H_\epsilon + H_\nu \tag{7.7}$$

and

$$u_{tt} - a^2 u_{tt} = K_\mu + K_\epsilon + K_\nu \,. \tag{7.8}$$

In these two equations

$$H_\mu = -u_t P_x - uP_{xt} + \gamma P u_x u_x + \gamma P u u_{xx} \,, \tag{7.9}$$

$$K_\mu = -u_t u_x - uu_{xt} + \frac{a^2}{\gamma P}(u_x P_x + uP_{xx}) \,, \tag{7.10}$$

$$H_\epsilon = \left(\frac{a^2}{\gamma P}\right)_x \gamma P P_x - \gamma P_t u_x \,, \tag{7.11}$$

$$K_\epsilon = \left(\frac{a^2}{\gamma P}\right) \gamma P_x u_x - \left(\frac{a^2}{\gamma P}\right)_t P_x \,, \tag{7.12}$$

$$H_\nu = Q_{1t} - \gamma P Q_{2x} \,, \tag{7.13}$$

and

$$K_\nu = Q_{2t} - \frac{a^2}{\gamma P} Q_{1x} \,. \tag{7.14}$$

The equations 7.7 and 7.8 are nonlinear. The left hand side of the equations are the homogeneous parts of the nonlinear wave equation. The boundary condition can be obtained by use of the momentum equation at each end. The boundary condition is

$$P_x\Big|_1^2 = \left(-\rho \frac{\partial u}{\partial t} - \rho u \cdot u_x\right)\Big|_1^2 + F\Big|_1^2 \tag{7.15}$$

at the boundary surface.

Consider flows which are perturbations of a mean flow. In these cases, choose

$$P = P_0 + P' \tag{7.16}$$

$$u = u_0 + u' \tag{7.17}$$

$$a^2 = a_0^2 + a_1^2 \,. \tag{7.18}$$

Assume that a mean flow exists and is determined by an unperturbed steady state. This implies that

$$P_{0t} = P_{0tt} = u_{0t} = u_{0tt} = 0 \,. \tag{7.19}$$

After considerable manipulation and some new definitions, the acoustic equations become

$$P'_{tt} - a_0^2 P'_{xx} = -a_0^2 (h_\mu + h_\epsilon + h_\beta + h_\nu) \,, \tag{7.20}$$

$$u'_{tt} - a_0^2 u'_{xx} = -a_0^2 (k_\mu + k_\epsilon + k_\beta + k_\nu) \,, \tag{7.21}$$

and

$$P'_x\Big|_1^2 = -(f_\mu + f_\epsilon + f_\beta + f_\nu) \tag{7.22}$$

where the h's are

$$-a_0^2 h_\mu = -u_0 P'_{xt} + \gamma P_0 u_0 u'_{xx} \tag{7.23}$$

$$-a_0^2 h_\beta = a^2 P_{0xx} - u_t' P_{0x} + \gamma(P_0 + P')(u_{0x}^2 + 2u_{0x}u_x' + u_0 u_{0xx} + u' u_{0xx}) + \left(\frac{a^2}{\gamma P}\right)_x \gamma(P_0 + P')P_{0x} - \gamma P_t' u_{0x} \tag{7.24}$$

$$-a_0^2 h_\epsilon = -u_t' P_x' - u' P_{xt}' + \gamma(P_0 + P')((u_x')^2 + u' u_{xx}') + \gamma P' u_0 u_{xx}' + \left(\frac{a^2}{\gamma P}\right)_x \gamma(P_0 + P')P_x' - \gamma P_t' u_x' + a_1^2 P_{xx}' \tag{7.25}$$

$$-a_0^2 h_\nu = Q_{1t}' + Q_{1t}^2 - \gamma(P_0 + P')(Q_{2x}' + Q_{2x}^2) \tag{7.26}$$

and the f's are

$$f_\mu = \rho_0(u_0 u_x' + u_t')\Big|_1^2, \tag{7.27}$$

$$f_\beta = ((\rho_0 + \rho')(u_0 + u')u_{0x} + P_{0x})\Big|_1^2, \tag{7.28}$$

$$f_\epsilon = (\rho'(u_0 + u')u_x' + \rho_0 u' u_x' + \rho' u_t')\Big|_1^2, \tag{7.29}$$

and

$$f_\nu = -(\vec{Q}_2)\Big|_1^2. \tag{7.30}$$

Similar equations can be found for the k's to be

$$-a_0^2 k_\mu = -u_0 u_{xt}' + \frac{a_0^2}{\gamma P_0} u_0 P_{xx}', \tag{7.31}$$

$$-a_0^2 k_\beta = -u_{0x} u_t' + \frac{a_0^2}{\gamma P_0}\left(1 - \frac{P'}{P_0} + \frac{a_1^2}{a_0^2}\right)(u_{0x}P_{0x} + u_{0x}P_x' + u_x' P_{0x} + u_0 P_{0xx} + u' P_{0xx} + \gamma P_{0x} u_{0x} + u_{0x} P_x' + P_{0x} u_x') - \frac{a_0^2}{\gamma P_0}\left(-\frac{P_t'}{P_0} + \frac{(a_1^2)_t}{a_0^2}\right) P_{0x}, \tag{7.32}$$

$$-a_0^2 k_\epsilon = -u_t' u_x' - u' u_{xt}' + \frac{a_0^2}{\gamma P_0}\left(1 - \frac{P'}{P_0} + \frac{a_1^2}{a_0^2}\right)(u_x' P_x' + u' P_{xx}') - \frac{a_0^2}{\gamma P_0}\left(-\frac{P_t'}{P_0} + \frac{(a_1^2)_t}{a_0^2}\right) u_0 P_{xx}', \tag{7.33}$$

and

$$-a_0^2 k_\nu = Q_{2t}' + Q_{2t}^2 - \frac{a_0^2}{\gamma P_0}\left(1 - \frac{P'}{P_0} + \frac{a_1^2}{a_0^2}\right)(Q_{1x}' + Q_{1x}^2). \tag{7.34}$$

The subscripts denote the physical importance of the particular terms. The subscript μ denotes mean flow contribution, β denotes the gradients in the mean flow contributions, ϵ denotes the strictly nonlinear terms (although β and ν terms are both linear and nonlinear), and ν denotes source contributions from mass, force, and entropy sources.

7.1.1 Linear Sturm-Liouville Problem

Consider the linearized acoustics equations and boundary conditions for a duct from l_1 to l_2 where boundary conditions are given at l_1 and l_2. Then 7.20 and 7.21 can be put in the form

$$P'_{tt} - a_0^2 P'_{xx} = -a_0^2 h_{lin} \tag{7.35}$$

and

$$u'_{tt} - a_0^2 u'_{xx} = -a_0^2 k_{lin} \tag{7.36}$$

with boundary conditions

$$P'_x(l_1) + \alpha_1(\omega) P'(l_1) = 0\,, \tag{7.37}$$

$$P'_x(l_2) + \alpha_2(\omega) P'(l_2) = 0\,, \tag{7.38}$$

$$u'_x(l_1) + \beta_1(\omega) u'(l_1) = 0\,, \tag{7.39}$$

and

$$u'_x(l_2) + \beta_2(\omega) u'(l_2) = 0\,. \tag{7.40}$$

General Sturm-Liouville Problem

The general form of the Sturm-Liouville equation is

$$\frac{d}{dx}\left(p\frac{d\phi_i}{dx}\right) + q\phi_i + \lambda_i r\phi_i = 0 \tag{7.41}$$

where p, q, and r are functions of x. When $p(x) = r(x) = 1$ and $q(x) = 0$, the S-L problem becomes

$$\frac{d^2}{dx^2}(\phi_i) + \lambda_i \phi_i = 0 \tag{7.42}$$

which is identical to 7.35 and 7.36 for the acoustics problem above where h_{lin} and k_{lin} both vanish. Consider

$$\phi_{ixx} + \lambda_i \phi_i = 0 \tag{7.43}$$

and

$$\phi_{jxx} + \lambda_j \phi_j = 0\,, \tag{7.44}$$

and multiply 7.43 by ϕ_j, 7.44 by ϕ_i. Then subtract to get

$$(\lambda_j - \lambda_i)\phi_i \phi_j = \phi_j \phi_{ixx} - \phi_i \phi_{jxx}\,. \tag{7.45}$$

Integrate over the volume, or spatially average, to get

$$(\lambda_j - \lambda_i) \int_a^b \phi_i \phi_j dV = \int_a^b \phi_j \phi_{ixx} dV - \int_a^b \phi_i \phi_{jxx} dV\,, \tag{7.46}$$

but,

$$\int \phi_i \phi_{jxx} dV = \phi_i \phi_{jx}\Big|_a^b - \phi_j \phi_{ix}\Big|_a^b + \int \phi_{ixx} \phi_j dV\,. \tag{7.47}$$

Then

$$(\lambda_j - \lambda_i) \int_a^b \phi_i \phi_j dV = \phi_j \phi_{ix}\Big|_a^b - \phi_i \phi_{jx}\Big|_a^b\,, \tag{7.48}$$

so that the right-hand side of 7.48 is

$$R.H.S. = \left(\left(\frac{1}{\alpha_2}\right)_j - \left(\frac{1}{\alpha_2}\right)_i\right) \phi_i(b)\phi_j(b) + \left(\left(\frac{1}{\alpha_1}\right)_i - \left(\frac{1}{\alpha_1}\right)_j\right) \phi_i(a)\phi_j(a)\,. \tag{7.49}$$

Hence, the proper result is obtained that the functions ϕ_i are orthogonal to each other under the inner products defined by

$$< \phi_i, \phi_j > = (\lambda_j - \lambda_i) \int_a^b \phi_i \phi_j dV \tag{7.50}$$

as long as the boundary conditions are not a function of frequency. Similarly, one can show that if ϕ_i is a solution, then $\dot{\phi}_i$ is also a solution and thus $< \dot{\phi}_i, \dot{\phi}_j >$ is also orthogonal.

Hence, for the special case of constant boundary conditions, it is easy to get simple orthogonal eigenfunctions. For the case h_{lin} and $k_{lin} \neq 0$ due to mean flow or sources, then the eigenfunctions will in general not be orthogonal.

7.1.2 Galerkin Expansion of P' and u'

The following section sets up the formalism required to solve the nonlinear acoustics in a constant area duct with arbitrary boundary conditions at each end. As shown in Chapter 6, the hot section of the combustor ($x_f < x < L_C$) is terminated by reflectances that are not ideal (real and of magnitude 1). To actually calculate a general combustor problem similar to Runs 3 through 6 of Chapter 6, a general formulation with arbitrary boundaries is required. The actual nonlinear problem to be solved in this chapter , however, is one of ideal boundary conditions. The results of the problem solved indicate that for the coupling of the classical acoustic modes, the acoustic-entropy interactions are relatively small compared to the acoustic-acoustic interactions. Thus, it is not necessary to use all of the capability of the more general formalism. More will be said about use of the general formalism in Section 7.2.

To summarize, the procedure for obtaining an approximate solution involves the following steps:

1. solve the linear eigenvalue problem;
2. express the fluctuation pressure and velocity as an expansion in the linear modes;
3. spatially average to obtain the nonlinear second order oscillator equation;

4. time average to obtain an approximate first order set of equations which govern the slow time scale evolution;

5. solve the first order slow time evolution equations with a fourth order Runge-Kutta method.

In the linear problem as posed in Section 4.3, β_I, the inlet boundary condition, and β_E, the exit boundary condition, are needed to find the eigenvalues, $\Omega_n = \omega_n + i\alpha_n$. The linear solution is used as the foundation from which the nonlinear problem is formulated. The fluctuation pressure and velocity are expressed as a summation of modes which are based on the linear separation of variables techniques to get

$$P'(x,t) = P_0 \sum_{n=1}^{\infty} \eta_n(t)\psi_n(x) \tag{7.51}$$

and

$$u'(x,t) = \sum_{n=1}^{\infty} \frac{\dot{\eta}}{\gamma k_n^2}\dot{\psi}_n(x)\,. \tag{7.52}$$

This choice of $u'(x,t)$ is chosen so that the momentum equation is exactly satisfied for the case of

$$\rho_0 \frac{\partial u'}{\partial t} = -P'_x\,. \tag{7.53}$$

For 7.53 to be true, the influences of the mean flow and of the body forces must be ignored.

Retaining the condition of accounting for complex boundary conditions that can be frequency dependent in the zeroth order problem, consider

$$P'_{tt} - a_0^2 P'_{xx} = -a_0^2 h \tag{7.54}$$

where

$$u'_t = \frac{a_0}{P_0}\left(A^{(r)}P'_t - \frac{1}{\omega}A^{(i)}P'_{tt}\right) \qquad \text{at} \quad x = x_f \tag{7.55}$$

$$u'_t = \frac{a_0}{P_0}\left(B^{(r)}P'_t - \frac{1}{\omega}B^{(i)}P'_{tt}\right) \qquad \text{at} \quad x = L\,. \tag{7.56}$$

This includes the approximation that i times the pressure, iP', is replaced by $(-1/\omega)P'_t$.

The zeroth order problem used will also be required to satisfy the nonhomogeneous boundary conditions. Then the zeroth order problem is

$$\psi_{tt} - a_0^2\psi_{xx} = 0 \tag{7.57}$$

where

$$\psi_x = -\frac{\gamma}{a_0}(A^{(r)}\psi_t - \frac{1}{\omega}A^{(i)}\psi_{tt}) \qquad \text{at} \quad x = x_f\,, \tag{7.58}$$

$$\psi_x = -\frac{\gamma}{a_0}(B^{(r)}\psi_t - \frac{1}{\omega}B^{(i)}\psi_{tt}) \qquad \text{at} \quad x = L\,. \tag{7.59}$$

Hence P' and ψ satisfy the same boundary conditions

$$\frac{d}{dx}\begin{Bmatrix} P' \\ \psi \end{Bmatrix} = \mathcal{L}_t^1 \begin{Bmatrix} P' \\ \psi \end{Bmatrix} \qquad \text{at} \quad x = x_f \tag{7.60}$$

and

$$\frac{d}{dx}\begin{Bmatrix} P' \\ \psi \end{Bmatrix} = \mathcal{L}_t^2 \begin{Bmatrix} P' \\ \psi \end{Bmatrix} \qquad \text{at} \quad x = L \tag{7.61}$$

where $\mathcal{L}_t^1$ and $\mathcal{L}_t^2$ are differential operators defined by 7.60 and 7.61. Choose $\psi_n = \hat{\varphi}_n(x)e^{-ia_o k_n t}$ from which

$$\hat{\varphi}_{nxx} + k_n^2\varphi_n = 0 \tag{7.62}$$

and

$$\hat{\varphi}_{nx} = i\gamma k_n A\varphi_n \qquad \text{at} \quad x = x_f \tag{7.63}$$

$$\hat{\varphi}_{nx} = i\gamma k_n B\psi_n \qquad \text{at} \quad x = L\,. \tag{7.64}$$

Expand P' as

$$P' \approx \sum_m P_0\eta_m(t)\hat{\varphi}_m(x)\,. \tag{7.65}$$

Return to the original partial differential equation 7.35 with 7.65, multiply by $\hat{\varphi}_n$ and spatially average from $x = x_f$ to $x = L$. Use Green's theorem and integration by parts to get

$$(\ddot{\eta}_m + \omega_m^2 \eta_m) \int_{xf}^{L} \hat{\varphi}_n \hat{\varphi}_m dx = -\int_{xf}^{L} \hat{\varphi}_n h dx - [\hat{\varphi}_n P_x' - \hat{\varphi}_{nx} P']_{xf}^{L} . \tag{7.66}$$

It is here that the issue of orthogonality appears. It can be shown that

$$\begin{aligned}(k_n^2 - k_m^2) \int_{xf}^{L} \hat{\varphi}_n \hat{\varphi}_m dx \;\; = \;\; & [\hat{\varphi}_n i k_m B_m \hat{\varphi}_m - \hat{\varphi}_m i k_n B_n \hat{\varphi}_n]_{x=L} \\ & -[\hat{\varphi}_n i k_m A_m \hat{\varphi}_m - \hat{\varphi}_m i k_n A_n \hat{\varphi}_n]_{x=x_f} . \end{aligned} \tag{7.67}$$

When the right-hand side of 7.67 vanishes the eigenfunctions $\hat{\varphi}_n$ are orthogonal. Since k_m , B_m , and A_m are generally functions of frequency, the right hand side will not vanish and the functions $\hat{\varphi}_n$ are *not* orthogonal. A_m is dependent upon the geometry of the inlet duct, inlet shock, dump plane, and the plane flame. Since the shock response is frequency dependent it is inevitable that A_m be a function of frequency. B_m is also frequency dependent since the reflectance of entropy waves as pressure waves at the exit nozzle is a frequency dependent process. From the work on entropy modes in Chapter 4 it is apparent that the set $\hat{\varphi}_n$ includes both the acoustic modes and the entropy modes.

When $\hat{\varphi}_n$ are not orthogonal, however, the Gramm-Schmidt Orthogonalization theorem guarantees that an orthogonal set, φ_i, can be constructed where

$$\varphi_1 = \hat{\varphi}_1 , \tag{7.68}$$

$$\varphi_2 = \hat{\varphi}_2 - c_{21} \hat{\varphi}_1 , \tag{7.69}$$

and

$$c_{21} = \frac{1}{E_1^2} \int_{xf}^{L} \hat{\varphi}_2 \hat{\varphi}_1 dx \tag{7.70}$$

and so on for all modes of the system. If only a few modes are to be considered then only a few orthogonal functions φ_n need be generated.

Recall that each of the $\hat{\varphi}_n$ are complex; choose P' so that

$$P' \approx P_0 \sum_i \eta_i \chi_i \tag{7.71}$$

where

$$\chi_i = \hat{\varphi}_i + \hat{\varphi}_i^* \tag{7.72}$$

and the $(\ )^*$ denotes the complex conjugate. Then

$$\int_{x_f}^{L} \chi_m \chi_n dx = \delta_{mn} \mathcal{E}_n^2 \tag{7.73}$$

and compute

$$\varphi_{nx} = \hat{\varphi}_{nx} - \sum^{n<j} c_{nj} \hat{\varphi}_{jx} \,. \tag{7.74}$$

Then 7.74 can be rewritten using 7.64 to get

$$\varphi_{nx} = i\gamma k_n A_n \hat{\varphi}_n - \sum^{n<m} c_{nm} i\gamma k_m A_m \hat{\varphi}_{mx} \qquad \text{at} \quad x = x_f \tag{7.75}$$

and

$$\varphi_{nx} = i\gamma k_n B_n \hat{\varphi}_n - \sum^{n<m} c_{nm} i\gamma k_m B_m \hat{\varphi}_{mx} \qquad \text{at} \quad x = L \,. \tag{7.76}$$

This produces a set of real, orthogonal functions that are suitable for determining the nonlinear response of problems with arbitrary boundaries that are not approximately ideal. Although not done here, the real functions are used in the time averaging and Runge-Kutta solution technique just as the simpler set of real functions considered next.

Example Problem

The actual problem treated is a combustor that originates at $x = x_f$ and terminates at $x = L$. The inlet reflectance (at $x = x_f$) is taken to be one (a rigid wall). The exit reflectance is taken to be β_{EXIT} as defined by 4.85. The set of eigenfunctions are given by

$$\psi_{ixx} - a_0^2 \psi_{xx} = 0 \tag{7.77}$$

where

$$\psi_{ix} = 0 \quad \text{at} \quad x = x_f \tag{7.78}$$

and

$$\psi_{ix} = 0 \quad \text{at} \quad x = L \tag{7.79}$$

This is the set of classical acoustics eigenfunctions. For typical values of the entropy magnitude, the entropy modes are highly damped and are not included in the set of eigenfunctions used in this expansion.

The nonlinear entropy will be present in the fluid mechanic terms between $x = x_f$ and $x = L$. The quadratic nonlinear terms consist of acoustic-acoustic interactions and acoustic-entropy interactions. Hence, the problem treated is the nonlinear interaction of the acoustic modes with contributions from entropy. It is possible to study the nonlinear acoustic mode and entropy mode with entropy contributions if an orthogonal set of eigenfunctions is constructed. This mode of nonlinear interaction is not treated here.

The actual problem to be done ,however, will use ideal boundary conditions at $x = x_f$ and $x = L$ to give orthogonal eigenfunctions directly and prevent the need to construct orthogonal functions. In this way the original set of eigenfunctions will be an orthogonal set.

Spatial Averaging

Spatial averaging uses the linear solution as an approximation to the spatial distributions. These are then averaged to reduce the influence of small discrepancies between the exact solution and the linear solution. The resulting set of equations has only one variable — time.

Again consider 7.77-7.79 where ψ_n satisfies the homogeneous boundary

conditions at $x = x_f$ and $x = L_C$, is real, and

$$\psi_n = \cos\left(\frac{n\pi(x - x_f)}{(L_C - x_f)}\right), \tag{7.80}$$

where ψ_n is the orthogonal set of eigenfunctions. Assuming a_0 is not a function of position (with the exception of step change across x_f) spatially average and use Green's Theorem to find

$$\ddot{\eta}_m + \omega_m^2 \eta_m = \frac{-a_0^2}{P_0 E_m^2}\left\{\iiint \psi_n h dV + \oint \psi_n f dA\right\}. \tag{7.81}$$

Then with the definitions in 7.1.2, this equation can be written in the form given by Culick [10] to be

$$\ddot{\eta}_n + \omega_n^2 \eta_n = F_n \tag{7.82}$$

and

$$\begin{aligned} -F_n \;=\; & \frac{a_0^2}{P_0 E_n^2}\left\{\iiint \psi_n h_\mu dV + \oint \psi_n f_\mu dA\right\} \text{linear terms} \\ & + \frac{a_0^2}{P_0 E_n^2}\left\{\iiint \psi_n (h_\epsilon + h_\beta) dV + \oint \psi_n (f_\epsilon + f_\beta) dA\right\} \text{nonlinear terms} \\ & + \frac{a_0^2}{P_0 E_n^2}\left\{\iiint \psi_n h_\nu dV + \oint \psi_n f_\nu dA\right\} \text{source terms}. \end{aligned} \tag{7.83}$$

Time Averaging

There are three obvious possible ways to solve the nonlinear problem:

1. Two-timing
2. Method of Time Averaging
3. Numerical Calculation.

Numerical analysis gives solutions to specific examples but, in general, often provides little insight into the mechanics of the solution. The method of two-timing is very attractive but, due to the large number of terms in F_N, can be a formidable bookkeeping problem. In the cases treated to date, two-timing

and time-averaging have given the same results; however, they were simple cases where $\omega_n = n\omega_1$. The method used here is the method of time averaging. In the past, questions have been raised as to the general validity of time averaging [55]. These issues have usually resulted from either the incorrect application of time-averaging or a failure to recognize its limitations.

From previous experience with nonlinear limit cycles [56] we expect that two time scales will be important. The fast time scale, which is associated with the oscillation frequency, is dominated by the linear characteristics. The slow time scale, which may contain linear damping or growth, contains the effect of the nonlinearity and controls the magnitude envelope of the fast time oscillations.

The method of averaging will average out the fast time oscillations and leave an ordinary differential equation for the slow time evolution of the slow time varying variables. In addition, the time averaging will reduce each second order ordinary differential equation to two first order ordinary differential equations. Consider the oscillator equation

$$\ddot{\eta}_n + \omega_n^2 \eta_n = F_n \,. \tag{7.84}$$

Multiply by $\dot{\eta}_n$ to get

$$\frac{d}{dt}\left(\frac{1}{2}\dot{\eta}_n^2 + \frac{1}{2}\omega_n^2\eta_n^2\right) = \dot{\eta}_n F_n \tag{7.85}$$

from which an acoustic energy, $\mathcal{E}_n$, is defined to be

$$\mathcal{E}_n = \left(\frac{1}{2}\dot{\eta}_n^2 + \frac{1}{2}\omega_n^2\eta_n^2\right) . \tag{7.86}$$

The time average is given by

$$< Q(t) > = \frac{1}{\tau}\int_t^{t+\tau} Q(t')dt' \,. \tag{7.87}$$

Since the linear time dependence is sinusoidal, try η_n of the form

$$\eta_n = A_n(\tau)\sin(\omega_n t) + B_n(\tau)\cos(\omega_n t) \tag{7.88}$$

where the functions $A_n(\tau)$ and $B_n(\tau)$ are slowly varying functions of time with respect to $\sin(\omega_n t)$. Differentiate η_n to get

$$\begin{aligned}\dot{\eta}_n &= \omega_n A_n \cos(\omega_n t) - \omega_n B_n \sin(\omega_n t) \\ &\quad + \dot{A}_n \sin(\omega_n t) + \dot{B}_n \cos(\omega_n t) . \end{aligned} \tag{7.89}$$

Since the unknown function η_n is replaced by two functions, A_n and B_n, it is not an approximation but a valid requirement that

$$\dot{A}_n \sin(\omega_n t) + \dot{B}_n \cos(\omega_n t) = 0 . \tag{7.90}$$

Thus the acoustic energy, $\mathcal{E}_n$, can be written as

$$\mathcal{E}_n = \left(\frac{1}{2}\dot{\eta}_n^2 + \frac{1}{2}\omega_n^2 \eta_n^2\right) = \left(\frac{1}{2}A_n^2 + \frac{1}{2}\omega_n^2 B_n^2\right) . \tag{7.91}$$

Calculating $\ddot{\eta}_n$, it is easy to get

$$F_n = \omega_n \left(\dot{A}_n \cos(\omega_n t) - \dot{B}_n \sin(\omega_n t)\right) \tag{7.92}$$

which when combined with 7.84 gives

$$\dot{A}_n = \frac{1}{\omega_n} F_n \cos(\omega_n t) \tag{7.93}$$

and

$$\dot{B}_n = \frac{-1}{\omega_n} F_n \sin(\omega_n t) . \tag{7.94}$$

The equations for A_n and B_n are first order ordinary differential equations and can be solved numerically by a fourth order Runge-Kutta stepping procedure. No time averaging has been done. To save computational efforts these equations can be time averaged over the fast time scale of the period of the first longitudinal mode. The errors produced by the time averaging will be small as long as the change in A_n and B_n with respect to time. In other words, the slope in an A_n vs.

time plot should not to be very large. The steady state limit cycle should have little error due to the averaging. The time averaged equations are

$$\dot{A}_n = \frac{1}{\omega_n \tau} \int_t^{t+\tau} F_n(t') \cos(\omega_n t') dt' \tag{7.95}$$

and

$$\dot{B}_n = \frac{-1}{\omega_n \tau} \int_t^{t+\tau} F_n(t') \sin(\omega_n t') dt' . \tag{7.96}$$

Specific Problem

The specific problem to be studied allows an assessment of the influence of entropy on steady limit cycles. The first attempt was to consider a case where the mean flow was neglected in the acoustics (but not the entropy), no sources were included, and mean flow gradients were assumed zero. After completing this, one factor obviously required special attention. The mean flow in the acoustics cannot be neglected since this contribution is of the same order as the nonlinear terms to be studied.

There are two ways the mean flow can be included. It is possible to solve the linear equations with mean flow and to use these results as the input to the approximate integral equations to determine the nonlinear behavior. This procedure is not used because: (1) the non-orthogonality of the linear terms (see section on Sturm-Liouville problem), and (2) this results in retaining terms in the approximate solution of the same order as ones already neglected. The correct way to retain the mean flow terms is to use the correction perturbation terms in F_n while using solutions with no mean flow as the basis functions in the Galerkin expansion,

$$P' = P_0 \sum_m \eta_m \psi_m . \tag{7.97}$$

The form of the final oscillator equation should look like

$$\ddot{\eta}_n + \omega_n^2 \eta_n = \alpha_{nm} \eta_m + \epsilon_{nm} \dot{\eta}_m + \beta_{nm} \ddot{\eta}_m$$

$$+A_{nml}\,\dot{\eta}_m\dot{\eta}_l + B_{nml}\,\eta_m\eta_l + C_{nml}\,\eta_m\dot{\eta}_l$$
$$+D_{nml}\,\eta_m\ddot{\eta}_l + E_{nml}\,\dot{\eta}_m\ddot{\eta}_l\,. \qquad (7.98)$$

Consider the case where gradients in the mean flow and sources are neglected. Then,

$$h_\beta = h_\nu = f_\beta = f_\nu = 0\,. \qquad (7.99)$$

The following assumptions are useful in calculating the above coefficient matrices.

- Neglect terms where the order is higher than 3.
  (i.e. $P'P'P'$,$u'u'P'$, $u's'P'$,etc.)
- Neglect terms of second order and containing mean flow.
  (i.e. $u_0u'P', u_0u'u', u_0s'u'$, etc.)
- Use the exit reflectances as defined in the simple entropy case section in any surface boundary conditions and not in volume integrals.

The terms $f_\mu, f_\epsilon, h_\mu, h_\epsilon$ need to be calculated. The expansions for the acoustic pressure and velocity are

$$P' = P_0 \sum_m \eta_m \psi_m \qquad (7.100)$$

and

$$u' = \sum_m \frac{\dot{\eta}_m \dot{\psi}_m}{\gamma k_m^2}\,. \qquad (7.101)$$

As mentioned earlier, the boundary conditions can be given in terms of an inlet and an exit admittance of the form

$$A_{NI} = \rho_0 a_0 \frac{u'}{P'} \qquad \text{at} \quad x = x_f \qquad (7.102)$$

and

$$A_{NEXIT} = \rho_0 a_0 \frac{u'}{P'} \qquad \text{at} \quad x = L_C\,. \qquad (7.103)$$

Whenever a u' or P' is encountered in a surface area calculation the admittance and the opposite term should be substituted. This is the way the linear boundary perturbations are incorporated into the spatial averaging formulation.

The entropy is assumed to be proportional to the pressure since the entropy at the inlet shock is proportional to the pressure. This is a convenient case for choosing the form of the entropy. The method could handle other functional forms of entropy but would require some development. Since the entropy is taken as proportional to the pressure then

$$s'(x,t) = \beta_m \eta_m \Phi_m \tag{7.104}$$

where

$$\Phi_m = \cos\left(\frac{\omega_m}{u_0} x\right). \tag{7.105}$$

After calculating the spatial averages of the terms f_ϵ, f_μ, h_ϵ, h_μ, the perturbation term F_n is

$$\begin{aligned} F_n &= \alpha_{nm}\eta_m + \epsilon_{nm}\dot{\eta}_m + \beta_{nm}\ddot{\eta}_m + A_{nml}\,\dot{\eta}_m\dot{\eta}_l \\ &\quad + B_{nml}\,\eta_m\eta_l + D_{nml}\,\eta_m\ddot{\eta}_l + E_{nml}\,\dot{\eta}_m\ddot{\eta}_l \end{aligned} \tag{7.106}$$

where the standard summation convention has been employed. Substituting for η_n from 7.88 it can be shown that

$$\begin{aligned} \dot{A}_n &= M^1_{nm}A_m + M^2_{nm}B_m + N^1_{nml}\,A_mA_l \\ &\quad + N^2_{nml}\,B_mA_l + N^3_{nml}\,A_mB_l + N^4_{nml}\,B_mB_l \end{aligned} \tag{7.107}$$

and

$$\begin{aligned} \dot{B}_n &= O^1_{nm}A_m + O^2_{nm}B_m + P^1_{nml}\,A_mA_l \\ &\quad + P^2_{nml}\,B_mA_l + P^3_{nml}\,A_mB_l + P^4_{nml}\,B_mB_l\,. \end{aligned} \tag{7.108}$$

where the time averages and spatial averages are incorporated into the coefficient matrices. The superscripts denote different coefficient matrices which are

explicitly given in Appendix I. The coefficients M^i_{nm} and O^i_{nm} govern the linear behavior while N^i_{nml} and P^i_{nml} govern the nonlinear behavior. In the absence of entropy, 7.107 and 7.108 reduce to

$$\dot{A}_n = \alpha_n A_n + \theta_n B_n + n\frac{\beta}{2}\sum_{i=1}^{\infty}[A_i(A_{n-i} - A_{i-n} - A_{n+i}) - B_i(B_{n-i} + B_{i-n} + B_{n+i})] \tag{7.109}$$

and

$$\dot{B}_n = \alpha_n B_n - \theta_n A_n + n\frac{\beta}{2}\sum_{i=1}^{\infty}[A_i(B_{n-i} + A_{i-n} - B_{n+i}) + B_i(A_{n-i} - A_{i-n} + A_{n+i})] \tag{7.110}$$

as given by Awad and Culick [42]. In their notation, α_n is the growth constant, θ_n is the frequency shift (from the value used in the Galerkin expansion), and β is the only nonlinear gasdynamic parameter where

$$\beta = \frac{\gamma+1}{8\gamma}\omega_1 . \tag{7.111}$$

7.2 Results of Calculations

A computer program was written to actually calculate the coefficient matrices and to perform the Runge-Kutta solution of 7.107 and 7.108. The Runge-Kutta method was identical to that given by White [57]. The first obvious case was to set the entropy to zero and reproduce the results given by Awad and Culick [42]. The examples given by Awad were reproducible. Two sample acoustic-acoustic nonlinear limit cycles are shown in Figures 7.1 and 7.2. The first shows a case where the initial disturbance is smaller than the resultant limit cycle and for the second the initial disturbance was larger. The actual magnitudes of the limit cycles are dependent upon the initial linear damping coefficients, α_1 and α_2. Also, the approach to the limit cycle is dependent upon the damping coefficients. Figure 7.3 shows a case where $\alpha_2 > -2\alpha_1$. There is a definite overshoot as the

solution approaches the limit cycle. Figure 7.4 is a case where $\alpha_2 \approx -4\alpha_1$. In this case, the solution has no overshoot at all in its approach to the limit cycle.

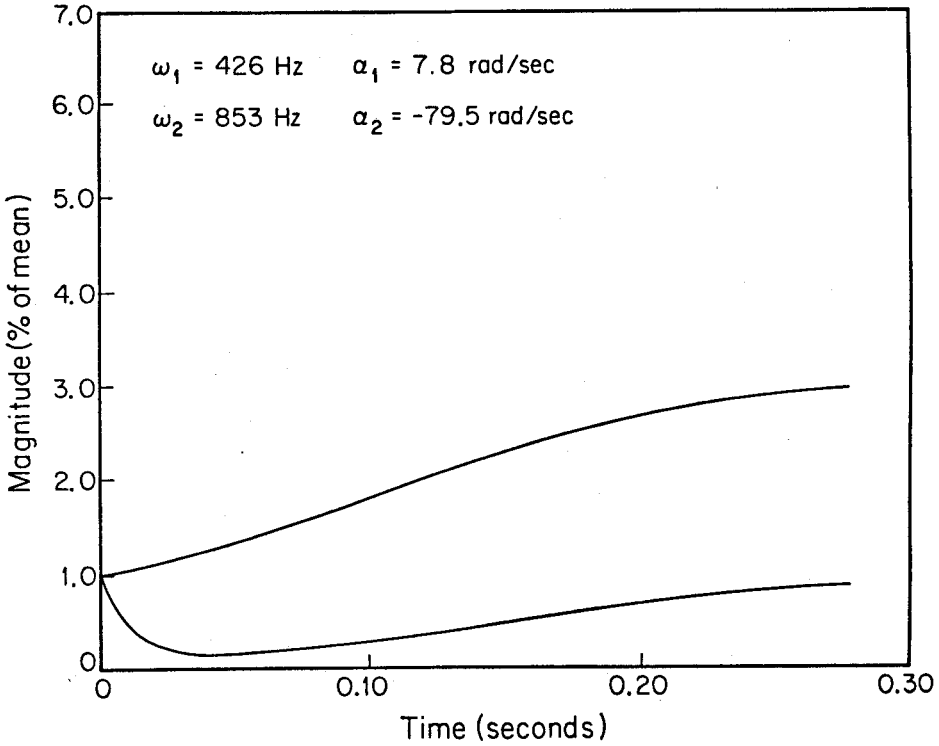

Figure 7.1: Acoustic-Acoustic Nonlinear Limit Cycles - Small Initial Disturbance.

For the case with entropy, the same procedure was executed. The magnitude of the acoustic-entropy terms in the coefficient matrices were very much smaller than the acoustic-acoustic terms. Even for cases where $\mathcal{H} \approx 3$, the acoustic-entropy interaction terms were less than one percent in magnitude of the acoustic-acoustic interaction terms. Since the acoustic-entropy terms are much smaller than the acoustic-acoustic terms in 7.107 and 7.108, it is not surprising that the nonlinear results are strongly dominated by the acoustic-acoustic interactions.

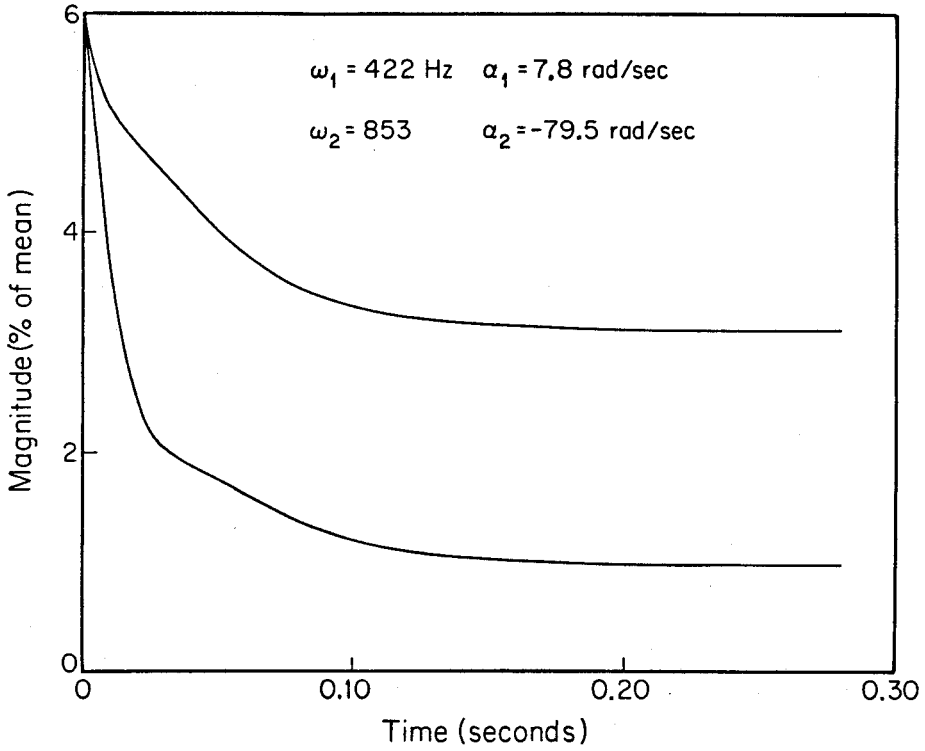

Figure 7.2: Acoustic-Acoustic Nonlinear Limit Cycles - Large Initial Disturbance.

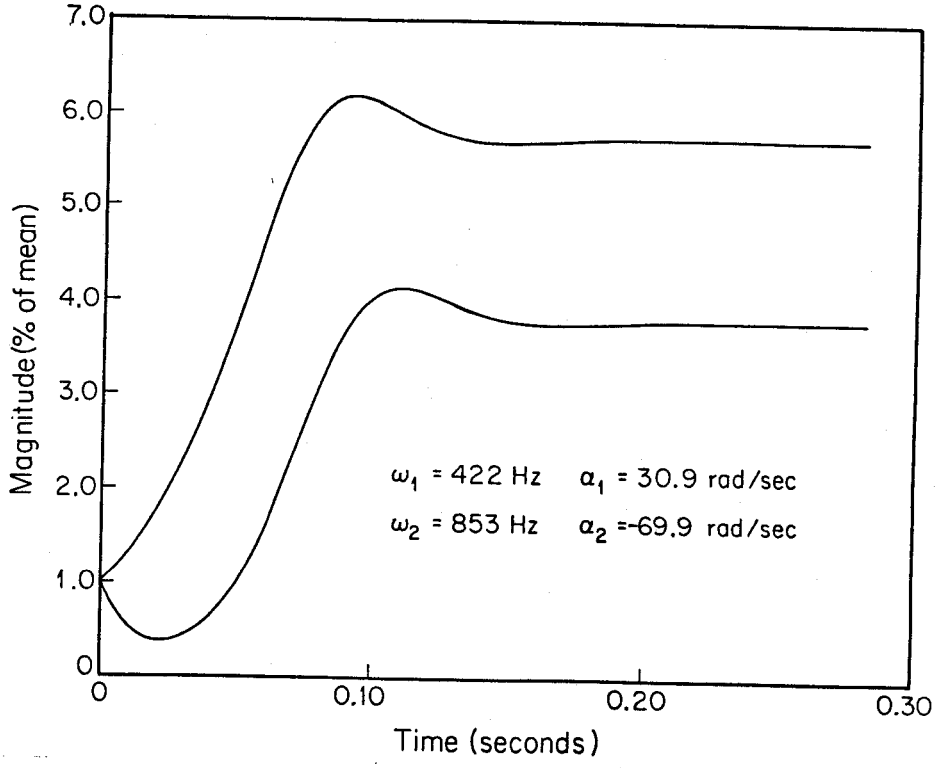

Figure 7.3: Acoustic-Acoustic Nonlinear Limit Cycles - Small Amount of Damping.

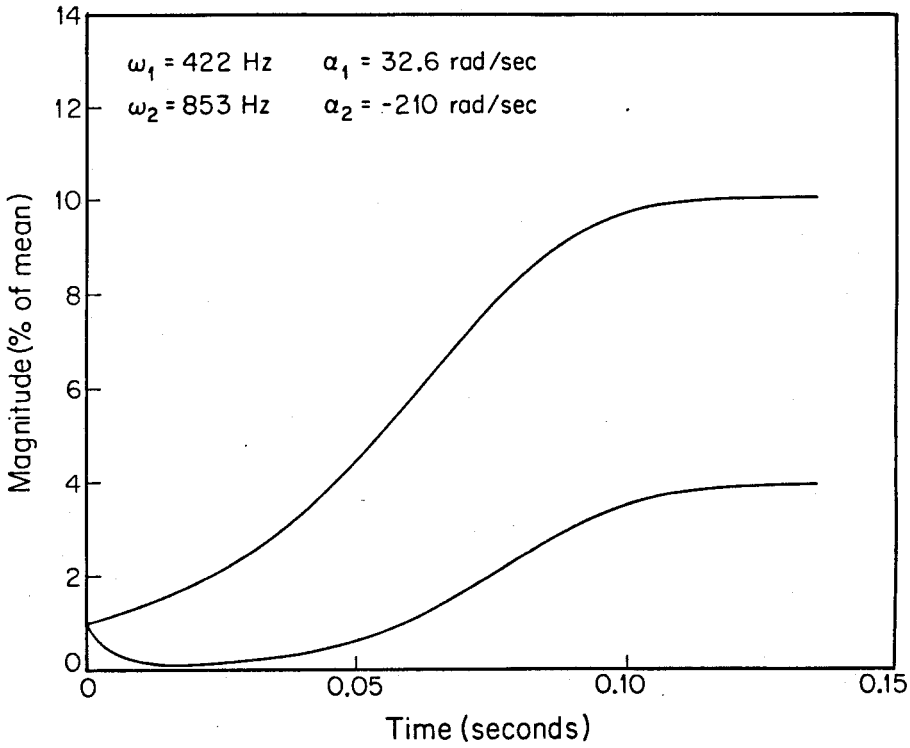

Figure 7.4: Acoustic-Acoustic Nonlinear Limit Cycles - Large Initial of Damping.

7.3 Discussion of Results

These results are very interesting. As shown in Chapters 4 through 6, the linear solutions are strongly dependent on entropy for the cases where $\mathcal{H} > .5$. Two important observations can be made about the linear eigenvalues (solutions):

1. The linear solutions are dependent upon entropy fluctuations.

2. The nonlinear behavior is strongly affected by linear solutions.

In general, the entropy will destabilize the linear solution when "in phase" driving occurs. Conversely, the entropy fluctuations will stabilize the linear solution when the driving is "out of phase". The phase of the driving is determined fluctuations will stabilize the linear solution when the driving is "out of phase". The phase of the driving is determined by the geometry and mean flow conditions. Hence, the linear coefficients in 7.107 and 7.108 (which are M^i_{nm} and O^i_{nm})

are dependent upon the entropy fluctuations.

The quadratic nonlinear processes are can be divided into four types:

1. Acoustic mode – acoustic mode coupling with

   (a) acoustic-acoustic interactions.

   (b) acoustic-entropy interactions.

2. Acoustic mode – entropy-induced mode coupling with

   (a) acoustic-acoustic interactions.

   (b) acoustic-entropy interactions.

The case studied is the acoustic mode – acoustic mode coupling. It is shown that the solution is dominated by the acoustic-acoustic interactions and not the acoustic-entropy interactions. Thus, the nonlinear coefficients, N^i_{nml} and P^i_{nml}, are not significantly influenced by the entropy fluctuations.

It is possible that the entropy contribution will be most significant to the nonlinear analysis when the acoustic modes and entropy-induced modes are interacting. This case was not investigated, but is the only remaining quadratic interaction between acoustics and entropy to be studied. It is expected that the influence of the acoustic-entropy interactions will be stronger than the case studied, but only for large values of linear interaction.

The coupling between two acoustic modes has the convenient result that the contribution of entropy is relatively easy to assess since the linear influence of entropy is easy to obtain from simple linear solutions. The nonlinear analysis can be done without entropy (while using the linear solutions with entropy). These observations apply only to the coupling between two acoustic modes and not for coupling between acoustic and entropy modes.

Chapter 8

Summary and Conclusions

There are several important conclusions which can be drawn from the previous chapters. Each of these will be discussed separately and are based on the low frequency assumptions. The low frequency assumptions require that the wavelengths of the oscillations be large with respect to the characteristic length of each compact element. The physical nature of the acoustic waves is propagation from any acoustic source with the acoustic velocity. The entropy waves on the other hand must be convected (or conducted which is not considered herein) away from its source with the mean flow.

A set of linearized equations of acoustics with entropy are developed in Section 4.3 for acoustic regions connected by compact acoustic elements. These were used in Section 4.4 to show that with entropy there are two distinct modes of acoustic oscillation: the acoustic mode and the entropy-induced mode. An acoustic mode reduces to classical acoustics in the absence of entropy. An entropy-induced mode is distinctly different and never reduces to an acoustic mode. The only reason that the entropy-induced mode exists is due to the coupling — a transfer of energy between fluctuating entropy waves and pressure (or velocity) waves. For small levels of entropy fluctuation and coupling, an entropy mode is

highly damped. For larger levels of entropy fluctuation, the entropy modes tend to be damped about the same as acoustic modes. It would be useful to set up an experiment where the entropy fluctuations are very large so that it would be easier to distinguish the acoustic mode and entropy-induced mode in the pressure oscillations. For the larger levels of entropy ($\mathcal{H} > .5$) the geometry determines which modes are "in phase" and thus driven.

In Chapter 5, a previous treatment of a plane flame is expanded and applied to an acoustic combustor system. It is shown that the condition for a stable deflagration in subsonic flow is that the flow be in a diverging channel (in the absence of viscosity, heat conduction, and dissipation). This is analogous to the case of shock wave stability in a diverging diffuser. The acoustic and entropy response of a flame is examined in detail. Of primary interest is the coupling of a flame to the acoustics upstream and downstream. The motion of the flame is part of the acoustic solution. It is significant to note that for the cases studied, the dominant response was due to the temperature discontinuity. The motion of the flame and the fluctuating heat release were minor influences. The important characteristic of the flow on the response of the flame to entropy is the mean flow Mach number into the flame which is usually small for the cold flow into the flame.

In Chapter 6, the compact acoustic elements of a plane flame, exit nozzle and inlet section are assembled into a combustor-inlet system model. For these linear boundary value problems, the geometry and mean conditions play the dominant role in determining the stability of the system. It is very important to include in the model all components which are acoustically coupled to the combustor. That is to say: it is incorrect to neglect the coupling of the inlet shock, inlet duct, and dump plane when determining the acoustic modes of the combustor. The flow is subsonic through the inlet and combustor and thus acoustically

coupled. For an experimental apparatus that does not have an upstream shock, the upstream ducting and plenum chambers which are acoustically coupled to the combustor must be included in determining the acoustic modes of the system.

When the nondimensionalized inlet entropy coupling term, characterized by $\mathcal{H}$, is greater than approximately .1, entropy plays a significant role in the linear stability. Some modes may be damped while others are amplified. In general, the entropy modes are damped more than the acoustic modes, but for values of entropy fluctuation proportional to pressure fluctuation, the entropy modes should not be ignored.

The contribution of the plane flame to the combustor model is to essentially act as a fluctuating heat release term proportional to the fluctuating mass flux across the flame. This heat release manifests itself in two physical mechanisms. First, the heat release changes the density and produces a pressure wave similar to a mass source. Second, a fluctuating entropy convecting downstream is created which is similar to an entropy source. The actual motion of the flame is several orders of magnitude smaller than the wavelength and for calculations can be treated as fixed at the mean position. The fluctuating entropy downstream of the flame will interact at the exit nozzle to produce pressure oscillations. The stability of the combustor system is determined by each of the contributing processes and their phase relationships. Hence, each frequency generally has a distinct damping coefficient.

The magnitude of the inlet shock reflectance is much less than 1 and hence, tends to damp out the driving produced by the coupling of entropy and pressure downstream. As seen from the examples, the driving from the shock is insufficient even when the acoustic reflectance is high. This implies that there is still an important driving mechanism in the combustion process which is not contained in the present model. It is the belief of the author that the fluctuating heat release

at the flame is still underestimated due to the one-dimensional assumptions. A two-dimensional model of an axisymmetric flame should be worked out while still using one-dimensional acoustics (as done by Yang [37]). The flame may still be treated as very thin, but flame sheet stretching due to vortex rollup and growth could greatly amplify the fluctuating heat releases. (This is due to the larger surface area and the fluctuating surface area of the flame.) It is not expected that such a two-dimensional flame model is easy to formulate but it could be applicable to many combustion flows with significant shear layers.

The nonlinear results of Chapter 7 apply only to coupling between two acoustic modes with acoustics and entropy contributions to the interactions. The entropy is shown to be insignificant in these nonlinear processes. The nonlinear solutions are dependent on the linear solutions and to this extent are significantly dependent upon the linear contributions of entropy. This is a direct consequence of the dependence of the nonlinear solution on the linear coefficients M^i_{nm} and O^i_{nm}. These coefficients reduce to linear coefficients given by Awad and Culick, α_n and θ_n, in the absence of entropy fluctuations and mean flow [42]. Further study is suggested to extend this work to the case of coupling between acoustic modes and entropy-induced modes of acoustics with entropy, since this is the last remaining fundamental issue of acoustics with fluctuating entropy.

The importance of the small influence of entropy in the nonlinear acoustic mode interactions is that the influence of entropy can be determined entirely from the linear analysis of entropy. This is a nice result since the linear analysis is, in general, much easier to perform and generalize for the purposes of design and prediction.

The practical application of this work should be apparent from the specific examples chosen to illustrate the processes. With renewed emphasis on airbreathing propulsion systems to increase range, specific impulse, and reduced size, the

issues of pressure oscillation stability may be crucial to feasibility and reliability. It is hoped that this work will help to dispel some confusion as to the importance of entropy with respect to pressure oscillations in combustion chambers.

Appendix I

The time averaged equations for $\dot{A}_n$ and $\dot{B}_n$ (7.107 and 7.108) are

$$\begin{aligned}\dot{A}_n &= M^1_{nm}A_m + M^2_{nm}B_m + N^1_{nml}\,A_mA_l \\ &\quad + N^2_{nml}\,B_mA_l + N^3_{nml}\,A_mB_l + N^4_{nml}\,B_mB_l\end{aligned}$$

and

$$\begin{aligned}\dot{B}_n &= O^1_{nm}A_m + O^2_{nm}B_m + P^1_{nml}\,A_mA_l \\ &\quad + P^2_{nml}\,B_mA_l + P^3_{nml}\,A_mB_l + P^4_{nml}\,B_mB_l\,.\end{aligned}$$

The coefficient matrices can be calculated directly with the use of time averaging. The time average is defined in the usual way as

$$< Q(t) > = \frac{1}{\tau}\int_t^{t+\tau} Q(t')dt'\,.$$

Apply time averaging to

$$\dot{A}_n = \frac{1}{\omega_n}F_n\cos(\omega_n t)$$

and

$$\dot{B}_n = \frac{-1}{\omega_n}F_n\sin(\omega_n t)$$

where

$$\begin{aligned}-F_n &= \frac{a_0^2}{P_0E_n^2}\left\{\iiint \psi_n h_\mu dV + \oint \psi_n f_\mu dA\right\}\text{linear terms} \\ &\quad + \frac{a_0^2}{P_0E_n^2}\left\{\iiint \psi_n(h_\epsilon + h_\beta)dV + \oint \psi_n(f_\epsilon + f_\beta)dA\right\}\text{nonlinear terms} \\ &\quad + \frac{a_0^2}{P_0E_n^2}\left\{\iiint \psi_n h_\nu dV + \oint \psi_n f_\nu dA\right\}\text{source terms}\,.\end{aligned}$$

By defining several coefficients, $-F_n$ can be rewritten as

$$\begin{aligned} F_n &= \alpha_{nm}\eta_m + \epsilon_{nm}\dot{\eta}_m + \beta_{nm}\ddot{\eta}_m + A_{nml}\,\dot{\eta}_m\dot{\eta}_l \\ &\quad + B_{nml}\,\eta_m\eta_l + D_{nml}\,\eta_m\ddot{\eta}_l + E_{nml}\,\dot{\eta}_m\ddot{\eta}_l \end{aligned}$$

Using the expansion in 7.88, 7.89, and 7.90 for the time dependent variable, η_n, obtain F_n as a function of A_n and B_n. With these, one can find

$$\begin{aligned} \dot{A}_n &= M^1_{nm}A_m + M^2_{nm}B_m + N^1_{nml}\,A_mA_l \\ &\quad + N^2_{nml}\,B_mA_l + N^3_{nml}\,A_mB_l + N^4_{nml}\,B_mB_l \end{aligned}$$

and

$$\begin{aligned} \dot{B}_n &= O^1_{nm}A_m + O^2_{nm}B_m + P^1_{nml}\,A_mA_l \\ &\quad + P^2_{nml}\,B_mA_l + P^3_{nml}\,A_mB_l + P^4_{nml}\,B_mB_l\,. \end{aligned}$$

where

$$M^1_{nm} = \frac{1}{\tau_1\omega_n}\{\tilde{\alpha}_{nm}SC_{nm} + \omega_m\tilde{\epsilon}_{nm}CC_{nm}\}\,,$$

$$M^2_{nm} = \frac{1}{\tau_1\omega_n}\{\tilde{\alpha}_{nm}CC_{nm} - \omega_m\tilde{\epsilon}_{nm}SC_{nm}\}\,,$$

$$N^1_{nm} = \frac{1}{\tau_1\omega_n}\{+\tilde{A}_{nml}\omega_m\omega_lCCC_{nml} + \tilde{B}_{nml}SSC_{nml} + \tilde{C}_{nml}\omega_mCSC_{nml}\}\,,$$

$$N^2_{nm} = \frac{1}{\tau_1\omega_n}\{-\tilde{A}_{nml}\omega_m\omega_lSCC_{nml} + \tilde{B}_{nml}CSC_{nml} - \tilde{C}_{nml}\omega_mSSC_{nml}\}\,,$$

$$N^3_{nm} = \frac{1}{\tau_1\omega_n}\{-\tilde{A}_{nml}\omega_m\omega_lCSC_{nml} + \tilde{B}_{nml}SCC_{nml} + \tilde{C}_{nml}\omega_mCCC_{nml}\}\,,$$

$$N^4_{nm} = \frac{1}{\tau_1\omega_n}\{+\tilde{A}_{nml}\omega_m\omega_lSSC_{nml} + \tilde{B}_{nml}CCC_{nml} - \tilde{C}_{nml}\omega_mSCC_{nml}\}\,,$$

and

$$O^1_{nm} = -\frac{1}{\tau_1\omega_n}\{\tilde{\alpha}_{nm}SS_{nm} + \omega_m\tilde{\epsilon}_{nm}CS_{nm}\}\,,$$

$$O^2_{nm} = -\frac{1}{\tau_1\omega_n}\{\tilde{\alpha}_{nm}CS_{nm} - \omega_m\tilde{\epsilon}_{nm}SS_{nm}\}\,,$$

$$P^1_{nm} = -\frac{1}{\tau_1\omega_n}\{+\tilde{A}_{nml}\omega_m\omega_l CCS_{nml} + \tilde{B}_{nml}SSS_{nml} + \tilde{C}_{nml}\omega_m CSS_{nml}\}\,,$$

$$P^2_{nm} = -\frac{1}{\tau_1\omega_n}\{-\tilde{A}_{nml}\omega_m\omega_l SCS_{nml} + \tilde{B}_{nml}CSS_{nml} - \tilde{C}_{nml}\omega_m SSS_{nml}\}\,,$$

$$P^3_{nm} = -\frac{1}{\tau_1\omega_n}\{-\tilde{A}_{nml}\omega_m\omega_l CSS_{nml} + \tilde{B}_{nml}SCS_{nml} + \tilde{C}_{nml}\omega_m CCS_{nml}\}\,,$$

$$P^4_{nm} = -\frac{1}{\tau_1\omega_n}\{+\tilde{A}_{nml}\omega_m\omega_l SSS_{nml} + \tilde{B}_{nml}CCS_{nml} - \tilde{C}_{nml}\omega_m SCS_{nml}\}\,.$$

The following definitions were used in the above equations. For $\omega_n \neq \omega_m$

$$SC_{nm} = \int_1^2 \sin(\omega_m t')\cos(\omega_n t')dt' = \left(-\frac{\cos(\omega_m+\omega_n)t}{2(\omega_m+\omega_n)} - \frac{\cos(\omega_m-\omega_n)t}{2(\omega_m-\omega_n)}\right)\Big|_1^2,$$

$$CS_{nm} = \int_1^2 \cos(\omega_m t')\sin(\omega_n t')dt' = \left(-\frac{\cos(\omega_m+\omega_n)t}{2(\omega_m+\omega_n)} + \frac{\cos(\omega_m-\omega_n)t}{2(\omega_m-\omega_n)}\right)\Big|_1^2,$$

$$SS_{nm} = \int_1^2 \sin(\omega_m t')\sin(\omega_n t')dt' = \left(-\frac{\sin(\omega_m+\omega_n)t}{2(\omega_m+\omega_n)} + \frac{\sin(\omega_m-\omega_n)t}{2(\omega_m-\omega_n)}\right)\Big|_1^2,$$

$$CC_{nm} = \int_1^2 \cos(\omega_m t')\cos(\omega_n t')dt' = \left(+\frac{\sin(\omega_m+\omega_n)t}{2(\omega_m+\omega_n)} + \frac{\sin(\omega_m-\omega_n)t}{2(\omega_m-\omega_n)}\right)\Big|_1^2.$$

For $\omega_n = \omega_m$

$$SC_{nn} = \int_1^2 \sin(\omega_n t')\cos(\omega_n t')dt' = -\frac{1}{4\omega_n}\cos(2\omega_n t')\Big|_1^2,$$

$$CS_{nn} = \int_1^2 \cos(\omega_n t')\sin(\omega_n t')dt' = -\frac{1}{4\omega_n}\cos(2\omega_n t')\Big|_1^2,$$

$$SS_{nn} = \int_1^2 \sin^2(\omega_n t')dt' = -\frac{1}{4\omega_n}\sin(2\omega_n t') + \frac{1}{2}t'\Big|_1^2,$$

$$CC_{nn} = \int_1^2 \cos^2(\omega_n t')dt' = +\frac{1}{4\omega_n}\sin(2\omega_n t') + \frac{1}{2}t'\Big|_1^2.$$

In addition,

$$\begin{aligned} SSS_{nml} &= -\frac{1}{4}\left[-\frac{\cos(+\omega_m+\omega_l+\omega_n)t}{(+\omega_m+\omega_l+\omega_n)} + \frac{\cos(+\omega_m-\omega_l+\omega_n)t}{(+\omega_m-\omega_l+\omega_n)}\right. \\ &\quad \left. +\frac{\cos(+\omega_m+\omega_l-\omega_n)t}{(+\omega_m+\omega_l-\omega_n)} + \frac{\cos(-\omega_m+\omega_l+\omega_n)t}{(-\omega_m+\omega_l+\omega_n)}\right]_1^2, \end{aligned}$$

$$\begin{aligned} SCC_{nml} &= -\frac{1}{4}\left[+\frac{\cos(+\omega_m+\omega_l+\omega_n)t}{(+\omega_m+\omega_l+\omega_n)} + \frac{\cos(+\omega_m-\omega_l+\omega_n)t}{(+\omega_m-\omega_l+\omega_n)}\right. \\ &\quad \left. +\frac{\cos(+\omega_m+\omega_l-\omega_n)t}{(+\omega_m+\omega_l-\omega_n)} - \frac{\cos(-\omega_m+\omega_l+\omega_n)t}{(-\omega_m+\omega_l+\omega_n)}\right]_1^2, \end{aligned}$$

$$\begin{aligned} CSC_{nml} &= -\frac{1}{4}\left[+\frac{\cos(+\omega_m+\omega_l+\omega_n)t}{(+\omega_m+\omega_l+\omega_n)} - \frac{\cos(+\omega_m-\omega_l+\omega_n)t}{(+\omega_m-\omega_l+\omega_n)}\right. \\ &\quad \left. +\frac{\cos(+\omega_m+\omega_l-\omega_n)t}{(+\omega_m+\omega_l-\omega_n)} + \frac{\cos(-\omega_m+\omega_l+\omega_n)t}{(-\omega_m+\omega_l+\omega_n)}\right]_1^2, \end{aligned}$$

$$\begin{aligned} CCS_{nml} &= -\frac{1}{4}\left[+\frac{\cos(+\omega_m+\omega_l+\omega_n)t}{(+\omega_m+\omega_l+\omega_n)} + \frac{\cos(+\omega_m-\omega_l+\omega_n)t}{(+\omega_m-\omega_l+\omega_n)}\right. \\ &\quad \left. -\frac{\cos(+\omega_m+\omega_l-\omega_n)t}{(+\omega_m+\omega_l-\omega_n)} + \frac{\cos(-\omega_m+\omega_l+\omega_n)t}{(-\omega_m+\omega_l+\omega_n)}\right]_1^2, \end{aligned}$$

$$\begin{aligned} CSS_{nml} &= +\frac{1}{4}\left[-\frac{\sin(+\omega_m+\omega_l+\omega_n)t}{(+\omega_m+\omega_l+\omega_n)} + \frac{\sin(+\omega_m-\omega_l+\omega_n)t}{(+\omega_m-\omega_l+\omega_n)}\right. \\ &\quad \left. +\frac{\sin(+\omega_m+\omega_l-\omega_n)t}{(+\omega_m+\omega_l-\omega_n)} - \frac{\sin(-\omega_m+\omega_l+\omega_n)t}{(-\omega_m+\omega_l+\omega_n)}\right]_1^2, \end{aligned}$$

$$SCS_{nml} = +\frac{1}{4}\left[-\frac{\sin(+\omega_m+\omega_l+\omega_n)t}{(+\omega_m+\omega_l+\omega_n)} - \frac{\sin(+\omega_m-\omega_l+\omega_n)t}{(+\omega_m-\omega_l+\omega_n)} + \frac{\sin(+\omega_m+\omega_l-\omega_n)t}{(+\omega_m+\omega_l-\omega_n)} + \frac{\sin(-\omega_m+\omega_l+\omega_n)t}{(-\omega_m+\omega_l+\omega_n)}\right]_1^2,$$

$$SSC_{nml} = +\frac{1}{4}\left[-\frac{\sin(+\omega_m+\omega_l+\omega_n)t}{(+\omega_m+\omega_l+\omega_n)} + \frac{\sin(+\omega_m-\omega_l+\omega_n)t}{(+\omega_m-\omega_l+\omega_n)} - \frac{\sin(+\omega_m+\omega_l-\omega_n)t}{(+\omega_m+\omega_l-\omega_n)} + \frac{\sin(-\omega_m+\omega_l+\omega_n)t}{(-\omega_m+\omega_l+\omega_n)}\right]_1^2,$$

and

$$CCC_{nml} = +\frac{1}{4}\left[+\frac{\sin(+\omega_m+\omega_l+\omega_n)t}{(+\omega_m+\omega_l+\omega_n)} + \frac{\sin(+\omega_m-\omega_l+\omega_n)t}{(+\omega_m-\omega_l+\omega_n)} + \frac{\sin(+\omega_m+\omega_l-\omega_n)t}{(+\omega_m+\omega_l-\omega_n)} + \frac{\sin(-\omega_m+\omega_l+\omega_n)t}{(-\omega_m+\omega_l+\omega_n)}\right]_1^2.$$

Although not listed here, care must be taken in the above 8 equations to consider $n = m = 1$, $n = l = 1$, and $m = l = 1$ just as above for SS_{nm} where $n = m$.

The matrices $\tilde{A}_{nml}$, $\tilde{B}_{nml}$, $\tilde{C}_{nml}$, $\tilde{\alpha}_{nm}$, $\tilde{\epsilon}_{nm}$ are determined from the spatial integrals of 7.83. To calculate the spatial integrals, one substitutes the assumed forms of u' and P' from 7.51 and 7.52 into the spatial integrals of 7.83 using 7.23 through 7.34. Since the time variable η_n is slowly varying, it is moved outside of the spatial integration. Then the integration is performed with ψ_n where in the special case chosen (from 7.80)

$$\psi_n(x) = \cos\left(\frac{n\pi(x-x_f)}{L_C - x_f}\right).$$

References

[1] Marble, F. E., "Personal communications," 1986.

[2] Summerfield, M., "A Theory of Unstable Combustion in Liquid Propellant Rocket Systems," *Journal of the American Rocket Society*, vol. 21, pp. 108–114, Sep. 1951.

[3] Crocco, L. and Cheng, S., *Theory of Combustion Instability in Liquid Propellant Rocket Motors.* Butterworths Scientific Publications, 1956.

[4] Crocco, L., "Aspects of Combustion Instability in Liquid Propellant Rocket Motors, Parts I and II," *Journal of the American Rocket Society*, vol. 21 and 22, pp. 163–178 and 7– 16, Nov. 1951 and 1952.

[5] Rayleigh, L., *Theory of Sound.* Dover Publications, second ed., 1894.

[6] Clark, W. H. and Humphrey, J. W., "Identification of Longitudinal Acoustic Modes Associated with Pressure Oscillations in Ramjets," *Journal of Propulsion and Power*, vol. 2, pp. 199–205, May-June 1986.

[7] Clark, W. H., "Expermental Investigation of Pressure Oscillations in a Side Dump Ramjet Combustor," *Journal of Spacecraft and Rockets*, vol. 19, no. 1, pp. 47–53, 1982.

[8] Clark, W. H., "Geometric Scale Effects on Combustion Instabilities in a Side Dump Liquid Fuel Ramjet," *Proceedings of the 19th JANNAF Combustion Meeting*, vol. 1, no. CPIA Pub. 366, pp. 595–604, 1982.

[9] Yang, V. and Culick, F. E. C., "Linear Theory of Pressure Oscillations in Liquid-Fueled Ramjet Engines," *AIAA 21st Aerospace Sciences Meeting*, Jan. 1983.

[10] Culick, F. E. C. and Rogers, T., "The Response of Normal Shocks in Diffusers," *Journal of the American Institute of Aeronautics and Astronautics*, vol. 21, pp. 1383–1390, Aug. 1980.

[11] Humphrey, J. W., "Computation of One-Dimensional Acoustic Modes as Applied to Ramjet Inlet/Combustors," NWC TM 5164, China Lake Naval Weapons Center, Oct. 1983.

[12] Smith, D. A., *An Experimental Study of Acoustically Excited, Vortex Driven, Combustion Instability within a Rearward Facing Step Combustor.* PhD thesis, California Institute of Technology, 1985.

[13] Crump, J. E., Schadow, K. C., Yang, V., and Culick, F. E. C., "Combustion Instability in a Research Combustor: Identification of Acoustic Modes," *Journal of Propulsion and Power*, vol. 2, pp. 105–109, March-April 1986.

[14] Schadow, K. C., Crump, J. E., and Blomshield, F., "Combustion Instability in a Research Combustor: Inlet Shock Oscillations," *Proceedings of the 18th JANNAF Combustion Meeting*, vol. 3, pp. 341–356, Oct. 1981.

[15] Schadow, K. C., Crump, J. E., Blomshield, F., and Bicker, C. J., "Combustion Instability in a Research Combustor: Pressure Oscillations," *Proceedings of the 18th JANNAF Combustion Meeting*, vol. 3, pp. 357–370, Oct. 1981.

[16] Schadow, K. C., Wilson, K. W., Crump, J. E., Foster, J. B., and Gutmark, E., "Interaction Between Acoustics and Subsonic Ducted Flow with Dump," *AIAA 22nd Aerospace Sciences Meeting*, Jan. 1984.

[17] Gutmark, E., Schadow, K. C., M.Parr, D., Wilson, K. W., and Harris, C. K., "The Mean and Turbulent Structure of Noncircular Jets," *AIAA Shear Flow Control Conference*, March 1985.

[18] Sajben, M., Bognar, T. J., and Kroutil, J. C., "Experimental Study of Flows in a Two-Dimensional Inlet Model," *Journal of Propulsion and Power*, vol. 1, pp. 109–117, March-April 1985.

[19] Bognar, T. J., Sajben, M., and Kroutil, J. C., "Response of a Supersonic Inlet to Downstream Perturbations," *Journal of Propulsion and Power*, vol. 1, pp. 118–125, March-April 1985.

[20] Hsieh, T., Bognar, T. J., and Coakley, T. J., "Numerical Simulation and Comparison with Experiments for Self-excited oscillations in a Diffuser FLow," *AIAA/SAE/ASME/ASEE 21st Joint Propulsion Conference*, July 1985.

[21] Davis, D. L., "Coaxial Dump Combustor Combustion Instabilities, Part 1 - Parametric Test Data," Tech. Rep., Aero Propulsion Laboratory, Air Force Wright Aeronautical Laboratories,Wright-Patterson AFB, 1981.

[22] Abouseif, G. E., Keklak, J. A., and Toong, T. Y., "Ramjet Rumble: The Low-Frequency Instability Mechanism in Coaxial Dump Combustors," *Combustion Science and Technology*, vol. 36, pp. 83–108, 1984.

[23] Craig, R. R., Buckley, P. L., and Stull, F. D., "Large Scale Low Pressure Dump Combustor Performance," *Aero Propulsion Laboratory (RJT), Air Force Wright Aeronautical Laboratories, Wright-Patterson AFB*, Aug. 1976.

[24] Reardon, F. H., "Analysis of Very Low Frequency Oscillations in a Ramjet Combustor by use of a Sensitive Time Lag Model," *Proceedings of the 18th JANNAF Combustion Meeting*, vol. 3, pp. 307–316, Oct. 1981.

[25] Rayleigh, L., *The Theory of Sound*, ch. XVI, p. 226. Dover Publications, second ed., 1896.

[26] Culick, F. E. C., "Nonlinear Behavior of acoustic Waves in Combustion Chambers–I," *Astronautica Acta.*, vol. 3, pp. 715–734, 1976.

[27] Culick, F. E. C., "Nonlinear Behavior of acoustic Waves in Combustion Chambers–II," *Astronautica Acta.*, vol. 3, pp. 735–757, 1976.

[28] Culick, F. E. C., "Remarks on Entropy Production in the One-Dimensional Approximation to Unsteaady Flow in Combustion Chambers," *Combustion Science and Technology*, 1976.

[29] Culick, F. E. C., "An Elementary Calculation of the Combustion of Solid Propellants," *Astronautica Acta.*, vol. 14, pp. 171–181, 1969.

[30] Culick, F. E. C., "Stability of Longitudinal Oscillations with Pressure and Velocity Coupling in a Solid Propellant Rocket," *Combustion Science and Technology*, vol. 2, pp. 179–201, 1970.

[31] Culick, F. E. C., "The Stability of One-Dimensional Motions in a Rocket Motor," *Combustion Science and Technology*, vol. 7, pp. 165–175, 1970.

[32] Culick, F. E. C., "Calculation of the Admittance Function for a Burning Surface," *Astronautica Acta.*, vol. 13, pp. 221–2371, 1967.

[33] Culick, F. E. C., "Rotational Mean Flow and Damping of Acoustic Waves in a Solid Propellant Rocket," *Journal of the American Institute of Aeronautics and Astronautics*, vol. 4, pp. 1462–1464, Aug. 1966.

[34] Clark, W. H., "Personal communications," 1983-84.

[35] Rogers, T., "Ramjet Inlet/Combustor Pulsations Study," NWC TP 6053, China Lake Naval Weapons Center, Jan. 1980.

[36] Rogers, T., "Ramjet Inlet/Combustor Pulsations Analysis and Test," NWC TP 6155, China Lake Naval Weapons Center, Jan. 1980.

[37] Yang, V., *Pressure Oscillations in Liquid-Fueled Ramjet Engines.* PhD thesis, California Institute of Technology, May 1984.

[38] Whitham, G. B., *Linear and Nonlinear Waves*, ch. 6. John Wiley and Sons, 1973.

[39] Awad, E. A., *Noninear Acoustic Instabilities in Combustion Chambers.* PhD thesis, California Institute of Technology, Aug. 1983.

[40] Kovasznay, L. S. G., "Turbulence in Supersonic Flow," *Journal of the Aeronautical Sciences*, vol. 20, pp. 657–682, Oct. 1953.

[41] Chu, B. T. and Kovasznay, L. S. G., "Non-linear interactions in a viscous heat-conducting compressible gas," *Journal of Fluid Mechanics*, vol. 3, no. 5, pp. 494–512, 1957-58.

[42] Awad, E. and Culick, F. E. C., "On the Existence and Stability of Limit Cycles for Longitudinal Acoustic Modes in a Combustion Chamber," *Combustion Science and Technology*, vol. 46, pp. 195–222, 1986.

[43] Tsien, H., "The transfer functions of rocket nozzles," *Journal of the American Rocket Society*, vol. 22, no. 1, pp. 139–143,162, 1952.

[44] Marble, F. E. and Candel, S. M., "Acoustic Disturbance from Gas Nonuniformities Convected Through a Nozzle," *Journal of Sound and Vibration*, vol. 55, no. 2, pp. 225–243, 1977.

[45] Chu, B. T., "Stability of Systems Containing a Heat Source - the Rayleigh Criterion," Tech. Rep., National Advisory Committee for Aeronautics, June 1956. Engineering Library, Lockheed Aircraft Corporation. NACA RM 56D27.

[46] Chu, B. T., "Mechanism of Generation of Pressure Waves at Flame Fronts," Tech. Rep., National Advisory Committee for Aeronautics, Oct. 1956. NACA TN 3683.

[47] Chu, B. T., "On the Generation of Pressure Waves at a Plane Flame," *Fourth International Symposium on Combustion*, pp. 603–612, 1953.

[48] Chu, B. T., "Pressure Waves Generated by Addition of Heat in a Gaseous Medium," Tech. Rep., Johns Hopkins University, June 1955. NACA TN 3411.

[49] Aaron, K. M., *Edgestones and Acoustic Resonances in a Duct.* PhD thesis, California Institute of Technology, 1985.

[50] Morse, P., *Vibration And Sound.* McGraw-Hill Book Company, Inc., first ed., 1936.

[51] Culick, F. E. C. and Rogers, T., "Modelling Pressure Oscillations in Ramjets," in *AIAA/SAE/ASME 16th Joint Propulsion Conference*, June 1980.

[52] Kantrowitz, A., "The Formation and Stability of Normal Shock Waves in Channel Flows," NACA TN 1225, National Advisory Committee for Aeronautics, Nov. 1946.

[53] Chu, B. T., "Mechanism of Generation of Pressure Waves at Flame Fronts," Tech. Rep. NACA TN 3683, National Advisory Committee for Aeronautics, Oct. 1956. See page 11.

[54] Morse, P., *Vibration And Sound*, ch. VI, pp. 215–227. McGraw-Hill Book Company, Inc., first ed., 1936.

[55] CULICK, F., "Communications between F.E.C. Culick, B.T. Zinn, and W. Andrepont.," 1976.

[56] Cole, J. D., *Perturbation Methods in Applied Mathematics.* Blaisdell Publishing Company, 1968.

[57] White, F. M., *Viscous Fluid Flow*, pp. 675–678. McGraw-Hill Book Company, Inc., first ed., 1974.